3D Neuronal Innervated Corneal Tissue Model

A dissertation submitted by
Siran Wang
in partial fulfillment of the requirements for the degree of
Doctor of Philosophy
in
Biomedical Engineering Department
Of
Tufts University
May, 2017

Advisor:
Dr. David L. Kaplan
Committee Members:
Dr. James L. Funderburgh
Dr. Qiaobing Xu
Dr. Kenneth R. Kenyon

Abstract

The cornea is the outermost layer of human eye and is an important part of the ocular light path. The cornea is medically significant as corneal diseases account for 25% of blindness in the world population [4]. Dense neuronal innervation provides vital functions and a protective role for the cornea including initiation of eye blinking. In addition to neuronal innervation, aligned ECM and stromal cell distribution maintain the transparency of cornea, while the multilayer epithelium forms an important barrier to protect ocular tissue. Despite the essential functions of these different structures, the interactions between nerve and corneal tissue are not clear. Current research methods are limited to *in vivo* rabbits, mice and pigs models which do not represent the human corneal anatomy and physiology. The goal of this research was to establish an *in vitro* tissue model to mimic the biological and mechanical environment of the cornea, using human cells. This *in vitro* tissue model can be used to study the physiology and pathology of the human cornea. In this work, a corneal tissue model containing epithelium and stroma with neuronal innervation was established, using silk protein as the scaffolding material to mimic the architecture of the cornea. This tissue model provided aligned growth of stromal cells, multiple layers of epithelial cells and innervation. Interactions between neurons and corneal cells were investigated in static culture first. Next, a dynamic culture system, that provides intraocular pressure and tear flow, was developed to study the impact of the physical environment on *in vitro* corneal tissue and nerves. Last, capsaicin nociceptive stimulation was introduced in the culture to study the impact on the corneal tissue and to establish functionality of the tissue model. This tissue model and dynamic culture system would benefit drug screening, testing of implant materials, cornea disease diagnose and related fields. Further, this tissue system can be used to replace animal models in pre-clinical test for drugs.

Acknowledgment

The work in this thesis would not have been accomplished without many people. They are my mentors, my friends, and my families. First, I would like to express my deepest gratitude to my advisor, Prof. David Kaplan. You are a great mentor, who taught me to think creatively when facing a scientific challenge and be brave to try what seems to be impossible. You have provided the right amount of guidance when it is most needed and let me grow in this lab to the level I have never imagined before. Also, you gave me the chance to come to the US, introduced me to this extraordinary lab where I met the career and the man I love. I will forever be thankful for all the opportunities you provide in the past and the future.

Then I would like to thank all my committee members. Prof. Qiaobing Xu, who has advised me in research, life and career development from the day I enter BME department. Your help has eased me in both scientific and cultural adventures. Thank you to Dr. Kenneth Kenyon, you have provided the crucial clinical perspective in my research, and always appreciating my results. You are also a fun friend often inspire me with your passion for life and ophthalmology. Prof. James Funderburgh, you are the collaborator that all scientist dream of. Your precious knowledge of corneal stroma has provided valuable guidance in my lab work and publications. Your generosity in providing human corneal stromal stem cells is the foundation of this work.

I will forever be indebted to my lab mentor Dr.Chiara E. Chezzi, who has always been there to provide guidance in writing and research planning. I was so touched when she came to the lab to meet with me and chat about data problems when she was going through her back problem after

the child birth. She has done so much for me, but for most she has trained me in critical thinking and experimental design which may be the essential portions in a Ph. D's work.

Dr. James D White is the most special person in my life. He started as my earliest lab mentor, and then become my best friend, my boyfriend, my fiance and now my husband. He was the one taught me cell culture, pipette, immunostaining, ELISA, and so much more. He is the kindest and most patient person I have ever seen. It took a lot of effort to train a student who didn't know the English name of any lab equipment to become a scientist mentoring three undergraduate students now. And most of all, thank you for all your love, support, and understanding.

Thanks to other members of tissue regeneration and neuro groups past and present: Rachel Gomes, Sarah. Lightfoot Vidal, Rosalyn Delia, Phillip Deardorff, Whitney Stoppel, Min Tang-Schomer, Amy Hopkins, Tom Valentin, Elise DeSimone, Yuting Dingle, Volha Liaudanskaya, Disha Sood, Will Cantley and Karolina Chwalek. Your input has helped me avoid extra miles on the way, and discussion with you is always insightful and exciting.

Thank you to Ying Chen, Erica Kimmerling, and Jonathan Grasman, for all the help with my work. To Dana Cairns, thank you for supplying the neuronal stem cells and help with my thesis.

To my officemate in room 124C, Nicole Raia, Zaira Martin Moldes, Nina Dinjaski, Eleana Manousiouthakis, William Cantley, Aswin Sundarakrishnan, Benjamin Partlow and Sophia Szymkowiak, you guys are the best. Your joyful company has made this office truly the den of optimistic even the experimental results are sometimes not.

Many thanks to all the Kaplan lab members, Lorenzo Tozzi, Chunmei Li, Wenwen Huang, Wenda Zhou, Jin Guo, Siwei Zhao, Anne Golding for all the great ideas helped me moving on my research.

To Tiger Tao, Miaomiao Yang and Prof. Fiorezo Omenetto, thank you a lot for the help in designing the NGF functionalized silk film.

My undergraduate students, Rachel Pollard, David Alvarez, Andrew Stephenson, Janani Baskaran, thank you for help out in lab. It is such a pleasure to be your mentor. Especially thanks to Rachel who helped me so much with my PCR and ELISA assay.

Sincere thanks to Milva Ricci, Laura Saurez, Carmen Preda, Martin Hunter, and Keleigh Sanford whose tireless behind the scenes effort kept my work going. We are lucky to have you.

Last, but for most I want to thank my family and my in-laws. Thank you for being my backbones through the process, being the cheerleader when I felt difficult to carry on, and being the most enthusiasm audiences for every little progress. Especially my father who have encouraged my chase of dream with strong financial and emotional support. I love you all.

Table of Contents

List of Figures

List of Tables

Abbreviations

HCSSCS: human corneal stromal stem cells
HCECS: human corneal epithelial cells
DRG: dorsal root ganglion
RGD: Arg-Gly-Asp
GDNF: Glial cell derived neurotrophic factor
BDNF: brain-derived neurotrophic factor
NGF: nerve growth factor
NT-3: neurotrophin-3
ECM: extracellular matrix
PDMS: polydimethylsiloxane
PEO: polyethylene oxide
EDC: 1-ethyl-3-(dimethyl aminopropyl) carbodiimide hydrochloride
NHS: Nhydroxysuccinimide
ITS: selenous acid
TCP: tissue culture plastic
TGF-β3: transforming growth factor-beta3
FGF: fibroblast growth factor
ELISA: enzyme-linked immunosorbent assay
FBS: fetal bovine serum
MSC: mesenchymal stem cells
KGF: keratinocyte growth factor
HGF: hepatic growth factor
EGF: epithelial growth factor
ED-LC: hCECs and DRG neurons co-culture in liquid
ED-ALIC: hCECs and DRG neurons co-culture at air-liquid interface
SD-LC: hCSSCs and DRG neurons co-culture in liquid
SD-ALIC: hCSSCs and DRG neurons co-culture at air-liquid interface
E-LC: hCECs cultured alone in liquid
E-ALIC: hCECs cultured alone at air-liquid interface
S-LC: hCSSCs cultured alone in liquid
S-ALIC: hCSSCs cultured alone at air-liquid interface
D-LC: DRG neurons cultured alone in liquid
D-ALIC: DRG neurons cultured alone at air-liquid interface
ESD-LC: hCSSCs, hCECs and DRG neurons tri-cultured in liquid
ESD-ALIC: hCSSCs, hCECs, and DRG neurons tri-cultured at air-liquid interface
KERA: keratocan
LUM: lumican
ACTA2: actin A2
ALDH3A1: aldehyde dehydrogenase 3 family member A1
IVL: involucrin
GJA4: gap junction protein alpha 4
KRT3: keratin 3
qPCR: quantitative real-time polymerase chain reaction
MUC: mucins gene family

CRCP: CGRP receptor component gene
SCN: sodium voltage gate gene
TAC1: Tachykinin, Precursor 1
TRPV1: transient receptor potential vanilloid 1
NTRK1: Neurotrophic Receptor Tyrosine Kinase 1)
IOP: Intraocular pressure
SP: Substance P
CGRP: Calcitonin gene-related peptide

Chapter I. Introduction and Background

I. Introduction

The ophthalmic pharmaceutical market has been continuously growing at a strong pace worldwide, from approximately $12 billion in 2010 to an estimated $52.4 billion in 2017 [12]. This growth has attracted investment from large drug companies including Pfizer, Merck and Danube Pharma [13]. Though research and development (R&D) expenditures have doubled in the past 10 years, the number of new drugs approved by the US Food and Drug Administration (FDA) has decreased [14]. For example, the FDA website notes that only 20 ocular drugs were approved in the past 10 years, and only 2 were approved in 2016 [15]. There are many reasons contributing to this situation, including the lack of understanding of fundamental cornea biology and repeatable and cost effective pre-clinical testing methods [16], among others.

The efficacy and safety of a drug are important evaluations in preclinical testing [17]. The current gold standard for evaluating drug toxicity and irritation for the eye is the *in vivo* Draize test on rabbit cornea [18]. Test substances are applied onto one eye of the rabbit to evaluate the level of irritation, while the other eye serves as a control. Other animals like pig, mouse, rat and monkey have also been used in pre-clinical trials of ocular drugs [18-20]. However, issues including lack of repeatability [21], reproducibility [22] and inconsistency with human responses have occurred, mainly due to the interspecies differences between animals and humans [23]. *Ex vivo* corneal models to identify substances that cause tissue damage have used isolated rabbit and porcine cornea [24, 25]. However, these *ex vivo* corneal models share the drawback of anatomical and physiological differences from human cornea as *in vivo* test methods [26]. Also, the *ex vivo* corneal models cannot be used to evaluate the irritation and pain response to the

substances due to the nerve damage during the excision of native tissue [27]. Means for preserving or reconstructing functional innervation in corneal model are needed to improve current models.

The limitations associated with *in vivo* and *ex vivo* corneal models have encouraged the development of new *in vitro* models that include the human cells which are more relevant for many diseases than animal corneas [28-30]. Meanwhile, these systems reduce ethical concerns, are more cost effective, and can provide high throughput analysis [26].

The current designs of corneal *in vitro* models are mainly focused on mimicking the corneal epithelium, as this layer is one of the major barriers for drug permeation into the cornea [31, 32]

Table 1. *Limitation of current corneal models.*

Limitations of Current Corneal Models		
Type	**Features**	**Limitations**
In vivo	Corneas in live animals	Anatomically, physiologically different from human cornea; expensive, difficult to control variation; ethical concerns
Ex vivo	Isolated animal corneas	Anatomically, physiologically different from human cornea; lack of innervation
In vitro	2D corneal tissue models	Lack cellular components and anatomy of human cornea
	3D collagen based corneal tissue models	Lack mechanical properties of cornea; lack innervation; do not support long term cultivation

(Table 1). These models have provided physiologically relevant pharmacodynamical data for drug testing [31-34]. However, it is difficult to perform toxicity and irritation testing on these corneal models due to the over-simplified cellular components, culture environment and lack of a neuronal component. To address these issues, an *in vitro* corneal model that includes functional innervation that can generate nociceptive reactions, scaffolds that mimic corneal anatomy and

mechanical properties, and dynamic cultivation condition that captures the native ocular surface environment is needed and

is the subject of the present thesis.

II. Purpose and Organization

The purpose of this research is to construct an innervated corneal model with epithelial and stromal layers. We hypothesized that by co-culturing corneal cells and neurons in scaffolds mimicking corneal anatomy with a bioreactor representing the ocular environment, a functional innervated corneal model could be achieved. Our research strategy is composed of three steps. First, develop a three-dimensional (3D) corneal model containing neurons, corneal epithelial and stromal cells. Second introduce intraocular pressure (IOP) and tear flow (TF) dynamic

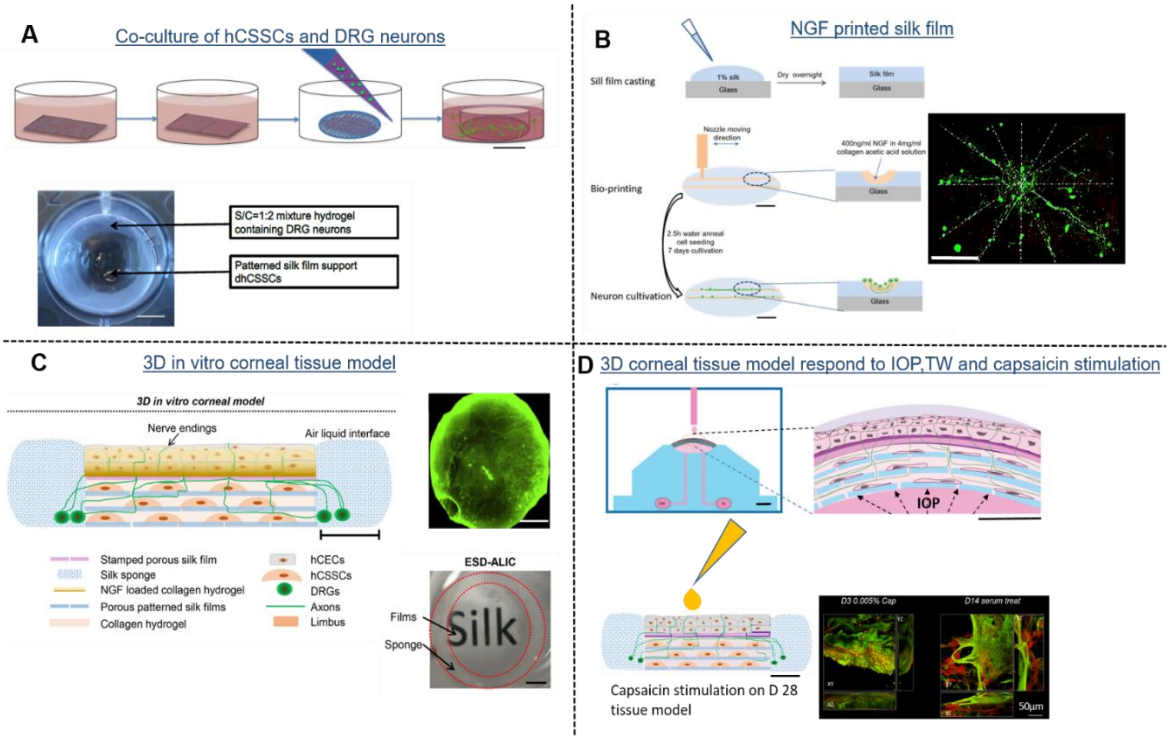

Figure 1. *Research outline figure leading to development of 3D tissue model of cornea. A. (Chapter II): Two-dimensional tissue model of innervated corneal stroma; B. (Chapter III): NGF bio-printing on silk films for neuronal extension guidance; C. (Chapter IV): Three dimensional tissue model of neuronal innervated cornea; D. (Chapter V and VI): 3D corneal tissue model responds to IOP, TW and capsaicin simulation.*

mechanical cues to mimic the native ocular environment and observe cellular responses. Third, determine how the tissue model responds to nociceptive stimulation. As a result, this innervated corneal epithelium and stroma model affords the cornea-neuron crosstalk to respond to physiological and pathological stimuli (Figure 1).

Chapters 2,3 and 4 describe the construction of the 3D innervated corneal tissue model. The content of Chapter 2 has been published in Journal of Biomedical Material Research Part A [35]. The focus of this chapter is on developing a co-culture system for differentiated human corneal stromal stem cells (hCSSCs) and dorsal root ganglion neurons (DRG) to mimic human cornea tissue interactions (Figure 1A). Axon extension, connectivity, and neuron cell viability were studied. DRG neurons developed longer axons when co-cultured with hCSSCs in comparison to neuron cultures alone. To assess the mechanism involved in the co-culture response, nerve growth factors secreted by hCSSCs including NGF, brain-derived neurotrophic factor (BDNF), glial cell-derived neurotrophic factor (GDNF), and neurotrophin-3 (NT-3) were characterized with greater focus on BDNF secretion. HCSSCs also secreted collagen type I, an extracellular matrix molecule favorable for neuronal outgrowth. This co-culture system provides a slowly degrading silk matrix to study neuronal responses in concert with hCSSCs related to innervation of corneal tissue with utility toward human corneal nerve regeneration and associated diseases.

In Chapter 3, methods to guide axonal extensions in the 3D corneal model were developed. Collagen type I and nerve growth factor (NGF) were printed on silk protein films by inkjet printing to generate patterned axonal tracts and regions of controllable stiffness (Figure 1B). These bio-printed silk films supported neuronal extension and guidance along the printed

patterns. This approach could be useful towards needs for improved nerve guides for implants and in the construction of *in vitro* innervated tissue models.

The data in Chapter 4 has been published in Biomaterials [36]. In this chapter a corneal tissue model was constructed to include the stroma, epithelium, and innervation. Thin silk protein film stacks served as the scaffolding to support the corneal epithelial and stromal layers, while a surrounding silk porous sponge supported neuronal growth. The neurons innervated the stromal and epithelial layers and improved function and viability of the tissues. An air-liquid interface environment of the corneal tissue was also mimicked *in vitro*, resulting in a positive impact on epithelial maturity. The inclusion of three cell types in co-culture at an air-liquid interface provides an important advance for the field of *in vitro* corneal tissue engineering, to permit improvements in the study of innervation and corneal tissue development, corneal disease, and tissue responses to environmental factors (Figure 1C).

In Chapter 5, intraocular pressure (IOP) and tear flow (TF) were introduced to the 3D model using a custom designed bioreactor system. We adopted a clinically used artificial anterior chamber to anchor our 3D corneal tissue model and generate pressure underneath the scaffold mimicking IOP (Figure 1D). A specially designed lid was fitted with a medium outlet that added tear solution dropwise to the surface of scaffold. In addition, human sourced sensory neurons were used in the scaffold instead of chicken DRG neurons. After the dynamic cultivation, the stromal ECM and neuronal functional markers were upregulated in both RNA and protein measurements, confirming such dynamic environment can be mimicked *in vitro* (Figure 1D).

In Chapter 6, we investigated the effect of capsaicin nociceptive stimulation on corneal cells and neuronal innervation in the cornea model (Figure 1 D). Decreased hCECs, hCSSCs and neuronal innervation density were observed after capsaicin stimulation. Pain mediators, substance P (SP) and calcitonin gene-related peptide (CGRP), were measured from capsaicin stimulated innervated samples. This pain-like response indicated the tissue model was innervated with functional human sensory neurons. To test the ability of recovery after trauma, serum treatment, which is used in clinic to treat epithelium defects, was applied on the injured corneal model. Corneal cell confluency and neuronal innervation were improved after treatment, revealing the feasibility of applying this tissue model in drug development.

Finally, Chapter 7 includes several ideas for future research using the corneal tissue model. Strategies for further optimization for epithelium and neuronal innervation in the model, proposed methods for investigating acute pain response and introducing inflammation are presented.

III. Background

Tissue engineering of *in vitro* corneal tissue models can provide understanding of corneal physiology, pathology and pharmacology. An ideal *in vitro* corneal tissue model should mimic the corneal anatomic structure, innervation and dynamic ocular environment. Here we discuss background of corneal anatomy, function, significance of corneal innervation in healthy and diseased state, and the state of art for corneal *in vitro* models.

3.1 Corneal Anatomy

The cornea is the transparent outermost part of human eye and accounts for approximately 2/3 of the eye's optical power [37]. The human, cornea has 0.5-0.6mm thickness in the center and 0.6-0.8mm in the periphery with a diameter of 11-12mm [37]. The cornea has three distinct layers, the epithelium, stroma and endothelium (Figure 2A). The corneal epithelium contributes 10% of corneal thickness. It is composed of a superficial layer formed with flattened apical cells, 4-5 layers of stratified non-keratinized epithelial cells, and a basal layer [38]. These cell layers are held together by tight junctions and serve as a barrier against fluid loss and pathogen penetration. The corneal epithelial cell surface contains microvilli that secrete a polysaccharide-protein mixture, adhering and stabilizing the tear film, while the basal cells secrete basal lamina attaching epithelium to stroma [39, 40].

In between the corneal epithelium and stroma is an acellular layer composed with collagen, laminin, nidogen and perlecan, named the Bowman's layer [41] (Figure 2A). This layer mainly serves to protect the stroma.

The corneal stroma accounts for 85-90% of the corneal thickness and consists of regularly arranged collagen fibers along with sparsely distributed interconnected keratocytes [42]. These cells produce collagen and proteoglycans that comprise the corneal extracellular matrix [43]. Corneal ECM is especially rich in collagens. Collagen types I, V and VI compose the majority of corneal stroma [44]. The cornea also contains proteoglycans including decorin, lumican, mimecan, keratocan, and keratin sulfate. These proteoglycans participate in the control of inter-fibrillar spacing and in lamellar adhesion [45-47].The stromal collagen fibrils are organized into lamellae which form approximately 300 layers in central cornea and 500 close to limbus [48]. The anterior stromal lamellae interweave through layers ,directly insert into Bowman's layer and contribute to corneal curvature [49]. Posterior stroma lamellae are wider, thicker, more ordered and more hydrated than in the anterior stroma [50-52]. In the posterior lamellae, keratocytes are arranged parallel to the plane of corneal curvature [53]. Proteoglycan [54] and keratoepithelin [55] are expressed between the collagen fibrils to bind collagen lamellae together.

The endothelial layer consists of a monolayer of cells that lines the posterior corneal surface which contain 3500 cells/mm^2 [56]. In the adult, endothelial cells do not proliferate under normal circumstances [57] and mainly serve as an active pump that moves ions and draws water osmotically from stroma into aqueous humour. This pumping mechanism maintains the transparency of cornea and allows nutrients to permeate from the aqueous humour into the stroma [58].

The cornea is the most peripherally innervated surface in the human body [59, 60] (Figure 2 B). Corneal innervation is distributed throughout the epithelial and stromal layers but is not found in

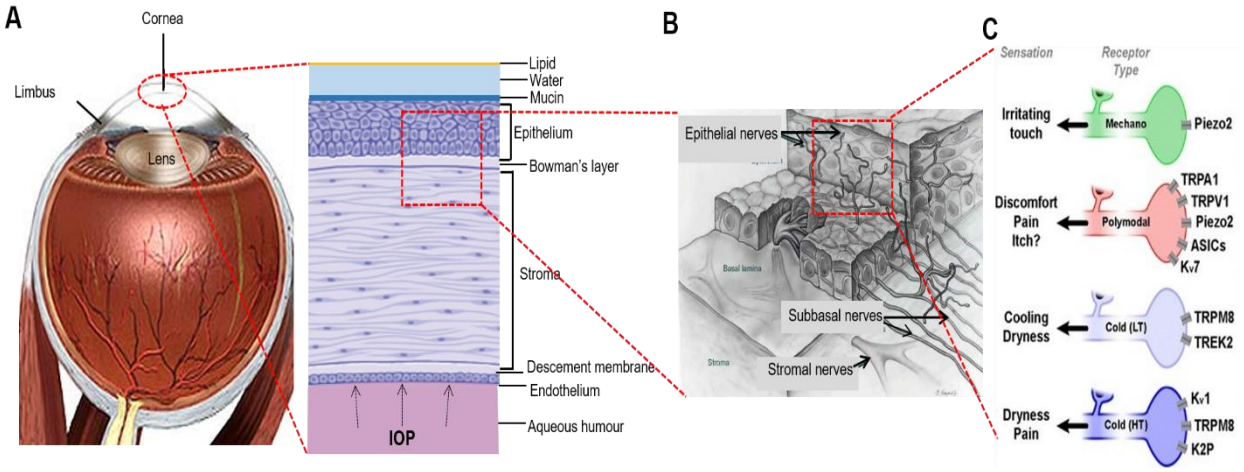

Figure 2. *Corneal anatomy structure (A), corneal innervation in epithelium and stroma (B) [5, 6], and different types of nociceptive receptor on the corneal surface[9].*

the endothelial layer [61] (Figure 2B). Stromal nerve trunks (33-71/mm^2) [62] arise from the limbal plexus and enter the peripheral corneal stroma radially. In the stroma, nerves are organized parallel to the collagen lamellae and branch into smaller fascicles as they proceed toward the superficial stroma [63]. The nerve fibers then penetrate the epithelium layer with an approximate density of 600 termini/mm^2 [61, 63]. During corneal development, nerve growth is modulated by many growth factors. Brain-derived neurotrophic factor (BDNF), nerve growth factor (NGF), glial cell line-derived neurotrophic factor (GDNF), and neurotrophin-3(NT-3) are expressed in the corneal epithelium and stroma [64-67]. Among these growth factors, NGF was found to be critical for corneal nerve survival, axonal branching, elongation, sprouting and regeneration [65].

3.2 Corneal Dynamic Environment

Dynamics of nutrient transfer, intraocular pressure, and tear flow all contribute to healthy cornea development and function. The cornea is a transparent, avascularized tissue located at air-liquid interface. Oxygen and nutrients diffuse into cornea via the aqueous humour and tear fluids. Corneal nerves secretes neurotrophic factors that contribute to the cytokine dynamics crucial to healthy cornea [64].

Corneal tissue is under constant tension generated by IOP, created by the aqueous humour in anterior chamber. In healthy human being, the IOP is maintained at around 15-20mmHg [68]. Variations of IOP within the normal range can be caused by heart rate [69], blood pressure [70], and respiration [71]. IOP determines the curvature of the cornea and influences corneal thickness [72-74] during corneal development [75]. An IOP value greater than 20mmHg is considered corneal hypertension, as observed in glaucoma, corneal trauma or overproduction of aqueous humour [76]. Multiple studies have shown that corneal cells react to mechanical stress *in vitro* and *in vivo*. Endothelial cell numbers decreased in glaucoma patients. Corneal stromal fibroblasts change morphology following the direction of tension [77, 78].

Aside from the constant application of tension, the surface of the cornea is immersed in the tear film, which serves as both a protective layer and a source of nutrients to the corneal epithelium. The tear film is composed of lipid, aqueous, and mucin layers [14]. Lipids in tear solution prevent drying [79]. An aqueous layer is secreted by the lacrimal gland, containing water and proteins [80]. The mucins secreted by conjunctival goblet cells and epithelial cells [81, 82]

provide lubrication as well as prevention of contaminantion [79]. The tear fluid is spread across the ocular surface by eye blinking with an average rate of once every 4.5 to 5.5 seconds [83].

3.3 Function of Corneal Innervation

Corneal innervation function provides a sensing platform for eye protection [84]. The corneal pain pathway originates in the dense, unmyelinated nerve endings in the tissue [85].These terminal nociceptors are woven in the epithelial layer of the cornea. The density and unique exposure of the nerve endings make the corneal nerve more sensitive and vulnerable to noxious stimuli [85, 86].

Different types of nociceptive fibers are found in the cornea, including mechanoreceptors, which make up about 20% of the nociceptors, cold receptors which make up about 10%, and polymodal receptors which make up 70% [87] (Figure 2C). When noxious stimuli reach above the pain threshold, the nociceptors fire an “all or nothing” action potential, signalling pain [85]. This signal travels to the trigeminal brainstem nuclear complex (TBNC) where the peripheral nociceptors originate, and are then transmitted to the central nervous system (CNS) [85].

Beside sensing the stimuli and providing protection for the eye, neurons generate neuropeptides and neurotransmitters that are important to maintain a healthy cornea (Figure 3) [88, 89]. SP is secreted by corneal nerves in healthy conditions and its production increases during pain. This neuropeptide is sensed by corneal epithelial cells through the abundantly expressed SP receptors [90]. SP concentration regulates corneal epithelial proliferation [91] migration [92] and adhesion [93]. CGRP is often found co-localized with SP in most corneal nerve fibers. CGRP stimulates migration of epithelial cells [94] and induces intracellular cAMP synthesis and interleukin-8

(IL-8) gene expression [95]. The majority of corneal nerves secrete SP and CGRP into tears. Norepinephrine [96], vasoactive intestinal polypeptide [97] and neurotensin [98] have also been detected in corneal nerves. These neuropeptides induce corneal epithelium proliferation and contribute to maintenance of epithelium.

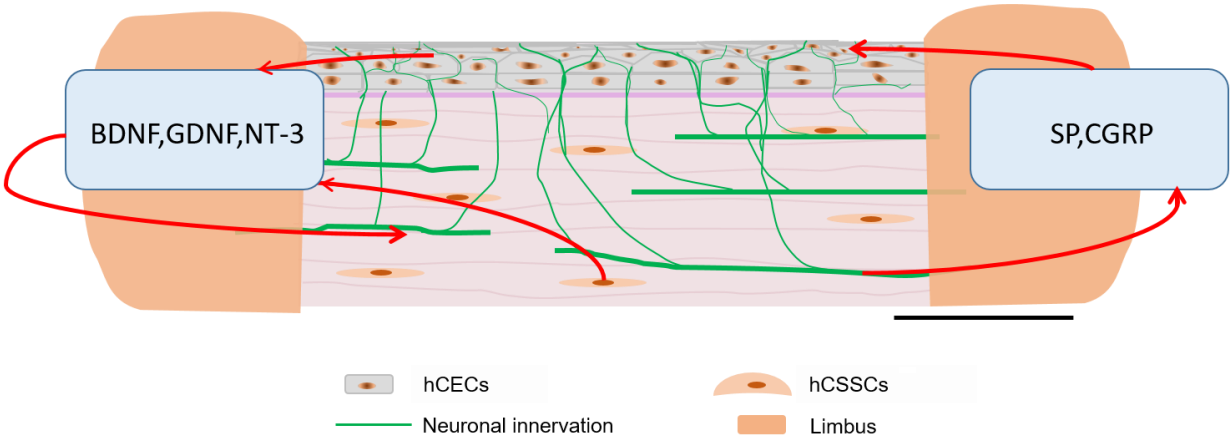

Figure 3. *The interaction between cornea and nerve. HCSSCs and hCECs secrete BDNF GDNF and NT-3 supporting neuronal innervation. Corneal nerve secretes SP and CGRP improve hCECs proliferation. Scale bar=3mm*

Despite the importance of corneal innervation, the role of neurons in healthy and diseased human cornea, as well as their role in cellular mechanisms are not fully understood [59]. This is partially due to the limitations of rabbits, mice and pigs *in vivo* corneal models. These limitations include the complexity of *in vivo* environments, differences between human and animal corneal nerves, and challenges with studying human embryo cornea. These drawbacks underscore the need for a new research platform.

3.4 Corneal Nerve in Diseases

Among patients who suffer from corneal opacity worldwide, 2.85 million people have diminished or absence of sensation due to corneal nerve dysfunction or degeneration [84]. In pathological environments, corneal nerve growth and function can be negatively affected [63].

During corneal infections, a 2-3 fold reduction of nerve fibers, bundles, and terminal branching was observed, while axon tortuosity increased [99]. Decrease of corneal nerve density is seen during keratoconus, a condition characterized by thinning of the cornea. Localized stromal nerve thickening, twisting, and looping were also observed [100-102]. Corneal nerve dysfunction was also found in autoimmune diseases as well as corneal ulceration and diabetic neuropathy [103-105]. In addition, corneal nerve injuries are side effects to surgery including corneal transplantation and UV treatment [63, 64]. However, the complex anatomical and biochemical disease pathways make it difficult to study corneal diseases *in vivo* [106-108]. An *in vitro* neuronal innervated model for clinical, biomedical, and pharmacological advances is needed.

3.5 Corneal Acute and Chronic Pain

Corneal pain often takes place along with ocular diseases including corneal trauma, infection and dry eye syndrome [109]. The understanding of pain in cornea and other organs, however, is limited by the complicated nociceptive pathways and associated physiological and psychological elements. As the most innervated organ on the human surface, the cornea is an ideal platform to study pain processes. Based on duration, pain can be categorized into acute and chronic pain. Acute pain is neuronal response that gradually resolves with healing and lasts less than 3 months

[110] whereas chronic pain persists for more than 3 months even after the original injury is no longer present [111, 112]. It is estimated that 20% of the population in developed countries suffer from chronic pain [111]. In the cornea, there are many causes of chronic pain, including diseases, infections, and injuries [113]. Corneal chronic pain is closely linked to dry eye disease (DED) which affects about 20% of adults over 45 years old in the US [112].

Confocal microscopy of patients with corneal neuropathic chronic pain showed reduced density and length of neuronal innervation. The most common symptoms in patients with chronic neuropathic pain, is allodynia (pain response to non-painful stimuli) and/or hyperalgesia (heightened pain response to normal stimuli) [114].These decreases in pain tolerance are directly correlated to a decrease in the activation threshold of the sensory neurons [114, 115]. Nociceptive neurons experiencing chronic neuropathic pain have alterations in the expression of sodium, potassium, and calcium ion channels [116]. Voltage-gated Ca^{2+} channels (VGCCs), which mediate the release of pain neurotransmitters and neuropeptides, are responsible for heightened sensitivity. In particular, VGCCs mediate the release of SP and CGRP, neuropeptides which are actively involved in chronic pain through tissue healing, pain, and inflammation [117].

In patients with chronic pain caused by injury or disease related DED-like symptoms, the corneal epithelial and stromal thickness was often reduced. The increase of dendritic cell count also provided evidence of an increased immune response during chronic pain response [87, 118]. These results show that chronic pain affects not only the nerves but the surrounding tissues as well [86, 119].

In response to these needs, current clinical solutions for corneal neuropathic pain are limited to eye drops containing nerve growth factors [65, 120, 121]. An *in vitro* corneal tissue model and improved understanding of corneal pain pathways would offer new options to study appropriate treatments.

3.6 Current corneal models

As a critical barrier for topical ophthalmic drugs, many corneal epithelial tissue models have been reported. The simplest model included cultured human primary epithelial cells (hCECs) on tissue culture plastic and served as platform for toxicology testing [122, 123] (Figure 4 A). HCECs in a fibrin gel formed tissue sheets were used for ocular surface reconstruction [33, 34]. Immortalized human corneal epidermal keratinocytes cells cultured at the air-liquid interface on a polycarbonate membrane have been commercialized as an EpiOcular ^{TM} system [124]. Other commercially available corneal epithelium models are HCE (skinEthic) and Clonetics (Lonza) [26, 125]. However, these epithelium models do not represent the complex eye structure and lack interactions between different cell types.

To address these limitations several multicellular models were investigated. A whole corneal *in vitro* model was developed and combined isolated primary bovine or rabbit endothelial stromal and endothelial cells [126, 127]. With the realization of importance that neuronal innervation plays in the cornea, tissue models that included neurons were developed. Chicken DRG neurons were used to innervate corneal epithelium and stroma cultured in a collagen hydrogel. The neurons were seeded in a collagen hydrogel ring surrounding layers of collagen hydrogel mimicking the lamellar structure of cornea. In this model, innervation increased epithelial

proliferation and SP secretion after capsaicin stimulation [128]. However, this model failed to recapitulate the alignment of the stromal cells and the multi-layer features of the epithelial cells. To date, the native density of nerve endings and branches have not been achieved using *in vitro* cultures. Furthermore, the use of collagen as the substrate poses significant limitations due to low mechanical stiffness, leading to mismatched mechanical properties and contraction in near and long-term culture [129, 130]. Thus far, all the current multi-cellular *in vitro* models do not represent the dynamic environment around cornea including composition of aqueous humor, tear fluid and tear flow [131].

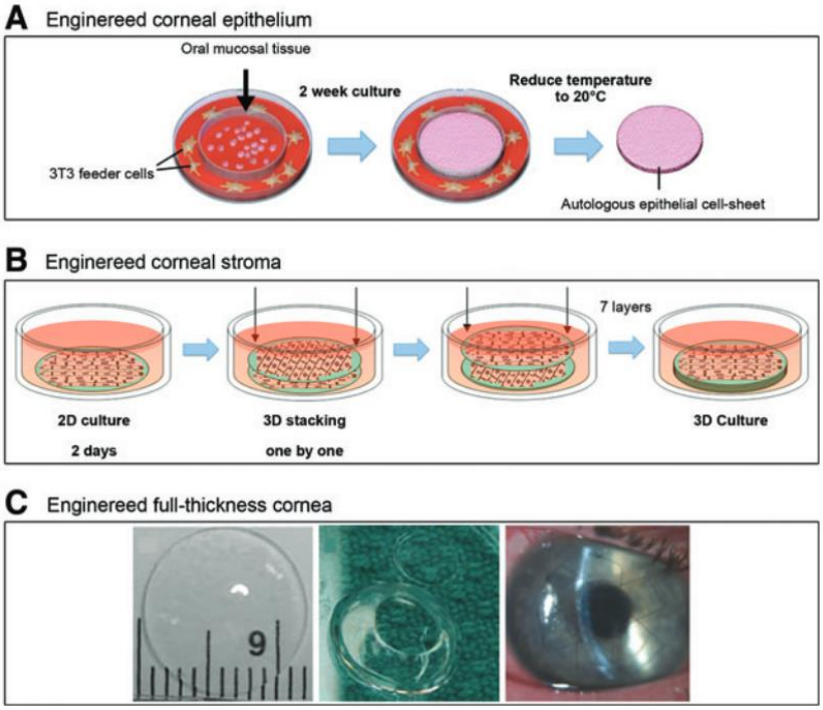

Figure 4. *Tissue-engineered approaches for corneal reconstruction. (A) Human epithelial cell sheet obtained from oral epithelial cells after removal of the cell sheet from poly(N-isopropylacrylamide)-pNIPAAM surface [6, 8]; (B) Assembly diagram of three-dimensional (3D) silk film corneal constructs seeded with human corneal fibroblasts. After 2 days, cell-seeded silk films were stacked one by one and three-dimensionally cultured[10]. (C) Synthetically cross-linked collagen molded into an implantable, full-thickness corneal substitute. Transparent samples were trimmed to prepare buttons for corneal implantation and held in place by sutures in the recipient eye[11].*

3.7 Application of Silk Fibroin in Corneal Tissue Engineering

Silk fibroin has many properties that make it advantageous for corneal tissue engineering. Silk is a biodegradable material with highly tunable mechanical properties [130, 132]. Optical clear films made with silk [130, 132] can provide elastic moduli of 67.7 kPa [133] that matched the stiffness of the cornea, which is 40-60 kPa [134, 135]. By casting on a surface with pattern, silk films can have topography with grooves ~1.67μm wide that provided aligned substrate for stromal cells [136]. Arginylglycylaspartic acid peptide (RGD) functionalization and polyethylene oxide (PEO)-induced creation of pores further improved cell attachment and growth to the films. Stromal cells seeded on these films were found to be differentiated into keratocytes and secrete

keratin sulfate, lumincan and keratocan [136]. These films also did not contract and slowly degraded *in vitro*, providing support for sustained *in vitro* tissue models (Figure 4B).

Silk material has also been applied in neural tissue engineering. Silk sponge seeded with primary cortical neurons showed innervation into the scaffold and responded *in vitro* with biochemical and electrophysiological outcomes, mimicking observations of brain homeostasis and mechanical injury responses [137-139]. Silk hydrogels have also been used as scaffolding material for DRG neuron cultivation and gave longer neuronal extension compared to collagen hydrogels. Nerve growth factors, collagen, and fibronectin can be used to decorate silk hydrogel and tune the nerve extension [140].

A key aspect of innervation of tissues is the guidance of the nerves towards the target location in the tissue. Axons can be guided by mechanical [141] and topographical inputs [142-144], response to growth factor gradients [145-147], and electrical stimulation [141, 142, 148, 149]. NGF loaded in silk matrix continuously released for 4 weeks with ~85% total weight of NFG retained in silk material [150]. Collagen hydrogels only released NGF for 4 days [151]. This result indicated that silk can serve as useful carrier of growth factors for axonal guidance. In all, the tunable topography, stiffness, degradation rate, and the ability to provide long lasting release of NGF make silk fibroin an ideal material for innervated *in vitro* tissue models.

3.8 Bioreactors for Corneal Tissue Model

In addition to substrate stiffness and chemical cues, the native dynamics around cornea including air-liquid interface, IOP and TF have not been fully mimicked. Multiple studies have illustrated

the importance of air-liquid interface in epithelium formation and differentiation [152-154]. Up to now, transwell cell culture is the main method for ALIC. However, cultivation of a thick tissue model is difficult in transwells due to the limited nutrient diffusion through pores on the transwell membrane. An alternative way of culturing thick tissues is to support sustained cell growth in a 3D scaffold.

As an important mechanical cue for corneal thickness and curvature, IOP (10-20 mmHg) needs to be mimicked through a pressure generating device. The Flexcell system is an air-driven device that has been used in many studies to apply tension on cells [155-157]. In the Flexcell system (Figure 5A), cells are seeded on a polydimethylsiloxane (PDMS) membrane which is connected to a sealed air chamber. By changing the air volume in the chamber with a pump, the cells can be stimulated with tension. Cultivated corneal stromal fibroblasts seeded in Flexcell plates expressed upregulated α-smooth muscle actin under tension [158]. Nonetheless, native IOP is generated by aqueous humour in anterior chamber, thus, air-driven pressure is not ideal for mimicking IOP.

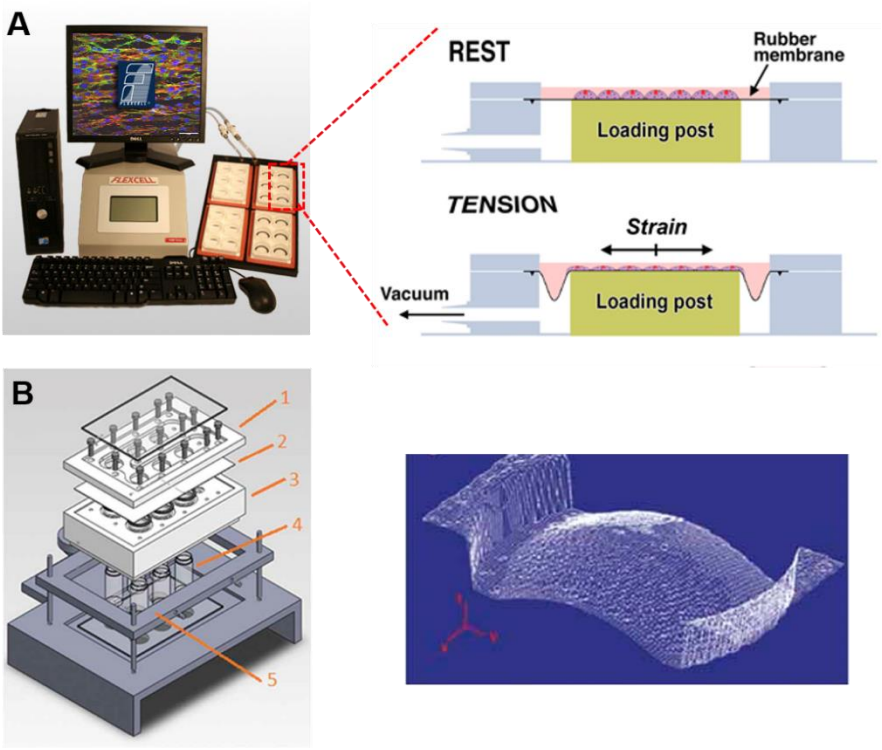

Figure 5. *Bioreactors used to mimic IOP. A: Flexcell system to apply tension to cells cultured on the rubber membrane[2]. B: A custom designed air driven bioreactor that created a curved surface mimicking IOP[7].*

Meanwhile, TF which provides nutrients for the cornea should be included in bioreactor designs for corneal tissue models. There has not yet been a bioreactor that can mimic the air-liquid interface, TF and IOP in one system. To do this, a liquid sealed chamber, a robust corneal tissue model, and tear flow mimicking accessories are needed. Much inspiration for this can be taken from the clinic. An artificial anterior chamber is used to inflate donor cornea with medium during the preparation for transplantation [159]. Though this chamber cannot provide persistent pressure, with optimization of sealing, this device can serve as *in vitro* bioreactor for generating IOP.

Taken together, silk protein can provide a robust scaffold supporting long-term dynamic culture and be decorated with growth factors to guide cell growth. Such scaffolds can be designed to

mimic corneal anatomy and seeded with corneal cells and neurons. A clinically used artificial anterior chamber can mimic IOP, but has not been utilized for *in vitro* bioreactor designs until now. Combining physiologically relevant cells, scaffolds, and a cultivation system, a functional corneal *in vitro* model can be achieved.

Chapter II. Two-Dimensional Tissue Model of Innervated Corneal Stroma

I. Introduction

In order to establish the silk-based corneal tissue model, a 2 D co-culture needs to be established first to optimize the medium components, material, seeding density and timing for co-culture. In this chapter, an *in vitro* silk protein-based co-culture system was developed to assess hCSSCs and DRG neuron interplay, with the goal of gaining a further understanding of the interactions between corneal stromal tissue and neuronal regeneration. The co-culture system was designed to closely mimic the anatomy of human corneal tissue, with thin silk films acting as the corneal stromal layer, and silk-collagen hydrogels containing DRG neurons resembling the surrounding corneal limbus tissue. BDNF and collagen I secretion from hCSSCs was observed and provided evidence that corneal stroma can improve neuronal innervation. Also, we explored silk-collagen mixture hydrogel as the scaffolding material for neuron culture. Collagen is rich in cell adhesion sites that supports neurons attachment and outgrowth[160], while silk provides a more mechanically robust matrix[140]. Together these proteins provide a tunable system to stimulate neuron outgrowth.

II. Materials and Methods

2.1 Preparation of Silk Solution

Silk solution was prepared from cocoons of Bombyx mori silkworm based on the procedures developed in our previous studies[133, 161, 162].Silk cocoons were supplied by Tajima Shoji Co. Yokohama, Japan) and boiled for 30 or 45 min in 0.02M Na2CO3 solution (Sigma-Aldrich. St Louis, MO). The boiled silk fibroin was rinsed with deionized water three

times and dried overnight. The extracted silk was then dissolved in a 9.3M LiBr solution and dialyzed against distilledwater for 2 days to obtain a silk fibroin aqueous solution (5–7% w/v).

2.2 Preparation of Silk Films

Patterned porous silk films were prepared using the procedure developed in our previous studies[163]. Silicone elastomer (PDMS; Corning, Midland, MI) was cast on optical dispersion angle grating (Edmund Optics, Great Barrington, NJ). The PDMS was cured at 60 C for 1 h, and then peeled off from the grating, and rinsed in 70% EtOH followed by Milli-Q water. A 1% w/v silk solution with 0.035% w/v of polyethylene oxide (PEO) was prepared and cast on the patterned PDMS mold and dried overnight. The film was annealed in a water filled desiccators at 220 mmHg for 2.5 h and then peeled off from the mold using our established methods[133]. The silk films were immersed in water for 2 days to extract the PEO and generate the pores.

2.3 RGD Surface Modification

RGD functionalized silk films were made using methods from our previous works[163, 164]. The silk films were presoaked in MES buffer (Thermofisher) for 30 min. A 1-ethyl-3-(dimethylaminopropyl) carbodiimide hydrochloride (EDC)/Nhydroxysuccinimide (NHS) solution (0.5 mg/mL of EDC and 0.7 mg/mL of NHS in MES buffer, pH 6.5) was reacted with the carboxyl groups from the aspartic and glutamic acid residues in the silk for 30 min at room temperature. These activated silk films were then washed with MES buffer two times and subsequently treated in 1 mg/mL Arg-Gly-Asp (RGD) solution (Bachem, Torrance, CA) for 2 hours.

2.4 Preparation of Silk Collagen Hydrogels

Collagen gels were prepared by adding 30 μL of 10X DMEM (GIBCO, Life Technology, Grand Island, NY) to 270 μL (4 mg/mL) acetic acid-type I collagen solution (rat-tail tendon, BD, Franklin Lake, NJ), followed by neutralization with 1M NaOH (Sigma). A 45 min boiled silk solution (2% w/v) was mixed with 10XDMEM (GIBCO) with ratio of 9 to 1, and then sonicated with a Digital Sonifier (Branson Ultrasonics, Danbury, CT) at 20% amplitude for 20 s to generate silk hydrogels using our establish protocols[140]. The sonicated silk was mixed with neutralized collagen solution at ratios (v/v) of 1 to 2 and 2 to 1, we refer as 1/2 hydrogel and 2/ 1 hydrogel, respectively.

2.5 Human Corneal Stromal Stem Cell Cultivation

HCSSCs were isolated from collagenase digestion of limbal stromal tissue of human corneas unsuitable for transplant. The cornea tissue was obtained from the Center for Organ Recovery and Education (Pittsburgh, PA)[162]. HCSSCs were passaged six times before seeding. Cells were detached with 0.25% trypsin (GIBCO) solution and seeded on the surface of the sterilized patterned porous silk film with concentration of 15,000 cells/cm^2. Cell seeding was accomplished by adding cell suspension dropwise on top of the film. The films were incubated for 30 min to allow time for cell attachment. Seeded silk films were cultured in proliferation medium containing DMEM/MCDB-201 in the ratio of 3 to 2(v/v) with 2% fetal bovine serum, 10 ng/mL platelet-derived growth factor, 1 mg/mL lipid-rich bovine serum albumin (Albumax, Life Technologies, Grand Island, NY), 10 ng/mL epidermal growth factor,5 mg/mL transferrin, 5 ng/mL selenous acid (ITS), 0.1 mM ascorbic acid-2-phosphate, 1028 M dexamethasone, 100 IU/ mL penicillin, 100 mg/mL streptomycin, 50 mg/mL gentamicin, and 100 ng/mL cholera toxin until confluent (~2 days).21 After hCSSCs confluence, silk films were cut into circular shapes

with a 12 mm diameter biopsy punch (McMaster-Carr, Robbinsville, NJ) and anchored in 24 well tissue culture plates (TCPs) with 8 mm diameter Teflon rings (McMaster-Carr). HCSSCs were differentiated on the silk films into keratocytes with differentiation medium using advanced DMEM (Life Technologies), containing 1.0 mM L-ascorbic acid-2-phosphate (Sigma-Aldrich, StLouis, MO), 50 ng/mL gentamicin (Life Technologies), 2 mM L-alanyl-L-glutamine (Life Technologies), 100 ng/mL penicillin, 100 ng/mL streptomycin (Mediatech, Manassas, VA) 0.1 ng/mL transforming growth factor-beta3 (TGF-B3,Sigma-Aldrich), and 10 ng/mL basic fibroblast growth factor (FGF-2, Sigma-Aldrich)[136]. HCSSCs were also differentiated on 24 well TCP for collagen staining and 6 well TCP for ELISA assays for neurotrophin secretion. HCSSCs were seeded with a concentration of 15,000 cell/cm2 and cultured for 14 and 22 days for collagen staining and ELISA experiments respectively.

2.6 DRG Neuron Culture in Hydrogels

DRG neurons were dissociated from DRG from chicken embryos (University of Connecticut, Poultry Farm, CT). The dissection and dissociation followed the protocol developed in our prior study[140]. Briefly, ganglia were trypsinized for 25 min and then centrifuged for 5 min at 1500 rpm. The pellets were triturated for 3 rounds, 12 times for each round. The dissociated neurons were transferred to 100 X 200 mm^2 TCPs and incubated for 4min, with neurons having less tendencies to attach to the bottom compared with other types of cells. The suspension was collected and centrifuged to isolate the neurons. All samples were seeded with 100,000 cells/mL. DRG neurons were cultivated in DRG growth medium prepared from DMEM/F12 medium supplemented with FBS (10%) and NGF (50 ng/mL, R&D Systems, Minneapolis, MN) for 7 days.

2.7 Co-Culture of Differentiated HCSSCs with DRG

Co-culture was processed on the film-hydrogel system, TCP, and transwell for cell morphology analysis and metabolism activity assays. Co-cultivation on film-hydrogel system was started by culturing hCSSCs on silk films for two weeks prior to initiating co-culture. The DRG neurons were incorporated into 300 μL of 1/2 hydrogel with 100,000 cells/mL. The hydrogels were then added gently around the silk film (Figure 6A). The samples were then incubated for 30 min to achieve gelation. A TCP co-culture group in which hCSSCs have direct contact with DRG neurons, and a transwell co-culture group where hCSSCs and DRG neurons were separated but

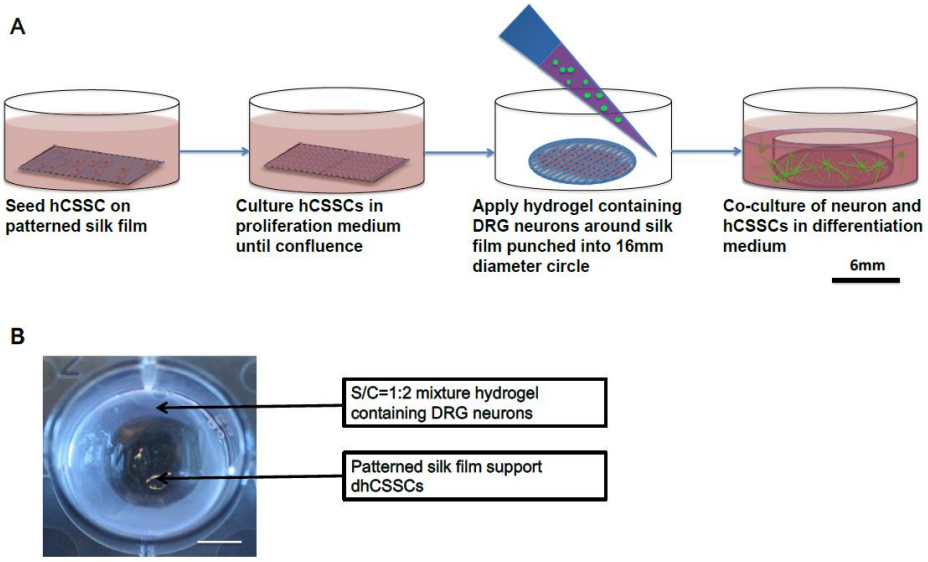

Figure 6*. Preparation of 2D co-culture scaffold of hCSSCs and DRG neurons. A: Human corneal stromal stem cells (hCSSCs) were seeded on the patterned silk films with a density of 15,000/cm2 and cultivated in proliferation medium to reach confluence. Differentiation of corneal stromal stem cell was then initiated to achieve differentiated hCSSCs. Silk films were cut into 12 mm diameter disks before co-culture. A silk-collagen mix hydrogel containing DRG neurons was applied around the silk film. The co-culture system was cultivated in hCSSC differentiation medium. B: Picture of co-culture system in 24 well TCP after 7 days of co-cultivation. The silk-collagen hydrogel retained its integrity after co-culture, the silk film remains anchored by the hydrogel after 7 days of cultivation. Scale bar = 6 mm.*

cultivated in the same system were also prepared. We refer to the groups as the TCP co-culture and transwell co-culture, respectively. The TCP co-culture group was prepared by seeding hCSSCs at 15,000 cell/cm^2 and DRG neurons at 30,000 cell/cm^2 in 24 wells TCP (Corning,

Corning, NY). The transwell co-culture group was prepared by seeding hCSSCs in the insert and DRG neurons in the well of 24 well polycarbonate membrane transwells (Corning, Corning, NY) with the same concentrations as in the TCP co-culture group. To analyze the uniqueness of hCSSCs co-culture impact on neurons, human corneal epithelial cells (hCECs) were also co-cultured with DRG neurons with the same seeding method and cell density on silk film and hydrogel systems. All co-cultures were maintained for 7 days in hCSSC differentiation medium with 50 ng/mL of NGF.

2.8 Cell Metabolic Activity

Cell metabolic activity was characterized using Alamar Blue (Invitrogen, Grand Island, NY) assay. Before the assay, the inserts from the transwell co-culture group were removed to separately analyze the two types of cells. Alamar blue dye was added to the medium at a ratio of 1–10 in both the TCP and transwell co-culture groups and incubated for 2 h. Fluorescence was measured with excitation and emission wavelengths of 530 and 590 nm, respectively.

2.9 Immunohistochemical Staining

Anti β-tubulin III staining was processed to observe neuronal extensions. Neurons cultivated in hydrogels were fixed on day7, while the co-cultured samples were fixed on day 1, 3, 5, and 7 in 4% paraformaldehyde in PBS (Affymetrix, Cleveland, OH) for 45 min. Samples were then treated with 0.03% Triton (Sigma) X-100 in PBS for 30 min. Anti β-tubulin III rabbit antibody (Sigma) was diluted 1:500 in 10% FBS/PBS solution, and applied on the samples. For quantifying collagen types I, V, VI secretion, hCSSCs cultured on TCP were fixed on days 3, 7, and 14. Anti-collagen types I, V, and VI antibodies (Abcam, Cambridge, MA) were diluted 1:200 in 10% FBS/ PBS solution and applied on samples. All samples were maintained at 4 °C

for 12 h and then washed 3 times, with soaking in PBS for 10 min each time. Anti-rabbit IgG-FITC antibody produced in goat (Sigma) was diluted 1:200 in 2% FBS/PBS solution and added to samples and incubated at 37 °C for 1 h. To observe hCSSCs in co-culture conditions, F-actin filaments were stained with Alexa Fluor VR 568 Phalloidin (Life Technologies). Phalloidin was diluted 1:20 in 10% FBS/PBS solution and incubated at the same time as anti-rabbit IgG-FITC antibody. Scaffolds without cells were also stained as negative controls. Immunostained samples were imaged using a fluorescence microscope (Leica DMIL, Buffalo Grove, IL) with FITC filter (513–556 nm) and Texas Red filter (604–644 nm).

2.10 Neural Axon Length Measurements

Positive staining of β-tubulin III was determined at 10X magnification for four regions on each sample of DRG neurons cultivated in hydrogels and co-cultured with hCSSCs or hCECs from n=6 samples from three independent experiments. All the images were then converted into 8-bit tiff files using Image J (NIH). The neuron J routine was applied to measure the axon length[165].

2.11 ECM Synthesis of hCSSCs

Images were collected at 10X magnification for four regions from each sample with anti-collagen type I, V, VI staining. using n=4 from three independent experiments. The integral pixel density was measured by Image J (NIH) for each image and normalized by dividing the cell number in the region.

2.12 HCSSCs Neurotrophin Secretion

To test hCSSCs ability to secrete neurotrophin and analyze their respective effects on neurons, ELISA experiments were performed against the medium in hCSSCs cultures. Briefly, hCSSCs were cultivated in 6 well TCP plate for 22 days and1 mL medium aliquots were collected every 3

days from each well. Media samples were then concentrated with Amicon Ultra 10K Filter Devices (Millipore, Merck KGaA, Darmstadt, Germany). ELISA assays for BDNF, GDNF, NT-3, NGF were processed with human BDNF, GDNF, NT-3, NGF Duo set (R&D system, Minneapolis, MN) with n53 from two independent experiments.

2.13 Statistical Analysis

All data analysis was performed with One-way ANOVA with Dunnett post hoc test. Significance level was set at $p<0.05$. All experiments were run in at least triplicates for two independent experiments.

III. Results and Discussion

3.1 Design of co-culture Scaffolds for DRGs and hCSSCs

The design of the co-culture system allowed for spatial confinement of the hCSSCs and DRGs while maintaining both cell types (Figure 6A). Silk-collagen hydrogels seeded with neurons were cast at the periphery of a silk film containing cultured hCSSCs. A silk-collagen hydrogel maintained DRG neuron viability while providing a suitable elastic modulus of 15 kPa for neuronal extension (Figure 6B) Porous patterned silk films functionalized with RGD supported the aligned growth of the hCSSCs as well as provided a transparent scaffold to mimic corneal tissue. The co-cultures were maintained for 1 week. During cultivation the silk films remained transparent and the hydrogels and scaffolds remained structurally stable (Figure 6B)

3.2 Optimization of Hydrogel Composition for DRG Neuronal Outgrowth

A silk-collagen hydrogel was chosen to support neuronal outgrowth. Collagen type I is a favorable substrate for many types of neurons[160, 166] while silk provided robust material to adjust the mechanical property of the hydrogel[140]. The optimal silk to collagen ratio for neuronal outgrowth was assessed. Silk alone, collagen alone, 1 to 2 silk-collagen hydrogel (1/2 hydrogel), and 2 to 1 silk-collagen hydrogel (2/1 hydrogel) were prepared. The concentration of silk and collagen in the 1/2 hydrogel was 6.67 and 2.67 mg/mL, respectively, and in the 2/1 hydrogel these values were 13.33 and 1.3 mg/mL, respectively. Within the silk hydrogel system (Figure 7A), there was limited neuronal extension with an average axon length of 30±14.8 μm after 7 days.

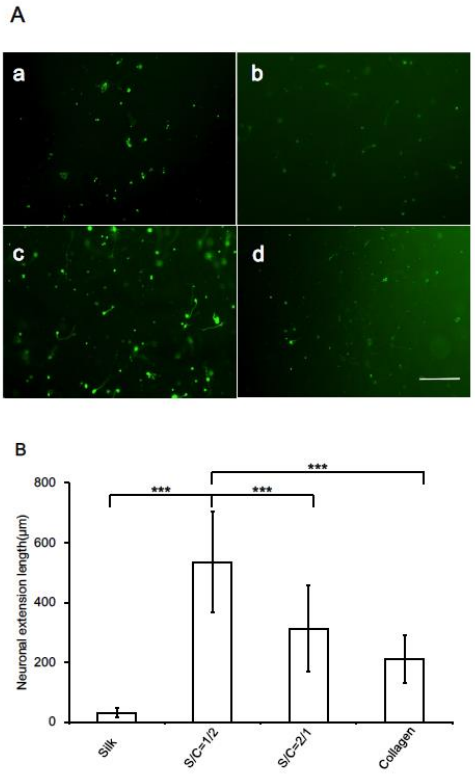

Figure 7. *DRG neuronal outgrowth in silk-collagen composite gels. A: Fluorescence images of DRG neuronal outgrowth in (immunostained with anti β-Tubulin III in green): (a) silk hydrogels, (b) silk/collagen = 2/1 (2/1) hydrogel, (c) silk/collagen = 1/2 (1/2) hydrogel, (d) collagen hydrogel. Images were taken on day 7 (Scale bar 100 μm). B: Quantification of neuronal extension length. 1/2 hydrogel gave statistically longer neuronal outgrowth than other hydrogels. N = 6 from three independent c cultures, respectively. ***p < 0.0001, one-way ANOVA with Dunnett post hoc test.*

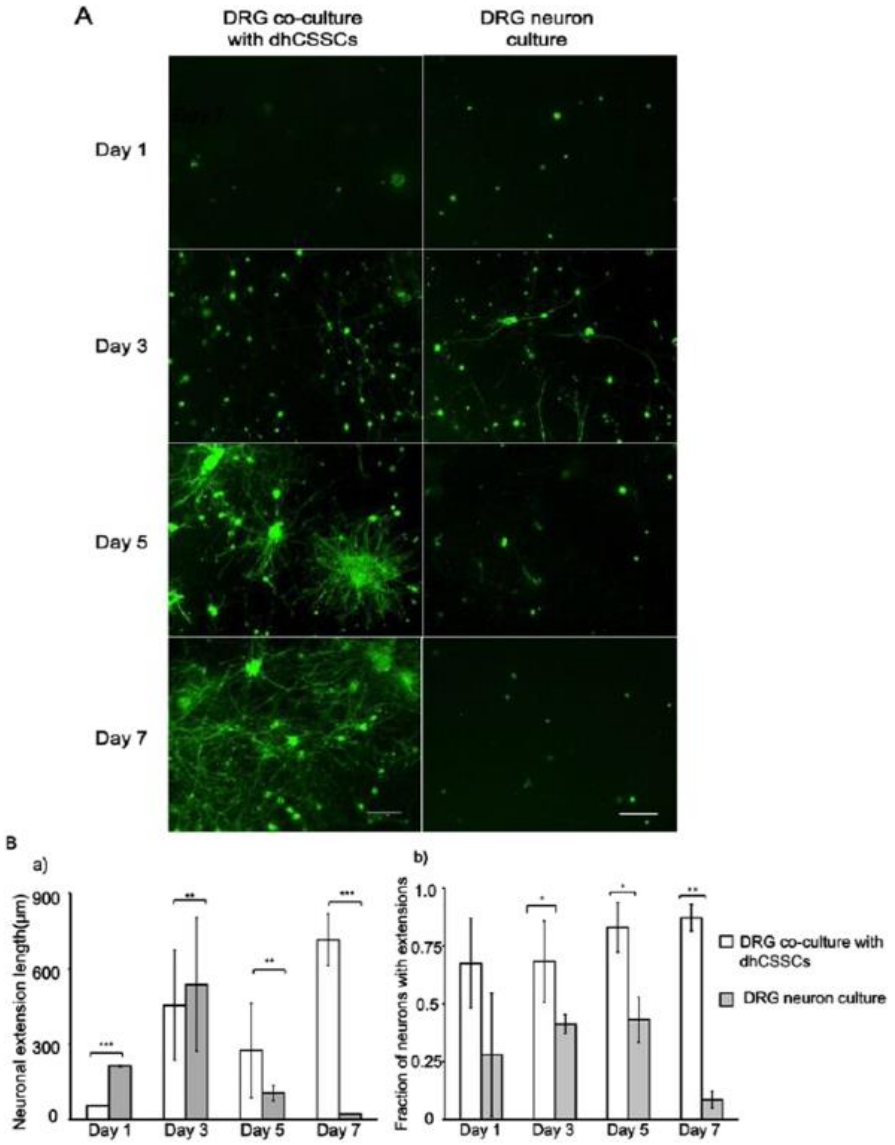

Figure 8. *DRG neuronal outgrowth in co-culture with hCSSCs and monocultures in 1/2 hydrogels. A: Representative fluorescence images of DRG neurons monoculture and co-cultured with hCSSCs. DRG neurons were immunostained with anti-β-Tubulin III in green on days 1, 3, 5, and 7 (Scale bars: 100 μm). (a) Quantification result indicated neuronal outgrowth during co-cultures with hCSSCs are statistically longer than monocultures on day 7. N = 3 from three independent cultures, respectively. **p < 0.001, *** p < 0.0001, one way ANOVA with Dunnett post hoc test. (b) Fraction of DRG neurons with extension in co-culture was statistical significantly more than DRG monocultures. N = 3 from three independent cultures, respectively. *** p < 0.0001 from one way ANOVA with Dunnett post hoc test.*

In comparison, within the collagen hydrogels, an increase in axon extensions was observed (210±78.6 μm), although axon morphology was thinner on the collagen hydrogels when

compared to the silk hydrogels. In the case of the composite hydrogels, the 1/2 hydrogel supported significantly longer axon extension compared with the other hydrogels with average axon length of 534±167.87 μm after 7 days, while 2/1 hydrogels supported an average 312±144.972 μm axon extensions. This study corroborated our previous work where silk hydrogels provided three times longer neuronal extension than collagen hydrogels[140]. Collagen concentration was reported previously to have an impact on neuronal extension with 1 mg/mL as the optimal concentration for axon extension[167]. However, the 1/2 hydrogel which contained 0.33 mg/mL of collagen provided longer axon length compare to the 2/1 hydrogel which contained 2.67 mg/mL of collagen. This result indicated that the silk fibroin provided some enhancement toward axon development. This may be due to primary (e.g., signaling) or secondary (mechanical, physical guidance) inputs. The results demonstrate that by varying the amount of silk relative to the collagen content in the hydrogels axon length could be tuned.

3.3 Effect of Co-culture on DRG Neuro Axon Extensions

The co-culture was maintained for 1 week and the results were compared with the DRG neuron cultured in 1/2 hydrogels alone. Staining for β-tubulin III showed that neurons co-cultured with hCSSCs have denser and longer axons, as well as increased cell aggregation, compared with neuron culture alone (Figure 8A). Quantification of neuronal extension showed comparable axon length in both co-culture and monoculture systems for the first 3 days (Figure 8B). However, from days 5 to 7 the DRG neurons co-cultured with hCSSCs reached an average length of 714 μm (±102 μm), 35 times longer than DRGs culture alone. The fraction of neurons with extensions (Figure 8B,b) was significantly higher in the co-culture group compared to the monoculture throughout the entire cultivation time. Long and dense neuronal extensions appeared on day 7 in the co-culture system (Figure 8A). The direct contact between hCSSCs and

DRG neurons were observed after 7 days of cultivation (Figure 8 A and B, Figure 10) indicating the system can be used to investigate the interactions between DRG and hCSSCs. To study the ability of hCSSCs to promote neuronal extension during co-culture, in comparison with another cell type, hCECs were also co-cultivated with DRG neurons using the same methods. In these co-cultures, there was no significant improvement in axon length or fraction of neurons with extensions compared with the DRGs when cultured alone (Figure 9). Even though the 2D co-culture of neurons with corneal epithelial cells was reported to provide longer neuronal extensions12 our results indicate that the neurons react differently in co-culture in scaffolds designed to mimic corneal anatomy. By co-culturing DRG neurons with hCSSCs, neuronal extension was significantly increased, illustrating co-cultivation of DRGs with other types of cell may provide a method for improving neuronal extension other than modifying scaffolding materials. To summarize, co-cultures of DRGs with hCSSCs grown on patterned porous silk films supported the growth of both types of cell and increased axon extension. The combined gel-film scaffold design allowed directed neuronal outgrowth from a peripheral seeding location toward hCSSCs cells, with neuron-cornea cell contacts observed.

3.4 Synthesis of Collagen I, V, VI of hCSSCs

To further study the impact of ECM on neuronal outgrowth, hCSSCs without permeabilization were stained to detect collagen I, V, VI secretion. These collagens have been detected from hCSSCs cultures[10, 164] but the effect of collagen secretion on neuronal outgrowth has not

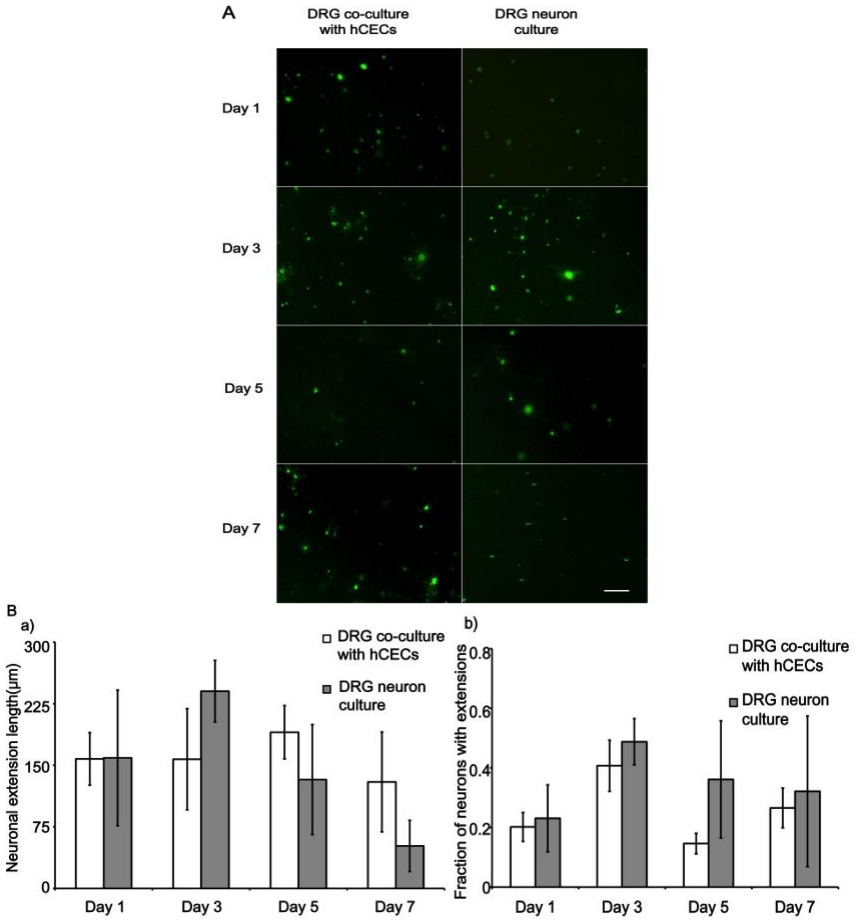

Figure 9. *DRG neuronal outgrowth in co-culture with hCECs and monocultures in ½ hydrogels. A: Representative fluorescence image of DRG neurons monoculture and co-cultured with hCECs. DRG neurons were immunostained with anti-β-Tubulin III in green on days 1, 3, 5, and 7 (Scale bars: 100 μm). (a) Quantification result indicated neuronal outgrowth during co-cultures with hCECs are statistically longer than monocultures on day 7. N = 3 from three independent cultures, respectively. **p < 0.001, *** p < 0.0001, one way ANOVA with Dunnett post hoc test. (b) Fraction of DRG neurons with extension in co-culture was not statistical significantly different from DRG monocultures. N = 3 from three independent cultures, respectively.*

been studied. The results indicated secretion of collagen types I, V, VI increased as time from days 3 to 14 (Figure 11A). Quantification of the relative increase showed that collagen type I, V,

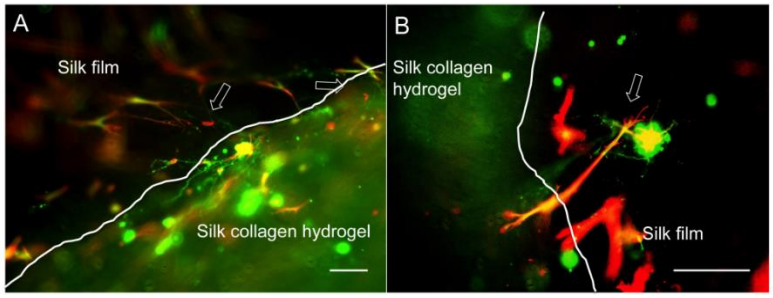

Figure 10. *DRG neuronal axons formed direct contact (indicated with arrows) with hCSSCs after 7 days of cultivation scale bars= 100µm.*

and VI production increased 100, 6, and 8-times from days 3 to 14, respectively. All 3 types of collagens were mainly located on the hCSSCs cell bodies on day 3, and were secreted into intercellular spaces on day 7 and 14. Collagen type I secretion was ~5-times that of collagen types V and VI on day14. Rat collagen type I was previously shown to promote neuronal outgrowth in culture[160], and may contribute to the increased neuronal outgrowth observed in the co-culture experiments. Conversely, collagen type V was found to inhibit axonal outgrowth by reducing cell adhesion[167, 168]. Collagen type VI was reported to affected Schwann cell differentiation, while its relationship with neuronal extension has not been reported[160]. Based on the known impact of collagen types I, V, VI to neurons[168, 169], the secretion of collagen type I from hCSSCs is one of the reasons that neurons achieved longer extension during co-cultivation with HCSSCs.

3.5 Neurotrophin Secretion from hCSSCs

Beside insoluble ECM molecules, BDNF, GDNF,NGF secreted from hCSSCs were quantified using ELISA. In order to improve accuracy, the medium collected from hCSSCs culture was

concentrated with a 10 K protein filter (Millipore, Billerica, MA). Among the four types of neurotrophins tested, only BDNF was found to be secreted from hCSSCs (Figure 12). The signals of GDNF, NT-3, and NGF from medium samples were not significantly higher than blank control, and lower than the detection range. RT-PCR study for corneal stromal tissue had previously detected mRNA expression of GDNF, NT-3, NGF, BDNF[121]. However, there was no protein assay for neurotrophin secretion of hCSSCs tested during *in vitro* culture. From ELISA result (Figure 12A), BDNF secreted from hCSSCs during the first week was ~0.3 and ~2.5 times higher than the second and third week. The concentration of neurotrophin for DRG viability and neuronal outgrowth improvement during *in vitro* cultivation is usually >1

ng/mL[170-172]. In this study, the accumulated secretion of BDNF over 22 days is only 80 pg/mL (Figure 11B). Thus, the BDNF secreted from hCSSCs during co-culture may have limited effect on the promotion of neuronal extension.

3.6 Cell Metabolism in TCP and Transwell Co-Cultures of hCSSCs and DRG Neurons

In this study, hCSSCs were found to promote neuronal outgrowth through ECM production and BDNF secretion. However, the separate contributions of soluble and insoluble factors remained unclear. To study this, cell metabolic activity was measured for co-cultures on TCP where cells

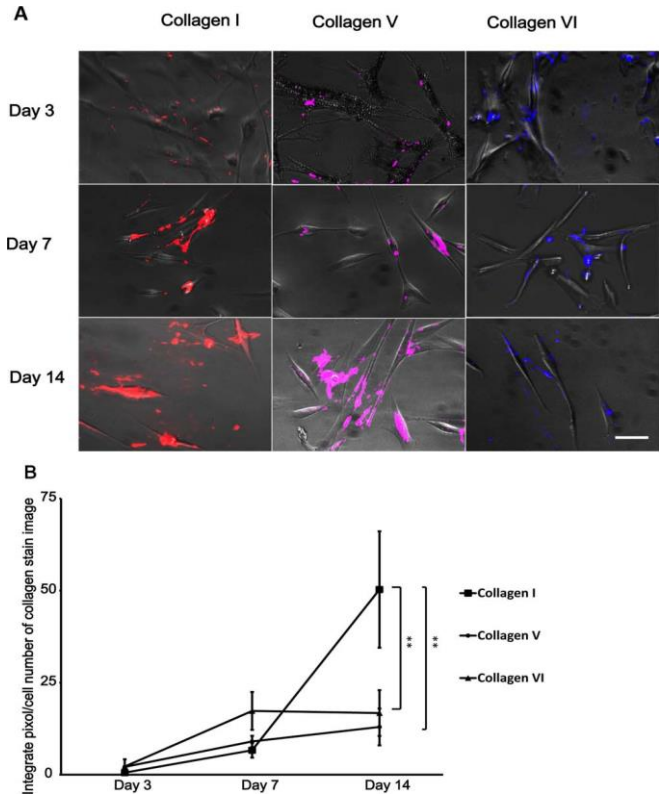

Figure 11. *Collagen types I, V, and VI secretion from hCSSCs. A: Fluorescence images of collagen types I, V, and VI immunostained in red, purple, and blue, respectively. Scale bars 50 μm. B: Quantification of fluorescence signals of collagen types I, V, VI on days 3, 7, 14, normalized against samples with no cells, showed secretion of collagen I was statistically significant higher than collagen type V and VI. n = 4 from three independent cultures, respectively. ** p < 0.001 from one-way ANOVA with Dunnett post hoc test.*

are exposed to both soluble and insoluble factors and compared to transwell co-culture groups where only soluble factors were available. Alamar blue results indicated that both types of co-cultures provided higher neuronal metabolism activity compared with the neuron monocultures (Figure 13A, B). In the transwell co-culture group (Figure 13A), however, the cell activity of neurons in co-culture was not statistically different to the monoculture, suggesting that soluble factor alone is not sufficient to promote neuronal viability. The activity of neurons in the TCP co-culture group was ~2times higher than TCP monoculture and ~2 times higher than the transwell co-culture group, after correction for the hCSSCs contribution (Figure 13B). This demonstrates that direct contact is necessary for hCSSCs to promote DRG neuronal extension with collagen secretion of hCSSCs playing an important role in promoting DRG neuronal extension. This is the first *in vitro* study to show the promotion of corneal

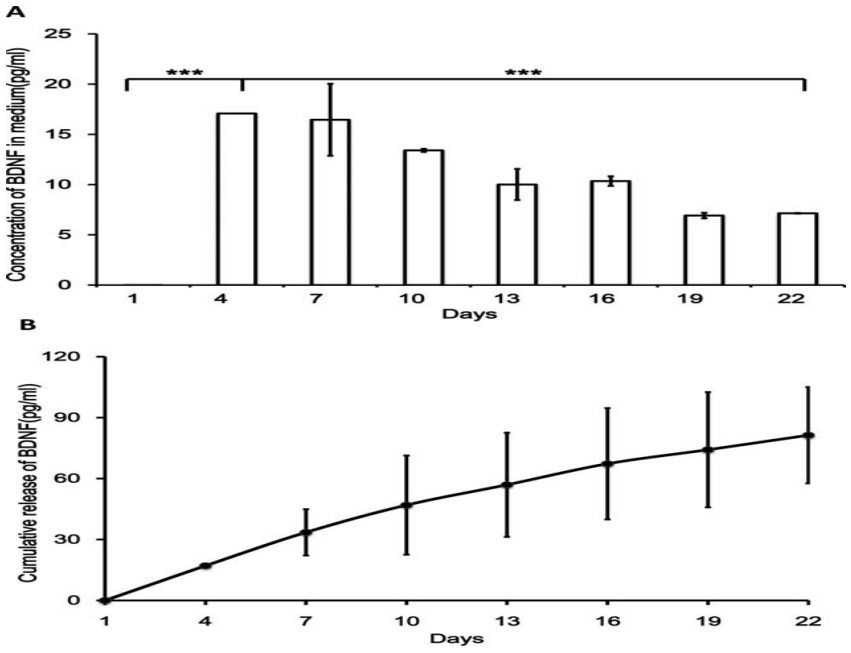

Figure 12*. ELISA assay for BDNF secretion from hCSSCs cultured on TCP. A: The concentration of BDNF in medium of hCSSCs culture from day 1 to day 22. Day 4 and 7 have the highest concentration, decreased on day 10, 13, 16, and remain on low level on day 19 and 22. B: The cumulative release of BDNF from day 1 to day 22. The cumulative release of BDNF reached 90 pg/mL after 22 days of culture. N = 3 from two independent culture, respectively. *** p < 0.0001 from one way ANOVA with Dunnett post hoc test.*

stromal cells effect on neuronal extension. Beside corneal stromal cells, co-cultivation of neuronal cells with other cell types has been previously reported to improve neuronal extension. Mesenchymal stem cells (MSCs) increased axon elongation by secreting BDNF and b-NGF, which contribute to neuron survival and regeneration[173]. Neural stem and precursor cells were also found to improve neuronal regeneration and survival through the secretion of fibronectin, laminin, and neurotrophins [174]. Furthermore, astrocytes and microglia were found to protect metabolically impaired neurons[175, 176]. The 2D co-culture of neurons with Schwann cells and corneal epithelial cell also provided longer neuronal extension[177, 178]. Although media

supplementation with neurotrophins such as NGF, GDNF, BDNF, and NT-3, can lead to longer neuronal extension[176, 179] data shown from this study indicate that ECM components also play an important role in promoting neuron development. Similarly, co-cultivation of neurons

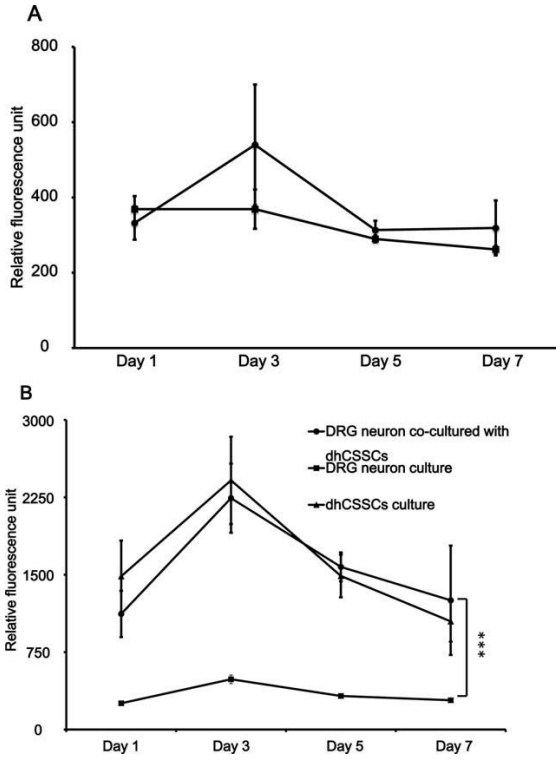

Figure 13*. Cell metabolism activity of DRG neurons co-cultured with hCSSCs and monocultures in 1/2 hydrogel. Fluorescence intensity from Alamar blue assay was normalized against day 0. A: Transwell TCP co-cultures showed higher activity compared with DRG neuron monocultures on TCP. N = 6 from three independent cultures, respectively. B: TCP co-cultures revealed cell activity in DRG neurons co-cultured with hCSSCs and hCSSCs monocultures were statistically significantly higher than DRG neuron monocultures, n = 6 from three independent cultures, respectively. ***p < 0.0001 from one-way ANOVA with Dunnett post hoc test.*

with other types of cells might provide an improved understanding of mechanisms of nerve development and regeneration in different tissues.

IV. Conclusion

A co-culture system was established to enable both hCSSCs and DRG neurons to grow, organize, and interact in culture. Using a two-component gel/film system based on silk and collagen, the structure of the cornea could be mimicked *in vitro* allowing to study the interactions between hCSSCs and DRG neurons. The impact of hCSSCs on neuronal outgrowth was observed and co-cultures significantly increased neuronal extensions likely due to collagen type I expression by the hCSSCs. The medium and scaffold optimized in this chapter provided knowledge for 3D corneal model establishment.

Chapter III. NGF Bio-printing On Silk Films

I. Introduction

In chapter 2 the growth of neuronal innervation was improved by co-culturing with hCSSCs. However, the axons were mainly located in the collagen-silk hydrogel and did not innervate the films seeded with hCSSCs. Tools for patterning neurons to control their extension and directions on biomaterial substrates is needed. These tools are important for both fundamental insights into phenotypic behavior as well as towards potential clinical treatments for peripheral nerves and innervated tissues in general. Neuronal extension can be guided by topographic cues, neurotrophic factors and extracellular matrix (ECM) decorations, with variables of mechanical properties, concentration gradients and interfaces as key in the process[180-182].

In this chapter we reasoned that printing axonal growth promoting tracks onto silk protein scaffolds would provide initial insight into biomaterial design strategies for studying innervated tissue models. Silk has been used extensively in tissue models [183-187] due to its biodegradability, tunable mechanical properties, slow degradation profile to maintain good mass transfer, biocompatibility with cells and the absence of cell-specific epitopes that would incorrectly signal cells [183]. Compared with conventional biomaterial deposition methods, inkjet printing can handle various types of materials including cells [188, 189] and proteins [190] with consistency in terms of control of the deposition process [191]. Our goal was to study bio-printed growth-promoting regions directly onto silk films and evaluate neuronal guidance. Silk physical crosslinking provided a suitable strategy with acidified collagen printing solutions to cross-link NGF and type I collagen to silk and support neuronal guidance. The conditions

described provide a relatively simple and rapid method to print complex patterns. This method could be utilized toward the design of nerve guides for peripheral nerve trauma treatment and in the construction of innervated tissue models.

II. Material and Methods

2.1 NGF Printing on Silk Films

The protein ink was composed of 4 mg/ml collagen type I in 0.02N acetic acid (Corning, Corning, NY) containing 400 ng/ml recombinant rat β-NGF (R&D System, Minneapolis, MN). The width of each NGF printed line was ~60 μm. Five layers of this ink was deposited by a commercial piezoelectric based inkjet printer (Dimatix DMP 2800, Fujifilm, equipped with cartridges DMC-11610) with a custom waveform, which had an average firing voltage at 25V (Figure 14).

2.2 Hand-drawn Films

The NGF collagen ink formulation was also used to make hand-drawn patterned silk films. The purpose was to study the effect of printing precision on neuronal response. A 50 μm diameter needle was dipped in the ink and used to draw the radial pattern used for the bio-printed films.

2.3 Cultivation of DRG Neurons On Printed Silk Films

DRG neurons were dissected and dissociated with same method as previous chapter. The samples for live cell imaging were seeded with DRG neurons labeled by DiI stain (Thermo Fisher). The neurons seeded on silk films were incubated at 37°C to allow cell attachment. DRG growth medium containing DMEM F-12 medium (Thermo Fisher, Grand Island, NY) containing 10% FBS (Thermo Fisher), 25 ng/ml recombinant rat β-NGF (R &D system) , 100 μg/mL

penicillin, and 100 µg/mL streptomycin (Mediatech, Manassas, VA) was used to culture the DRGs for 7 days.

2.4 Co-culture of Human Corneal Epithelial Cell (hCECs) and DRGs

In order to test the effectiveness of nerve guidance in a co-culture environment, primary hCECs (Thermo Fisher) were seeded on the silk films at a density of 15,000/cm ^{2} together with the 15,000/cm^2 DRG neurons. The co-cultures were maintained for 7 days.

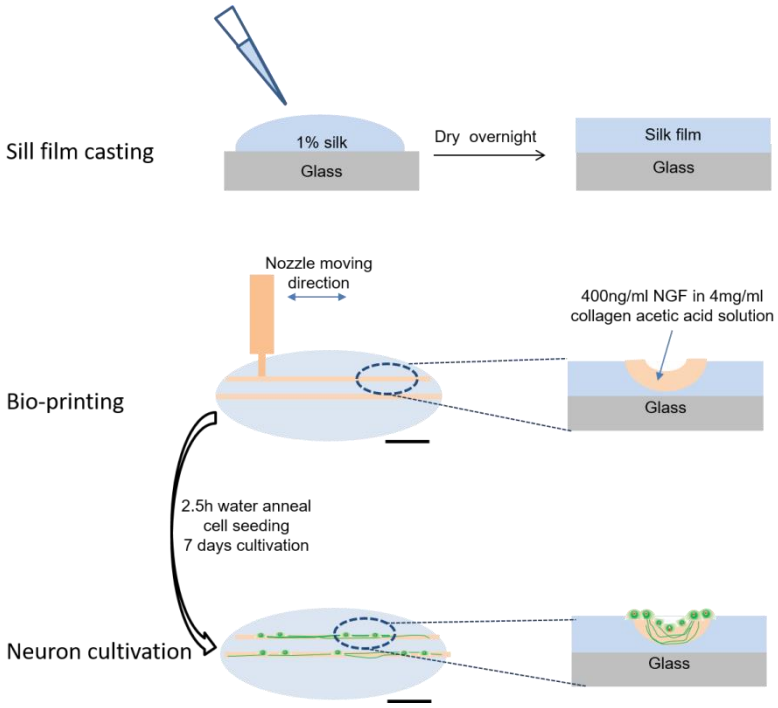

Figure 14. *Process of printing NGF and collagen on silk films: 1% silk solution was cast on 12mm diameter glass coverslips and dried overnight at room temperature on the bench top. Ink composed of 4 mg/ml collagen in 0.02N acetic acid containing 400 ng/ml NGF was printed on the surface of the silk films. The printed silk film was then water annealed for 2.5h and sterilized by exposure to UV for 30 min on both sides. The DRG neurons were seeded on the surface of the silk films and cultivated for 7 days to allow neuronal extension development. Scale bar = 3 mm.*

2.5 Atomic Force Microscopy (AFM) and Profilometry

Nano-indentation was performed in contact mode on a VEECO Dimension 3100 Atomic Force Microscope (Veeco Instruments Inc, Plainview, NY) to obtain mechanical profiles. The Young's

modulus (elastic modulus) for each sample was calculated by fitting the force-distance curves from the indentations with the Hertz model [192-194]. The protein networks obey rubber elasticity, and a Poisson ratio of 0.5 was used [193]. The spring constant of the AFM tips was in the range from 1 to 6 N m^{-1}, which was also confirmed by the thermal tune method. The half-opening angle of the cone was 25° according to the manufacturer's specifications. For each sample, at least 3 indentation points in different regions were measured and the average Young's modulus and standard deviation were determined. Topographic features were assessed using a stylus profilometer (Stylus XT) and pocket thickness gauge (Mitutoyo 7308, Aurora, IL, USA). The thickness was measured at 3 different spots on collagen-NGF printed region and on silk films.

2.6 Immunohistochemistry

Anti β-tubulin III staining was performed to observe neuronal extensions on the films. The neurons cultivated on the silk films were fixed at day 7 in 4% paraformaldehyde in PBS (Affymetrix, Cleveland, OH) for 20 min. Samples were then treated with 0.2% Triton (Sigma) X-100 in PBS for 30 min. Anti β-tubulin III rabbit antibody (Sigma) was diluted 1:500 in 5% BSA/PBS solution and applied on samples followed by incubation at 4°C overnight. The excess antibodies were removed by washing 3 times with PBS. Anti-rabbit IgG-FITC antibody produced in goat (Sigma) was diluted 1:200 in 5% BSA/PBS and added to samples before incubation at room temperature for 1 h. The samples were then washed 3 times with PBS before microscopy. Live cell images were collected on day 1, 3,5 and 7. All the images were collected using a fluorescence microscope (Leica DMIL, Buffalo Grove, IL) with FITC filter (513-556nm) and Texas Red filter (604-644nm). Angles between axons and printing direction were analyzed using ImageJ software (National Institute of Health, Bethesda, MD).

2.7 Axon Length and Angle Measurement

Positive staining of β tubulin III was determined at 4x magnification. The images were collected from *n=3* samples from 3 independent experiments. All the images were then converted into 8-bit tiff files using Image J (NIH). The neuron J routine [165] was then applied to measure axon length and angle.

2.8 NGF Release from Printed Silk Film

To quantify the release of NGF from the printed silk films, samples were incubated in DMEM at 37°C for 28 days with medium samples (1 mL) collected every 3 days. Enzyme linked immuno-sorbent assay (ELISA) using NGF Duo set (R&D system) was used to quantify the NGF.

2.9 Statistical analysis

All data analysis was performed with one way ANOVA with Dunnett *post hoc* test. Significance level was set at $p<0.05$. Data were collected from $n>3$ from 2 independent experiments.

III. Results

3.1 Topographic Assessment of NGF-collagen Printed Silk Films

Topographic assessments showed that printing NGF-collagen inks onto the pre-cast silk films resulted in grooves 60 µm wide and 0.5 µm deep (Figure 15A). AFM measurements of the film surfaces indicated that hydration with DMEM did not significantly vary the mechanical properties (Figure 15B) dry silk film: 0.2 GPa, hydrated silk film: 0.18 GPa). However, for the printed sites containing collagen depositions, the stiffness of collagen-ink after drying was 0.65GPa, which was significantly higher than the native silk films (0.2 GPa). After hydration

with DMEM, the stiffness of printed sites was 0.1± 0.04GPa, significantly decreased and softer than non-printed regions of the silk films.

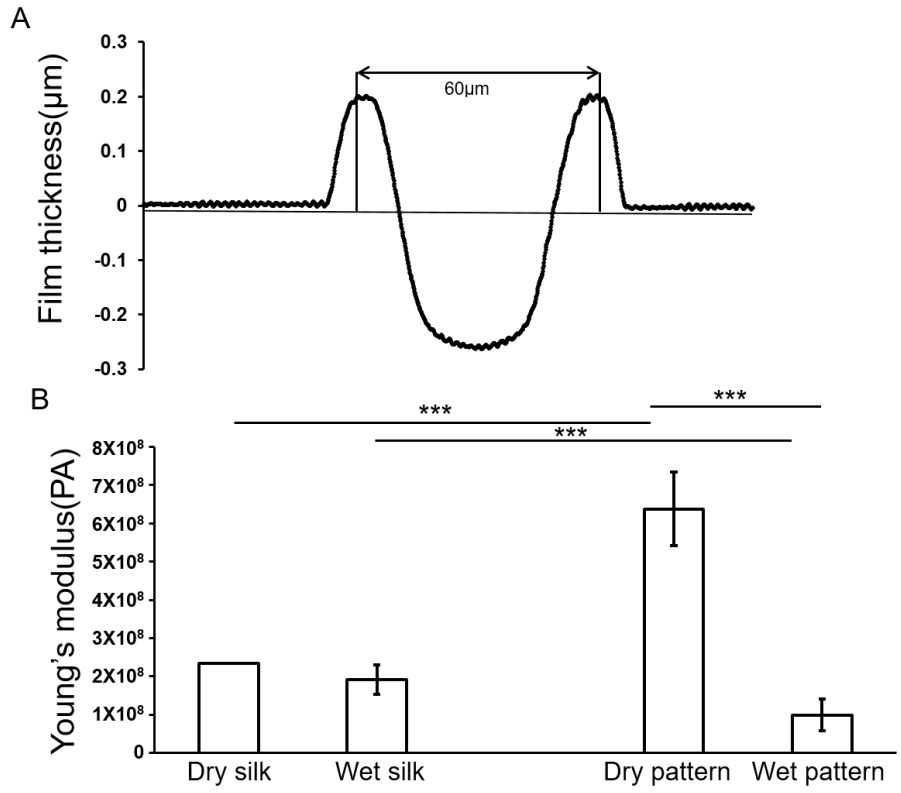

Figure 15*. Topography (A) and stiffness (B) of printed silk films. Profilometry indicated the printed site formed 60μm wide, 0.5μm depth grooves. When acidic solution hit the silk film surface the hydration and crosslinking process created a depression in the film at the printed site. The printed site was 3 times stiffer than silk films in the dry state and 1 time softer after hydration. The data was collected from n>3 from 2 independent experiments.*

3.2 DRG Neuronal Extensions Follow the Growth Factor Printed Pattern

After 7 days of cultivation, DRG neurons developed extensions on the surface of printed silk films and the majority of the axons were located on the printed regions. In the center of films, the axons had the highest density on printed regions compared to the other regions of the films (Figure 16). Less axons were observed on the hand-drawn silk films. The average axon length on

the printed silk film was 280 ±61 μm which is 4 times of hand drawn silk films (69 ±16 μm). The angle between the direction of axon growth and the direction that the nozzle of printer moved was 5.97 ±3.4 degrees. Whereas on the hand-drawn silk films the average angle was 97±36 degrees.

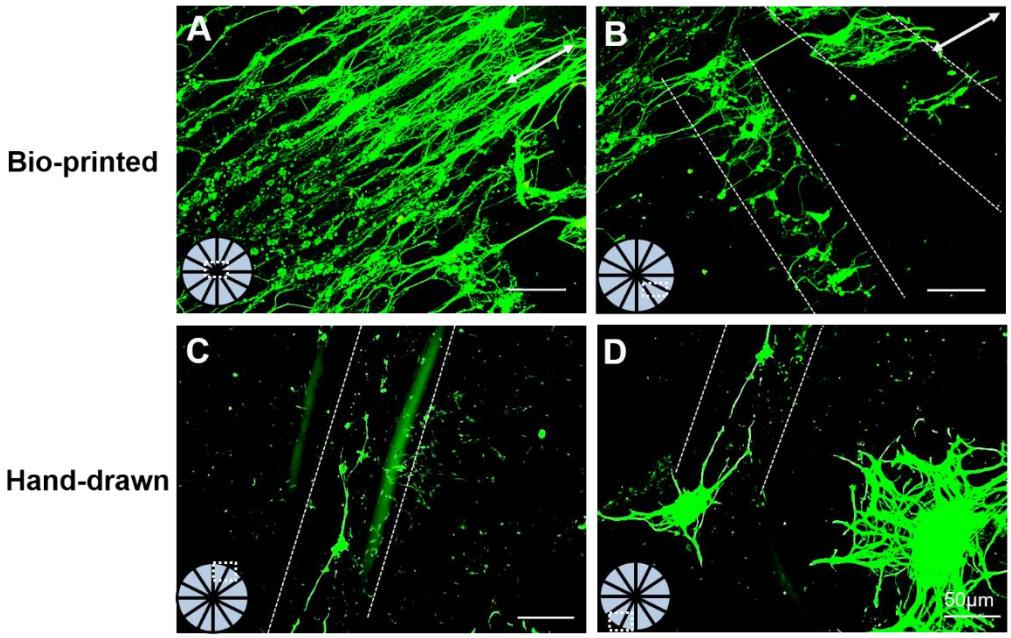

Figure 16. *Immunohistochemistry of DRG neurons cultivated on bio-printed and hand-drawn silk films for 7 days. The dash rectangles indicate the location of images on the silk films. The dash lines indicate the region being printed with ink. The white arrow represents the direction that the nozzle of printer moved. Rabbit anti-β III tubulin and FITC anti-rabbit produced in goat (Sigma) were used to visualize axons (green). Images were collected from n>3 from 2 independent experiments. Scale bars = 50μm.*

3.3 DiI Live Cell Labled Neuron Migrated Towards Printed Path

In order to study the attraction of neurons on the silk surfaces printed with NGF-collagen inks live cell imaging was processed (Figure 17). On the bioprinted silk films neurons were randomly located on day 1, with no extensions observed. On day 3 aggregation of neurons at the printed sites was observed, with short axons formed. On day 5, cell aggregation at the printed sites was more visible with the majority of neurons located on printed lines. By day 7, the majority of neuron clusters were located on printed lines, indicating that the neurons continued to migrate or

grow towards the printed lines over time. On the hand- drawn samples, the similar aggregation was observed with fewer axon extensions.

After 7 days of co-cultivation with hCECs the neurons developed extensions with the majority of these following the printed patterns on the silk films (Figure 18 A, B). The hCECs were randomly distributed on the silk films and did not appear to migrate or aggregate on the printed paths, unlike the neurons.

NGF release was quantified over a period of 28 d. For all measurements, the level of NGF detected was not significantly higher than the detection limit of the assay. These results indicated that the NGF was not released from the cross-linked bio-inks at a detectable level (15.6 pg/ml) and thus remained located with the inks during the cultivation period of study.

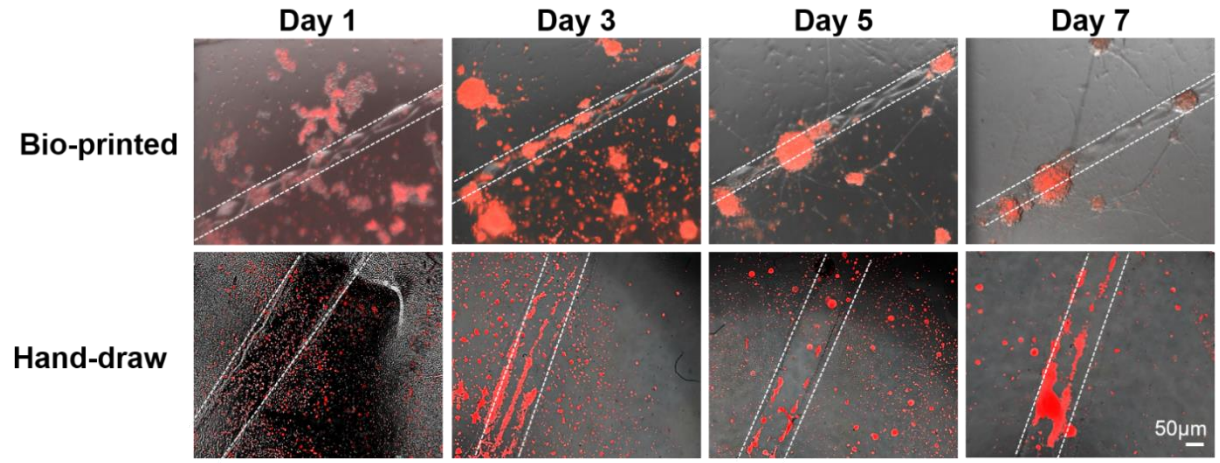

Figure 17. *Live cell imaging of DRG neurons cultivated on bio-printed and hand drawn silk films for 7 days. The neurons were labeled with DiI staining (red). The images were taken at the same location of the silk films on days 1,3,5,7. Aggregation of neuron towards the printed lines was observed on both types of films. Axons were visualized on the bio-printed silk film. Scale bars = 50µm*

IV. Discussion

Bio-printing has become a popular method to generate guidance cues for cells. The design of inks in this paper was focused on combining a favorable ECM protein (type I collagen) with a growth factor (NGF) to increase the efficiency of guidance for neuronal extensions. During the design optimization, acidic compositions were found to be able to achieve crosslinking of silk by

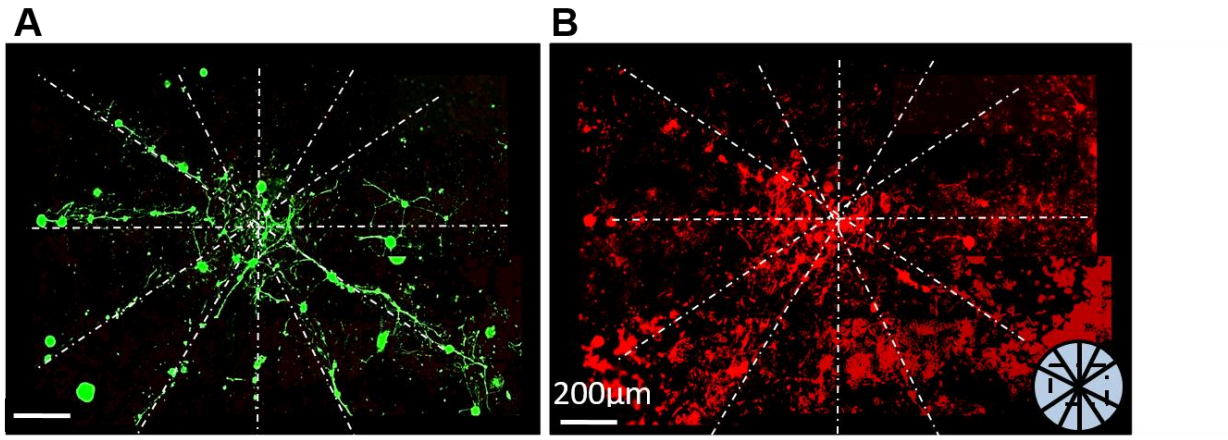

Figure 18. *Immunohistochemistry of DRGs (A) and hCECs (B) co-cultured on printed silk films for 7 days. βIII tubulin was stained (green) to show neuronal extensions while actin was stained (red) to reveal hCECs. A and B were imaged on the same location on the same film. White dash lines indicate the printed patterns on the silk films. The neuronal extensions (green) were guided by the printed patterns in co-culture conditions. HCECs (red) were randomly distributed on the surface of silk films and were not guided by the printed patterns. Scale bar = 200µm.*

trapping collagen and NGF during printing. Among the commonly used methods for surface decoration promoting neuronal extension, collagen was more stable in acid solution than laminin and poly-lysine [195, 196]. During the printing, the acidic collagen ink was physically entrapped in the crosslinked silk protein along with the NGF at the printed site. The procedure avoided the use of harsh NaOH often used in collagen crosslinking, while creating a non-soluble reservoir of growth factor and collagen where printed on the silk films.

According to the topography measurements, the printing procedure generated groove dimensions that were favorable for neuron guidance. The grooves were created by the hydration and

crosslinking process when acidic solution contacted the silk film. The stiffness indicated that the printed region was softer than elsewhere on the silk films upon hydration, perhaps supporting improved neuron response as well [140].The higher stiffness observed in the dry state on the printed sites is mainly due to the crosslinked silk protein. In the printing methods established in this study, the level of chemical guidance can be tuned through the concentration of collagen and NGF utilized in the process, while the mechanical guidance can be adjusted through the concentration of acetic acid and the amount of ink at the printed site. The width and depth of the grooves can also be modulated through the printing process based on the amount of ink deposited on the surface of film.

In order to provide continuous guidance for neuronal extension and innervation *in vitro* and *in vivo,* growth factors are required to be localized and at suitable concentrations. Here NGF was retained in the printed patterns through 28 days of incubation in DMEM at 37°C, suggesting utility for the approach for long term neuronal extension guidance. This is also supported by previous studies showing that NGF was able to be retained in silk protein based hydrogel and scaffolds [150, 197, 198].

With the live cell imaging and immunohistochemistry, neuronal extensions were observed to be mainly located on the printed sites. The neurons located originally on silk films and aggregated towards the printed paths through 7 days of cultivation, which indicated that the printed regions provided the required cutes and attraction for the neurons. The neurons mainly located on the printed pattern with axons extended following the direction of nozzle movement, suggesting that

in addition to the attraction effect created with the printed regions the direction that ink was sprayed on the silk film can also impact on the direction of axon growth.

In comparing the bio-printed and hand-drawn functionalized films, the bio-printed films provided longer neuronal extensions and stronger guidance of the axons. Also, the bio-printed silk films provided more precise width of the pattern. These features are crucial to the application of bio-printed silk film such as nerve guides.

In the human body the neuronal extensions are under the influence of the surrounding tissue environment, including other cell types that can influence fate and function. In this study, corneal epithelial cells were used as an example, as the corneal epithelium is the most innervated region in the human body with 600 nerve terminals/mm^2 [61, 64]. During co-cultivation with the hCECs, the neuronal extensions were mainly located on the printed paths while the hCECs remained randomly distributed on the silk films, confirming that the growth factor pattern had no effect on hCECs and *vice versa*. This result showed the potential of the silk film printing method for nerve guidance even under co-culture conditions or potentially in more complex *in vivo* environments.

V. Conclusions

A strategy for printing inks with growth factors and matrix molecules was developed to provide nerve growth promoting tracks on a biodegradable protein material for neuronal extension guidance. Growth factor printed silk films were advantageous in combining chemical and mechanical guidance for neurons. DRG neurons cultured on these films were attracted to the printed patterns with axons directed by the printing direction. The patterned axon outgrowth was

achieved in the presence of other cell types, enabling complex co-culture systems to be considered with this method. These collagen, growth factor printed silk films can be beneficial for generating nerve guides and innervated tissue models.

Chapter IV. Three Dimensional Tissue Model of Neuronal Innervated Cornea

I. Introduction

To further mimic the thickness, cellular components, and morphology of neuronal innervation in the native cornea, a 3D silk protein based co-culture system including the corneal stromal layer, epithelial layer, and DRG neurons, to further understand the interactions between corneal innervation and corneal tissues. The scaffold design was to closely mimic corneal anatomy, with silk film stacks for corneal epithelial and stromal cell growth surrounded by a silk sponge seeded with the DRG simulating the limbus tissue. The guidance for neuronal extensions was generated by the addition of NGF in the epithelial layer scaffold. An air-liquid interface was also designed for a bioreactor support system to house the corneal tissues and to better mimic the native corneal environment. This new corneal tissue construct supported dense innervation in the epithelial and stromal regions as well as sustained cultivation *in vitro*, critical outcomes for the system utility toward the further study of corneal development, function and dysfunction.

II. Material and Methods

2.1 Preparation of NGF, HGF, KGF, Collagen Stamped Silk Film

Flat, optically clear, porous silk films were prepared by casting 120 μL of 1% w/v silk solution with 0.05% w/v of polyethylene oxide (PEO, MW = 900,000, Sigma–Aldrich) on a 12 mm diameter glass coverslip (Electron Microscopy Science, Hatfield, PA) [186]. The films were then dried overnight. High and low concentration NGF inks were used for stamping the silk films. The inks were composed of 50 μl (4 mg/mL) acetic acid-type I collagen solution (rat-tail tendon, BD, Franklin Lake, NJ) containing 100 ng/ml keratinocyte growth factor (KGF) (Sigma), 100 ng/ml hepatic growth factor (HGF) (Sigma), 200 ng /ml epithelium growth factor (EGF)

(Thermo Fisher, Waltham MA), and either a high concentration of NGF (400 ng/ml) or a low concentration of NGF (200 ng/ml) (R&D Systems, Minneapolis, MN). Multi-circular, radial and uniform stamp patterns were employed (Figure 20). The multi-circular stamps were formed by dipping a 12 mm outside diameter and a 6 mm inside diameter donut shape polydimethylsiloxane (PDMS) (Fisher Scientific Co. Fair Lawn, NJ) stamp in the low NGF ink and pressing onto the dried silk film. The center was stamped with a 6 mm PDMS cylinder carrying the high concentration NGF ink. The radial pattern was stamped with the high NGF ink with its shape indicated in Figure 20. The whole surface of the uniformly stamped silk film was covered with high NGF ink. The silk films were annealed in water filled desiccators at -25 mmHg for 2.5 h for physical cross-linking. Before use, the silk films were exposed to UV light for 30 min on each side and the soaked in DI water for 48 h to extract any residual PEO to form the pores.

2.2 Preparation of Silk Sponges

Salt leached silk scaffolds with 500-600 μm pores were prepared using our previously reported procedure [199]. The scaffolds were mounted in a custom designed well fabricated to be 1 mm depth depressed into a Delrin sheet (McMaster-Carr, Robbinsville, NJ). The scaffold was sliced into 1 mm thick layers using microtome blade and cut into donut shapes (15 mm outer diameter, 12 mm inner diameter) with a biopsy punch (McMaster-Carr, Robbinsville, NJ). The silk sponge donuts were sterilized by autoclave before cell seeding.

2.3 Human Corneal Epithelial Cell Culture

Primary hCECs (C0185C, Thermo Fisher) were passaged 5 times before seeding. Cells were detached with 0.25% trypsin (GIBCO) and seeded on top of sterilized stamped silk

films at a density of 150,000 cells/cm^2. The films were then incubated for 4 hours to allow time for cell attachment and then cultured in keratinocyte SFM medium (Thermo Fisher) for 2 days to reach confluency.

2.4 Co-culture of hCSSCs hCECs and Neurons

The scaffolds for co-culture were designed to mimic corneal anatomy (Figure 19). For convenience, E, S, D and N will be used to represent hCECs, hCSSCs, DRG neurons and human neuron respectively. To prepare the co-culture scaffolds, 3 layers of patterned silk films seeded

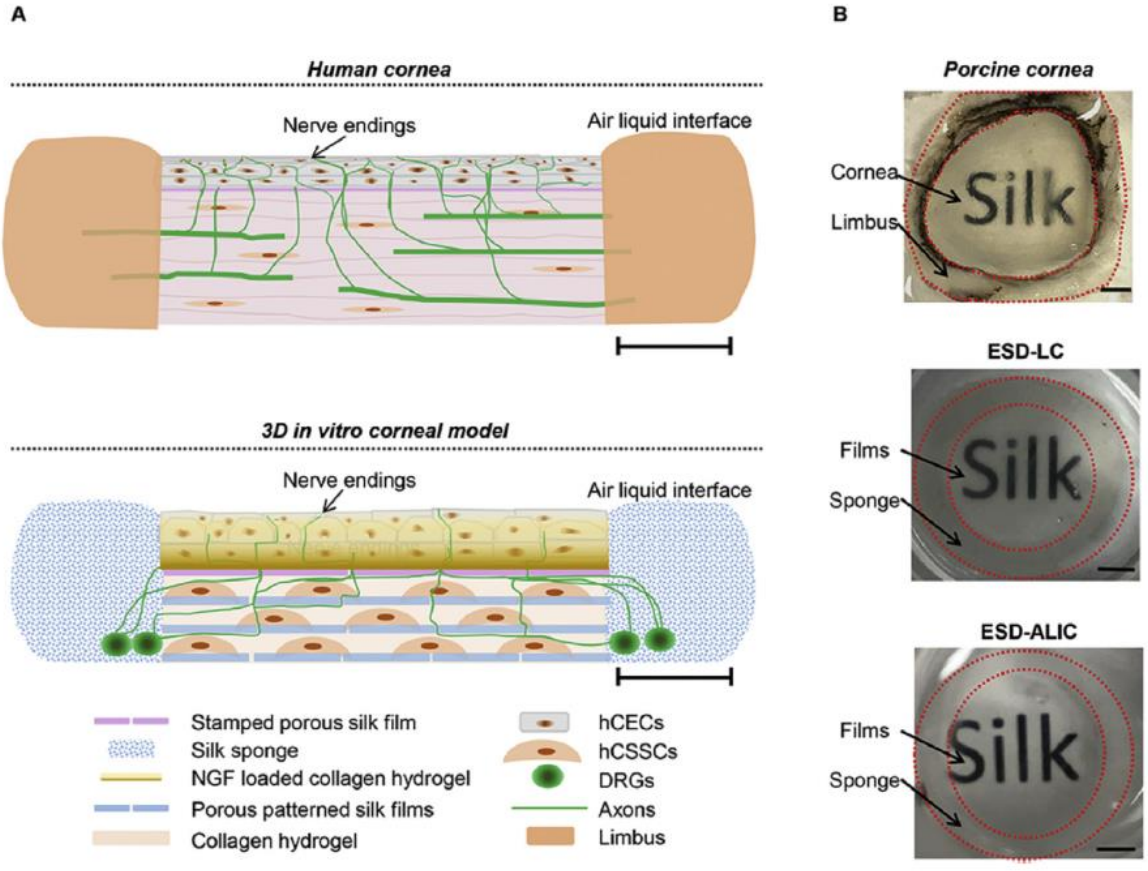

Figure 19. *Schematic and pictures of 3D corneal tissue model. A) Side view schematics of human cornea and in vitro 3D corneal tissue model. Scale bars=3 mm. B) Pictures of porcine cornea, day 28 co-culture of hCECs, hCSSCs and DRG explants in liquid (ESD-LC) and day 28 co-culture at air-liquid interface (ESD-ALIC) soaked in glycerol. Scale bars= 3 mm.*

with S were stacked with their patterns in a crisscross pattern. Then, the silk film stacks were cut to 12 mm diameter with a biopsy punch (McMaster-Carr) and transferred to the center of the silk sponge donuts. The flat silk films seeded with E were then transferred with forceps and gently placed on top of the film stacks. To achieve integrity of the scaffold, 500 µl type I rat tail collagen was casted on top and absorbed into the scaffold. In order to guide axons toward the top of the scaffolds, 50 µl of collagen hydrogel containing 400 ng/ml of NGF was cast on top of the film stack. The scaffolds were then incubated at 37^0C for 30 min to complete the crosslinking. After this, the whole scaffold was immersed in hCSSCs differentiation medium and cultivated for 2 days. A customized designed waffle-shaped PDMS floating shelf (5 mm thick, 5 cm diameter, with 16 X 1 mm^2 holes) was prepared by casting PDMS on top of Delrin ® molds (McMaster-Carr). This PDMS shelf allowed the top of the scaffold to remain at the air-liquid interface (ALIC) while the bottom was immersed in hCSSCs differentiation medium. The cultivation in liquid (LC) and air-liquid interface (ALIC) lasted 28 days. The co-cultures of E and D (ED-LC and ED-ALIC), S and D (SD-LC and SD-ALIC), and single cultures (E-LC, E-ALIC, S-LC, S-ALIC, D-LC, D-ALIC), were also processed as comparisons for the three cell types in tri-cultures (ESD-LC, ESD-ALIC). The scaffolds for two types of cell co-cultures and single cultures were prepared with the same methods as the ESD tri-cultures but only contained the respective cellular components.

2.5 Immunohistochemistry

The single cultured and co-cultured samples were fixed at days 14 and 28. Samples were fixed in 4% paraformaldehyde in PBS (Affymetrix, Cleveland, OH) for 45 min and then treated with 5% BSA for 30 min. Cellular morphology was revealed with anti β tubulin III staining. Keratocan was stained to reveal hCSSCs ECM secretion while involucrin was stained to reflect the maturity of hCECs. The dilution of antibodies is indicated in Table 2. The samples were treated with primary antibodies for 12 h at 4°C and then washed with PBS 3 times, 15 min each. The samples were stained with secondary antibodies for 8 h at 4°C and washed with PBS 3 times, 15 min each. DAPI was diluted 1:1000 in 5% BSA solution at the same time as the primary antibodies. Images were taken on a BZX-700 microscope (Keyence Corporation, Itasca, IL) at 10X and 4X. Maximum intensity projection images were generated using Advanced 3D Analysis software (Keyence Corporation, Itasca, IL). In order to compare transparency, the fixed samples for ESD-LC, ESD-ALIC and the porcine cornea were immersed in glycerol for 1h and placed over a paper with the word "SILK" printed. Photos were taken to indicate transparency.

Table 2. *Primary and secondary antibodies for immunostaining*

	Samples	Primary antibody dilution	Secondary antibody dilution
β tubulin III	ED,SD,ESD,E,S,D	Anti-β-tubulin III rabbit antibody 1:500 diluted in 5% BSA	Goat anti-rabbit IgG-FITC antibody(Sigma). 1:200 diluted in 5% BSA. Used donkey anti-rabbit IgG (FITC) (Abcam) when co-stained with keratocan 1:200 diluted in 5% BSA
Keratocan	SD,ESD,S	Anti-keratocan goat antibody 1:100 diluted in 5% BSA	Donkey anti –goat IgG, Alexa Fluor ® 568(Sigma), 1:200 diluted in 5% BSA
Involucrin	ED,ESD,E	Anti-involucrin mouse antibody 1:500 diluted in 5% BSA	Goat anti-mouse IgG H&L (TRITC) (Abcam), 1:200 diluted in 5% BSA

2.6 Q-PCR

Gene expression levels for keratocan (KERA), lumican (LUM), smooth muscle actin (ACTA2) aldehyde dehydrogenase 3A1 (ALDH3A1), involucrin (IVL), connexin 37 (GJA4), and cytokeratin 3 (KRT3) were quantified by RT-PCR (qPCR) [10, 136, 200]. In brief, total RNA was extracted using Trizol with single step acid-phenol guanidinium method [201], adsorbed onto a silica-gel membrane using the Qiagen RNeasy Kit protocol (Qiagen, Valencia, CA), eluted, and quantified [202]. The RNA extracted from the scaffolds was reverse transcribed to cDNA in a 20 µl reaction using high-capacity cDNA reverse transcription kit (Thermo Fisher). Quantitative RT-PCR of cDNA (~30 ng/µl) was performed using assays containing fluorescent hybridization probes (Taq Man: Thermo Fisher). Reactions were incubated at 95°C for 10 min and amplification was carried out on samples with 2 min incubation at 50°C, followed by 50 cycles of 15 seconds at 95°C and 1 min at 60°C. The reaction for RT-PCR was processed in a 15 µl solution containing 1X Universal PCR Master Mix (Thermo Fisher) with 6 µl cDNA samples. RNA expression at day 28 was compared to day0 samples using 18s as a reference gene.

2.7 Neuronal Extension Measurement

Positive staining of β tubulin III was determined at 4x magnification. The images were collected from $n=3$ samples from 3 independent experiments. All the stitched images were then converted into 8- bit tiff files using Image J (NIH). The neuron J routine [165] was then applied to measure axon length. The density of axons on 4X images was counted using Image J cell counter.

2.8 Statistical Analysis

Data analysis was performed using Student's T test. The significance level was set at $p<0.05$. All experiments were run in at least triplicates for two independent experiments.

III. Results

3.1 Guidance of Neuronal Innervation

After 14 days of cultivation, the uniformly stamped silk films provided higher axon density (112 ± 34 termini/mm^2) than multi-circular (26 ± 5 termini/mm^2) and radial stamped films (33 ± 8 termini/mm^2) (Figure 21). Thus, this strategy was selected to guide neuronal innervation towards the center of the scaffolds in the remaining studies. After 28 days of cultivation the axons were mostly located on the top surface of the scaffolds (Figure 21 A, B) indicating successful guidance of innervation. This guidance was also studied at the ALIC (Figure 21 C, D) where the top surface of scaffolds had twice the density of axons than in the LC. The length and density of axons reached an average of 3 ± 0.7 mm and 55 ±10.61 termini/mm^2 in the LC versus 4 ± 0.5 mm and 99 ± 13.5 termini/mm^2 in the ALIC. Thus, the combination of stamped silk films and NGF loaded collagen supported the effective guidance of neuronal innervation towards the top center of the scaffolds.

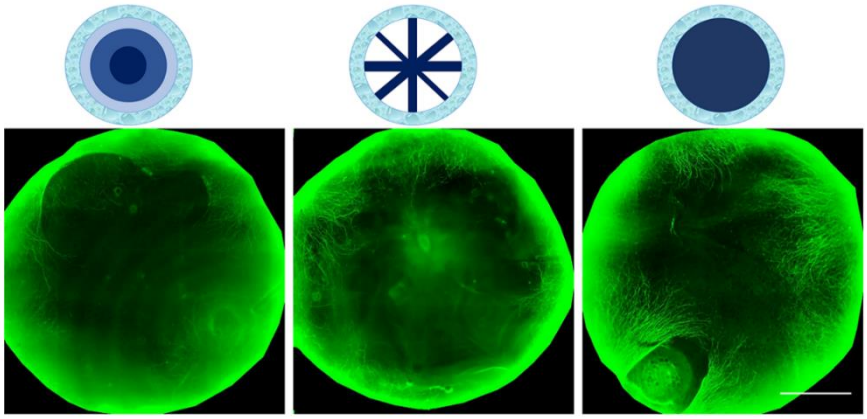

Figure 20. *IHC for axonal guidance on different stamped films. Immunohistochemistry staining of axonal guidance generated by multi-circular (left), radial (middle) and uniform (right) stamped patterns. β III tubulin was stained green. The uniform stamped patterns provided the strongest guidance and led to denser and longer innervation compared to the other two patterns. Images collected from n>3 from three independent experiments. Scale bar =3mm*

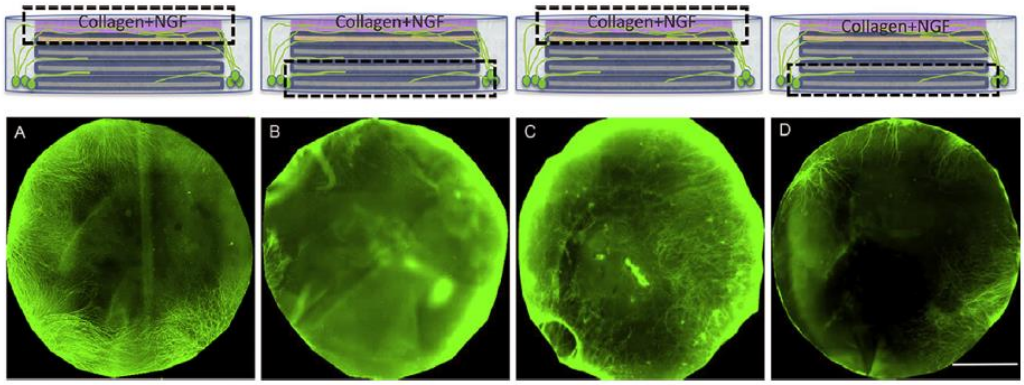

Figure 21. *IHC for neuronal extension guided towards the top of scaffold. Immunohistochemistry staining of β III tubulin (green) showed axons being guided towards the top center of the scaffolds in the LCs and ALICs. A) The top surface of day 28 D-LC sample. B) The bottom surface of day 28 D-LC sample. C) The top surface of day 28 D-ALIC sample. D) The bottom surface of day 28 D-ALIC sample. Scale bars = 6 mm.*

3.2 Co-culture, Tri-culture and Single Cultures In Liquid Phase

The scaffolds for tri-culture in liquid remained intact and transparent through 28 days (Figure 22 B). When hCECs were innervated in the ESD-LC and ED-LC groups, the morphology of the hCECs adopted a healthy polygonal epithelial cell morphology whereas in the E-LC group the cells were elongated (Figure 22). HCECs aggregation was observed in the liquid phase single cultures and co-cultures (Figure 22). The hCSSCs retained alignment at both cultivation time

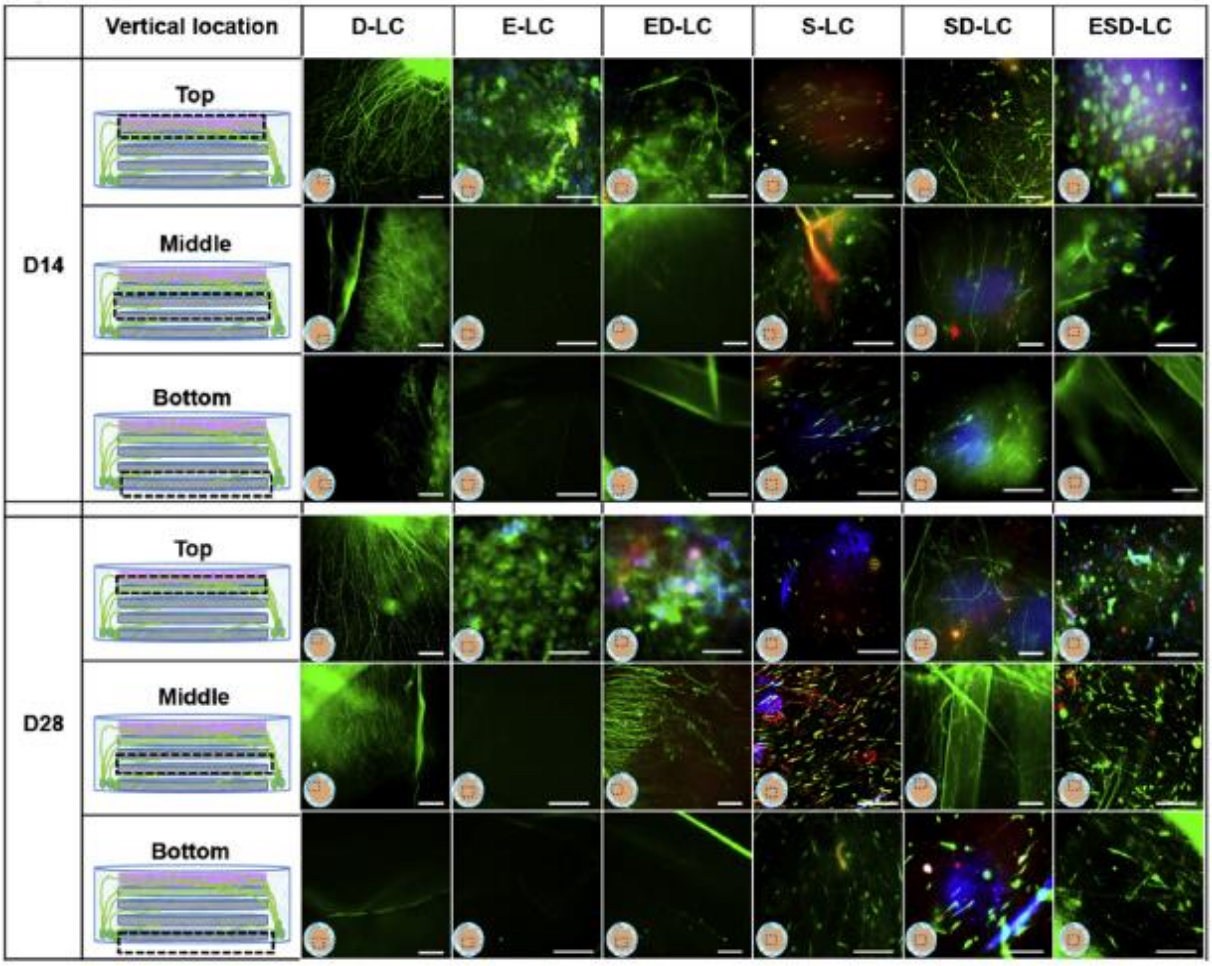

Figure 22. *IHC for cultures in liquid. Immunohistochemistry staining of DRGs, hCECs, and hCSSCs cultured alone (D-LC, E-LC, S-LC); hCECs, DRG co-culture (ED-LC); hCSSCs, DRG co-culture (SD-LC); hCECs, hCSSCs, DRG tri-culture (ESD-LC) in liquind. β III tubulin was stained green in all the samples. Involucrin was stained red in E-LC, ED-LC groups and the top layer of ESD-LC sample. Keratocan was stained red in S-LC, SD-LC groups, middle and bottom layers of ESD-LC sample. The dashed boxes indicate the location of images. Scale bars=100μm.*

points (Figure 22). Innervation was developed in all the co-culture groups, with the SD-LC group resulting in axons that were ~2 times longer than in the ED-LC group (Figure 25 A). The innervation was located on the top surface of scaffolds and between each layer of silk films (Figure 22). There was no significant difference in length and density of axons between the SD-LC and ESD-LC (Figure 25)**.**

3.3 Co-culture, Tri-culture and Single Cultures in Air-Liquid Interface

The integrity of the scaffolds and the transparency of the stacked films was maintained through 28 days of cultivation (Figure 19B). Immunostaining showed that the hCECs formed polygonal epithelial cell morphology (Figure 23) and developed into multicellular layers in the ESD-ALIC group (Figure 23). The involucrin, a marker for mature corneal epithelium, in the day 28 ESD-ALIC group was highest among the different conditions in ALIC and higher than the day 28 ESD-LC samples (Figure 27). The alignment of hCSSCs remained through the cultures in the S-ALIC, SD-ALIC and ESD-ALIC systems (Figure 23). The secretion of keratocan was also observed in the hCSSCs single cultures and co-cultures. The DRGs cultured alone at the ALIC had an axon density that was approximately two-fold higher than in the LC (Figures 25). Innervation was observed at the top surface and between the silk film layers in the scaffolds (Figure 23). The dense innervation appeared in the ESD-ALIC group (80 terminal/mm^2), which was 3 and 2 times higher than the ESD-LC and D-LC groups respectively (Figure 25 B). Calcium imaging was collected with menthal added to the medium to stimulate neuronal firing (Figure 26) showes increased neuronal firing whith menthol addition, supporting neuron function in the tissue constructs.

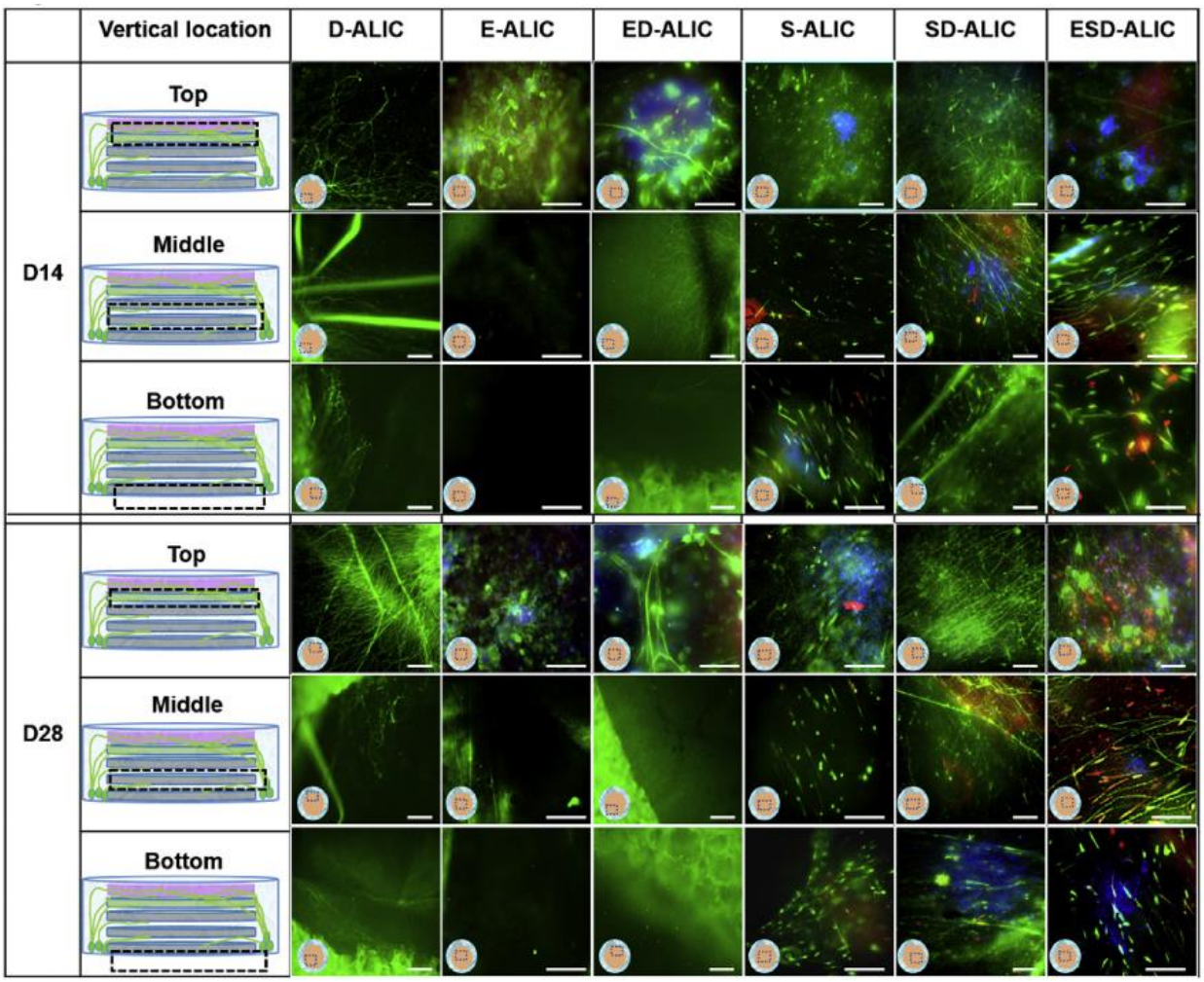

Figure 23. *IHC for air-liquid interface cultures. Immunohistochemistry staining of DRGs, hCECs, and hCSSCs cultured alone (D-ALIC, E-ALIC, S-ALIC); hCECs, DRG co-culture (ED-ALIC); hCSSCs, DRG co-culture (SD-ALIC); hCECs, hCSSCs, DRG tri-culture (ESD-ALIC) in liquind. β III tubulin was stained green in all the samples. Involucrin was stained red in E-ALIC, ED-ALIC groups and the top layer of ESD-ALIC sample. Keratocan was stained red in S-ALIC, SD-ALIC groups, middle and bottom layers of ESD-ALIC sample. The dashed boxes indicate the location of images. Scale bars=100μm.*

3.4 Q-PCR Analysis

In order to investigate the impact of innervation on the hCECs, expression of mRNA for involucrin (IVL), connexin 37 (GJA4), and cytokeratin-3 (KRT3) was quantified by qPCR. IVL

is a marker for maturity whereas GJA4 documents accumulation of cell-cell junctions in the epithelial layer. IVL and GJA4 were expressed in all groups, whereas KRT3 was only expressed in ED-ALIC, ESD-LC and ESD-ALIC samples (Figure 27 A). ED-ALIC had significantly higher expression of IVL and GJA4 compared to ED-LC. Also, the ESD-LC and ESD-ALIC groups had significantly higher IVL and GJA4 expression compared to ED-LC and ED-ALIC groups. The expression of mRNA for keratocan (KERA), lumican (LUM), aldehyde dehydrogenase (ALDH3A1) and smooth muscle actin (ACTA2) was quantified to analyze the functional state of the hCSSCs (Figure 27 B). KERA and LUM are corneal stroma ECM proteins that were previously shown to be expressed by keratocytes differentiated from hCSSCs [10]. ALDH3A1 is highly expressed in both epithelium and stromal cells of differentiated cornea and important for cornel transparency[203]. Smooth muscle actin (ACTA2) is a marker of myofibroblasts, cells involved in secretion of fibrotic non-transparent corneal tissue [204]. The expression of ACTA2 was down regulated in all the culture groups (Figure 27 B). The S-LC group had the highest KERA and LUM expression compared to all the other groups. When hCSSCs were innervated (SD-ALIC), the expression of KERA and LUM were not different from the SD-LC and were significantly higher than the S-ALIC. The expression of ALDH3A1 was significantly greater in groups with innervation compared to non-innervated samples

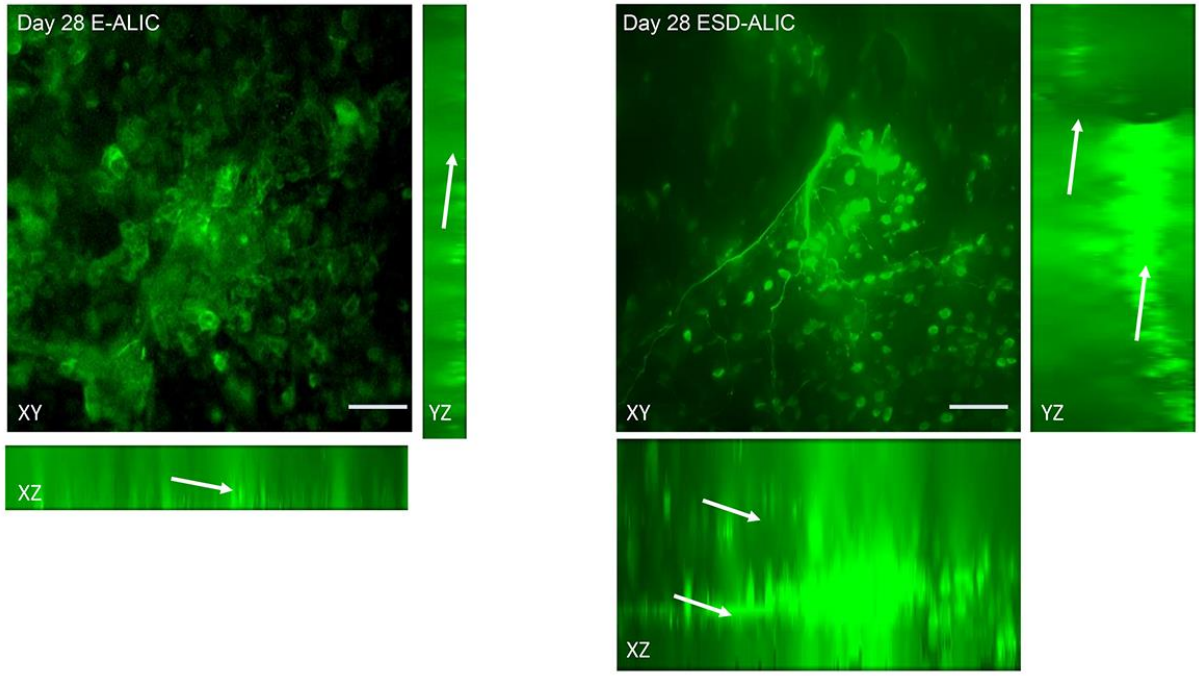

Figure 24. *Immunohistochemistry staining of day 28 E-ALIC and ESD-ALIC samples. βIII tubulin stained green. More cellular layers (white arrows) were observed in ESD-ALIC than in E-ALIC sample. Images were collected from n>3 from three independent experiments. Scale bars =100μm*

IV. Discussion

Compared to collagen-based corneal tissue models with innervation [128, 205], the silk protein provided tunable materials to match the mechanical properties of human cornea [129, 139, 206]. Films and sponges prepared from silk supported aligned hCSSCs growth and improved neuronal extensions [136, 137]. In collagen-based tissue models, NGF was loaded into hydrogels to create a concentration gradient to guide neuronal growth [12, 32]. However, the density and length of innervation were not quantified, and collagen undergoes consistent contraction over time that impacts cell functions. In our present study of corneal tissue models, NGF loaded collagen gels were combined with NGF stamped silk films to guide the axons towards the top center of the scaffolds, while concurrently avoiding the problem of material contraction.

Interactions between cells sourced from chickens in contact with human cells has been previously reported [207]. Dorsal root ganglion neurons were used to mimic corneal innervation, due to its roles as a critical component as sensory neurons [208]. The average terminal density and axon length reached 100 termini/mm^2 and 4 mm in the ALICs. The guided, dense, and long

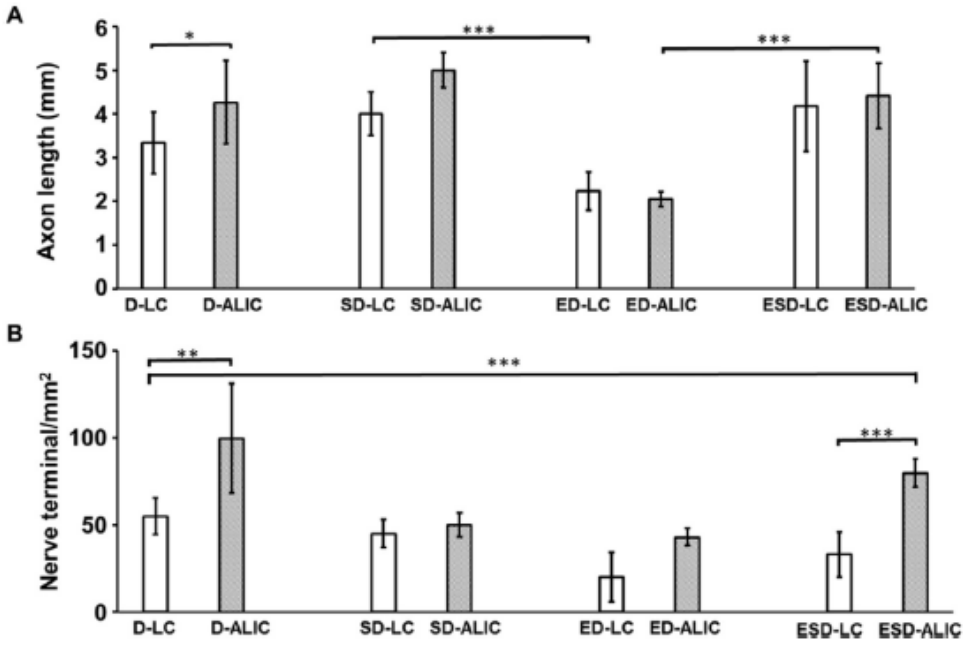

Figure 25. *Quantification of density and length of axons in day28 LC and ALIC. DRG single cultures in liquid phase(D-LC) and at air-liquid interface (D-ALI); DRG and hCSSCs co-culture in liquid phase(SD-LC) and at air-liquid interface (SD-ALIC); DRG co-culture with hCECs in liquid phase (ED-LC) and at air-liquid interfaces (ED-ALIC); DRG neuron , hCSSCs and hCECstri-culture in liquid phase (ESD-LC) and at air-liquid interfaces (ESD-ALIC). The air-liquid interface culture supported significantly longer axons compared to the liquid cultures. D-ALIC and ESD-ALIC groups provided the densest axons among the groups reaching an average of ~100 termini/cm2. Data was collected from n>3 from three independent experiments. ***P<0.0001; **P<0.001.*

axons establish an essential foundation to for innervated corneal tissue models. Further, these systems remained functional for at least one month in culture, supporting sustained cultivation to allow both acute and chronic studies with these new corneal tissues.

Previously, an air-liquid interface was achieved by culturing tissue constructs in trans-wells [153, 209, 210]. HCSSC survival in trans-wells was not robust in some of our preliminary experiments. Thus, PDMS shelves were designed to maintain a fluid environment for the stroma while the epithelium was positioned at the ALIC. As a result, the hCSSCs survived well in these systems.

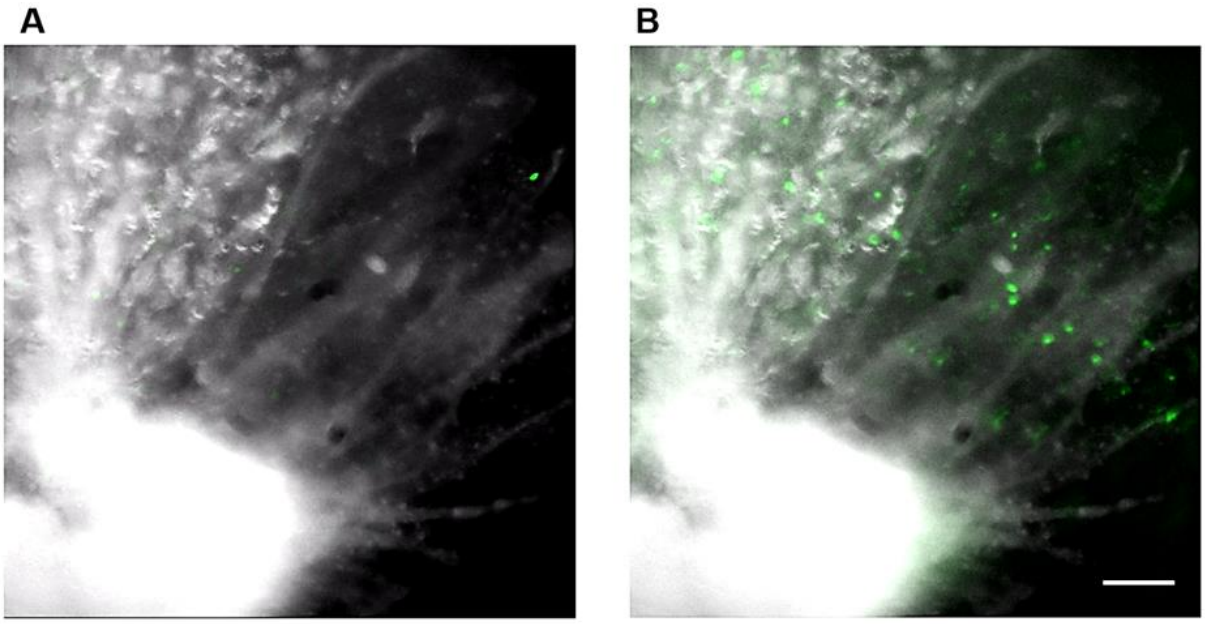

Figure 26. *Calcium imaging of DRG neuronal innervation before (A) and after (B) menthol stimulation. Scale bar=100µm*

After the scaffold design for neuronal innervation guidance and air-liquid cultivation was completed, the hCSSCs and hCECs were included in the cultures. In our previous studies, we developed patterned corneal stoma construct using RGD functionalized silk film stacks [26], which supported the secretion of aligned ECM from hCSSCs. In a more recent study, 2D co-culture systems with silk films and silk collagen hydrogels improved DRG axonal development when co-cultured with hCSSCs. In order to include the epithelium, an important barrier layer for the cornea [3], HGF, KGF and EGF were stamped on the top silk film layer. HCECs survived

through 28 days of cultivation in the LC and ALIC. Multilayer growth of hCECs (Figure 24) was achieved in the ALIC systems, reflecting the importance of the air-liquid environment to generate suitable outcomes for these cornea tissues.

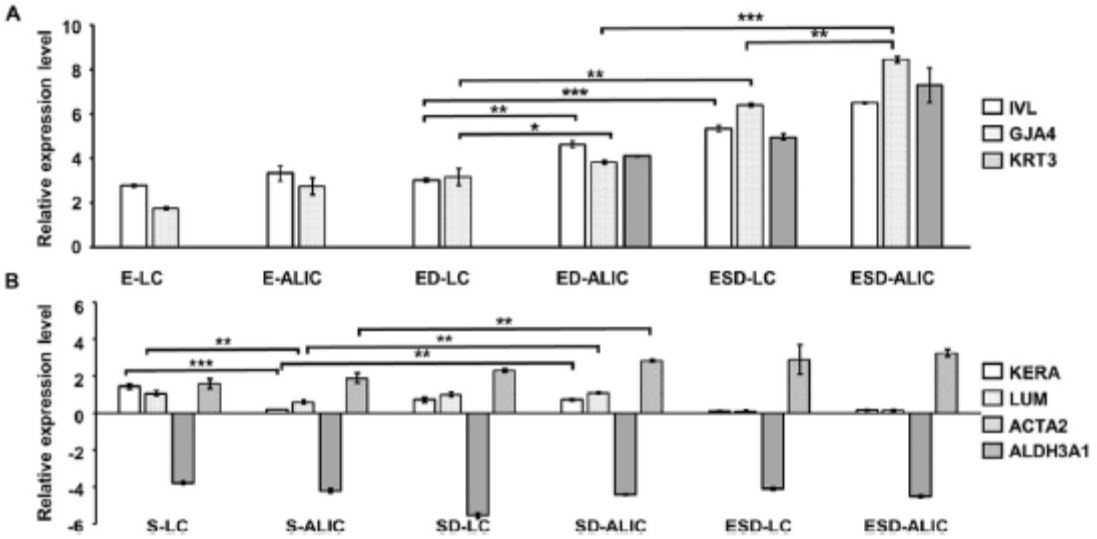

Figure 27. *Gene expression of hCSSCs (A) and hCECs (B) in LC and ALIC. The expression levels of mRNA for involucrin (IVL), connexin 37 (GJA4) and cytokeratin 3 (KRT3) were quantified through Q-PCR and normalized with day 0 samples of hCECs. The expression levels of mRNAs for keratocan (KERA), lumican (LUM), aldehyde dehydrogenase 3A1 (ALDH3A1) and smooth muscle actin (ACTA2) were quantified through Q-PCR and normalized with day 0 samples of hCSSCs. The expression level of IVL, GJA4 were significantly higher in ED and ESD co-cultures compared to hCECs single cultures. hCSSCs expressed the most keratocan when cultured in the liquid phase. SD-ALIC groups had significantly higher keratocan expression compared to the S-ALIC groups. The data were collected from n>3 from three independent experiments.*
****P<0.0001; **P<0.001.*

The expression of IVL, GJA4 and the number of epithelial cellular layers in the innervated and air-liquid interface cultured samples were significantly higher than in the non-innervated samples cultivated in liquid phase, suggesting innervation and the air liquid interface contributes towards achieving cell and tissue maturity of the corneal epithelium.

During the sustained cultivation in LC, the survival of hCSSCs appeared to decrease when hCECs were included in the system. This outcome was likely due to the hCECs remaining proliferative throughout the cultivation which created competition for nutrients. This issue did not appear in the ALICs, which again supported the key role of this environment maintaining a healthy epithelium and stroma. However, when hCSSCs were cultured alone, the LC provided better KERA expression compared to the ALIC, indicating the liquid environment enhanced the secretion of ECM in the stroma.

The highly expressed ALDH3A1 and KERA in the innervated stroma showed the essential role of innervation on corneal stromal transparency and function [211]. In humans, it was observed that the impairment of corneal innervation can cause corneal ulcers (neurotrophic keratitis) [212]. Patients with neurotrophic keratitis present decreased corneal sensitivity with alterations in corneal epithelium, nerve, keratocyte, and endothelium. Our findings corroborate that corneal sensory nerves play a critical role in maintaining the vitality, metabolism, and replenishment of corneal cells [213]. While preliminary in outcome in the present study, the data suggest that this new corneal 3D tissue model has potential to help to explore and address these types of corneal diseases.

The interaction between corneal cells and innervation was also observed through the morphology. The axons developed from the bottom of silk sponge and grew towards the top of the scaffold in single culture and co-culture groups. In the tri-cultures, the axons branched at the edge of scaffold and sprouted thin and long axons that grew in between stromal layers and on the epithelial layer. Epithelial innervation developed through cultivation formed close connections

with hCECs in the ALIC. In stromal layer, the axons were guided by the pattern on the silk film and grew parallel with hCSSCs. Through the longer and denser axons in the ESD-ALIC compared to the ED-ALIC, a synergistic effect by the hCSSCs was revealed. This finding is in agreement with our previous study which illustrated the importance of collagen type I and BDNF secreted by hCSSCs in improving neuronal extensions [35]. Interestingly, we observed longer axons in all the ALIC groups. A similar effect was shown in other DRG neuron single cultures and co-cultures with skin tissue at the air-liquid interface [214, 215]. The results indicate the importance of the ALIC in supporting long and dense neuronal innervation at *in vitro* environment.

The cultivation time for current cornea tissues models was limited to 1-2 weeks [128, 205]. Cornea development takes 2 months in the human embryo [61]. Interactions between innervation and corneal tissue in longer-term cultivation are critical in this study, the robust silk protein based scaffold retained integrity and transparency through 28 days of cultivation. These results support the utility of these scaffold designs and bioreactor support for sustainable cultivation of 3D cornea tissues for a range of studies in the future.

V. Conclusion

Innervated silk-based corneal tissue models were developed which supported long and dense neuronal innervation with multi-layer hCECs for the epithelium and aligned hCSSCs for the stromal layers. The impact of innervation on the corneal stroma and epithelium in sustained culture was demonstrated. With these advances in relevance, innervation, and time in culture,

these corneal tissue models can be considered as supplements to animal models in areas such as drug development, disease intervention and in general corneal physiology research.

Chapter V. *In vitro* Corneal Tissue Model in a Dynamic *in vitro* Environment

I. Introduction

Following the development of the 3D corneal tissue model, we investigated the effects of intraocular pressure (IOP) and tear flow (TF) on the system. In addition, we inserted human sensory neurons into the scaffold to more accurately mimic the cellular components of the human cornea. Analysis of cellular reactions to mechanical stimulation provides an important metric for evaluation of the functionality of the tissue model. In this chapter, we optimized the clinically-used Barron® artificial anterior chamber to serve as a bioreactor system and provide sustained IOP. The chamber was equipped with a customized lid with an auxiliary medium outlet to provide tear flow with a rate of 10 drops/min mimic human tear flow rate. The tears increased the viability of epithelium and stroma compared to the IOP group. Furthermore, IOP improved ECM protein expression and secretion in corneal stromal cells. Development of this novel dynamic cultivation system provides a new opportunity to study tears and IOP in a highly controlled *in vitro* environment.

II. Materials and Methods

2.1 Human Sensory Neuron Cell Culture

Human sensory neurons (hNs) were differentiated from human neuronal stem cells reprogramed from human fibroblasts [216]. Subsequently, neuronal stem cells were differentiated for 10 days on a gelatin-coated plate into sensory neurons, using 3 inhibitors and 3 growth factors

supplemented in neurobasal medium (Thermofisher) containing 2% B-27 (Sigma), 10% antibiotic-antimycotic (Thermofisher) , 10% glutamax (Thermofisher), 3 growth factors (25ng/ml NGF, 25ng/ml BDNF, 25ng/ml GDNF), and 3 inhibitors (3μM CHIR99021, 10μM SU5402, and 10μM DAPT) (Thermofisher) [217]. Silk sponges were immersed in 0.1mg/ml (poly-D-lysine) PDL solution at 4°C overnight before use. The PDL solution was aspirated prior to cell seeding. Then 5ml TrypL-select solution (Thermo Fisher Scientific) was added per dish of neurons and incubated at 37°C for 1min. The solution was subsequently neutralized with neurobasal medium to inactive the enzyme and detach neurons from the dishes. The cell solution was then collected and centrifuged at 1200 RPM for 5 min and suspended with the neurobasal medium at a concentration of 100,000,000 cells /ml. A 100μl of cell solution was then added to 300μl of neutralized collagen hydrogel and applied onto the silk sponge using133μl per scaffold. The sponges were then incubated for 1h to allow time for crosslinking before beginning culture in 3I+3G neurobasal medium.

2.2 Tri-cultivation of hCSSCs, hCECs and hNs

The methods for tri-culturing hCSSCs, hCECs and hNs was the same as with the ESD tri-culture in section 2.4 in Chapter IV.

2.3 Preparation of Artificial Anterior Chamber

The artificial anterior chambers were purchased from Barron®[1]. As can be seen in Figure 28 and 29, the chamber is composed of a base, a tissue retainer, and a locking ring. A porous silk film was made and applied on top of the base to serve as a bottom membrane. Following application, a 15mm inner diameter and 17mm outer diameter rubber o-ring (McMaster) was

placed on top of the film to improve sealing and decrease stress on the scaffold. The corneal tissue model, described in Chapter IV, was cultured for 14 days was then placed gently on top of the silk film and was anchored down by the tissue retainer. Sealing of the antieror chamber was achieved by fastening the locking ring. The co-culture medium was then pushed into the system through a luer lock connector. The pinch clamps were clipped once the pressure reached the range of 15-20mmHg. This pressure was maintained and measured by a tonometer (Medical Device Depot, Ellicott City, Maryland) [218] every 3 days throughout the duration of culture. Culture medium was changed every 2 days by complete aspiration and refilling the chamber.

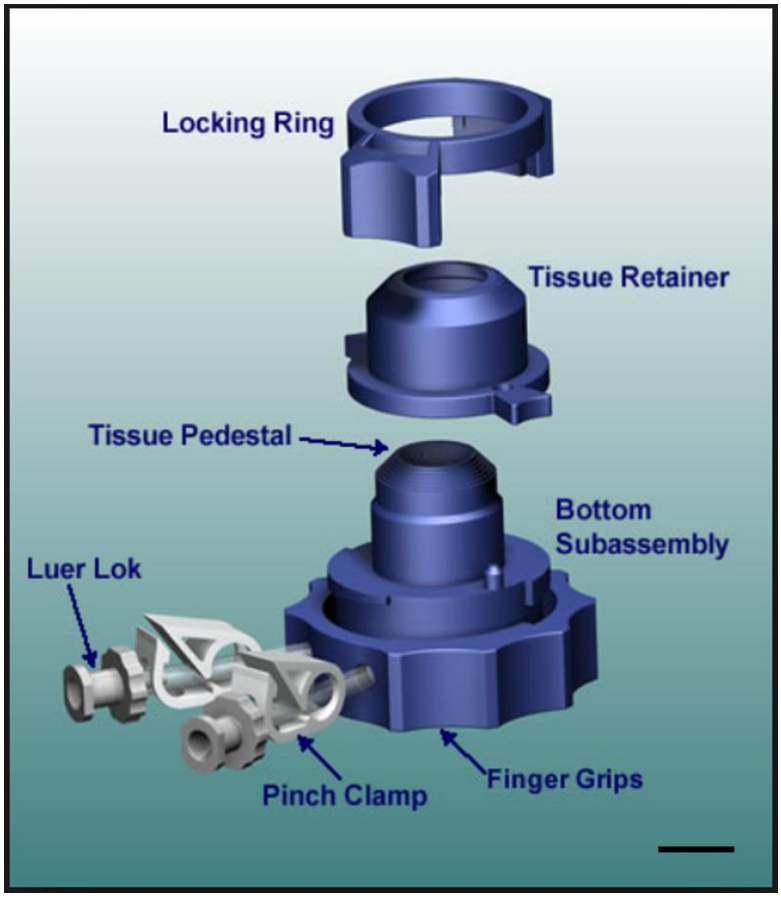

Figure 28. *The structure of artificial anterior chamber. The base of chamber is connected to luer lock which can be closed by tightening the pinch clamp. The tissue retainer and locking ring are used to seal the system[1]. Scale bar=6mm*

2.4 Preparation of Tear Dropping Device

A custom designed lid was made of polycarbonate with a 3mm medium inlet (Figure 29 A and B) and was fitted with a silicone pipe to provide tear flow (TF) on the surface of the scaffold (Figure

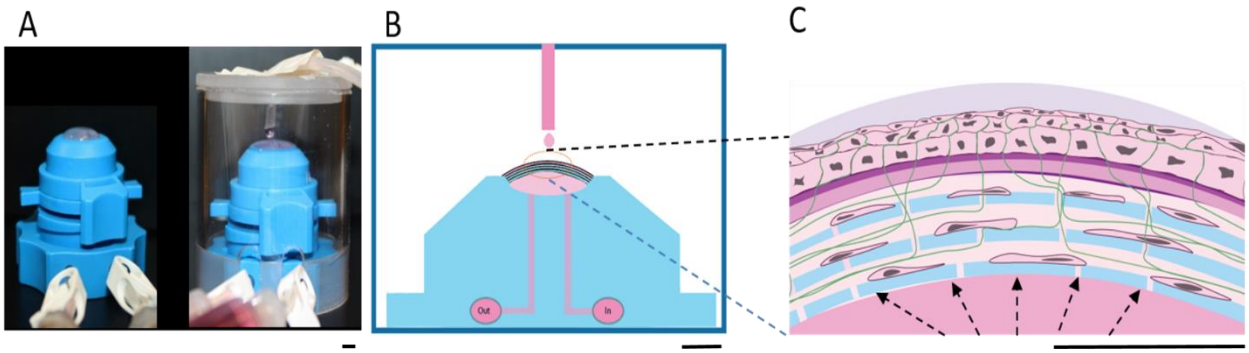

Figure 29. *Representative picture and schematic for bioreactor. A: The tissue model was pressurized and formed a dome shape under artificial IOP. A tear wash device was added with dropwise tear, to bathe the surface of tissue model. B: Schematic of the inner structure of bioreactor. The cellular component in the tissue model in bioreactor with dash line indicating the intraocular pressure. Scale bars=6mm*

29 A). The pipe was anchored to have 1 mm of distance from the top surface of the scaffold. The bioreactor was then placed on top of an absorbing gauze pad to collect tear flow run off from the top surface of the scaffold. The tear pipe was connected to a 50ml syringe containing TF fluid (hCSSCs differentiation medium supplemented with 25ng/ml EGF) (Sigma). To provide tear flow, 50ml syringes were then loaded in a syringe pump (Harvard Apparatus, Holliston, MA) programed for a 50ul /min flow rate.

2.5 Immunohistochemistry

Dynamic and static cultivated tissue models were fixed on day 28 and day 40 by soaking samples in 10% formalin PBS solution overnight. The samples were then rinsed with PBS to remove residual formalin before dehydration with ethanol, xylene and paraffin (Table 2). The samples were cut into 3 pieces, embedded and hardened in fresh paraffin (VWR). The samples were then sectioned into 8µm thick slices and rehydrated following the steps in Table 3 Antigen retrival was completed using unmasking solution (Vector Laboratory, Burlingame, CA) and heated for 20 min with a vegetable steamer. The primary antibodies were then added onto the slides, incubated at 4°C overnight and washed with PBS 3 times before application of the secondary antibody. Following 1h incubation at room temperature, the unbound secondary antibody was rinsed off the slides by washing with PBS 3 times prior imaging. The dilution ratio used for primary and secondary antibody preparation is included in Table 2.

Table 3. *Steps of tissue processing*

Dehydration		**Xylene exchange**		**Paraffin**	
Solution	time	Solution	Time	Solution	Time
50% Ethanol	10 min	2:1 Ethanol : Xylene	15 min	2:1 Xylene : Paraffin	30 min
70% Ethanol	10 min	1:1 Ethanol : Xylene	15 min	1:1 Xylene : Paraffin	30 min
80% Ethanol	10 min	1:2 Ethanol : Xylene	15 min	1:2 Xylene : Paraffin	30 min
95% Ethanol	10 min	100% Xylene	15 min	100% Paraffin	1hr
100% Ethanol	10 min	100% Xylene	15 min	100% Paraffin	1hr
100% Ethanol	10 min	100% Xylene	15 min		
100% Ethanol	10 min				

III. Results

3.1 Neuronal Stem Cell Differentiation

The expression level of CRCP, BDNF, TAC1, TRPV1 and NTRK1 at day 14 by the hNs was quantified by q-PCR to assess the effectiveness of differentiation of human iPS neurons. For neurons cultivated with 3I+3G neurobasal medium, the expression of pain mediators (CRCP, BDNF, TAC1), temperature and capsaicin nociceptor (TRPV1), and neurotrophic factor receptor (NTRK1) were upregulated compared to the group cultured with neurobasal medium alone (Figure 30). These data provide baseline information on relevance of these cells for the study of sensory/pain-related outcomes.

3.2 Neurons Responded to Dynamic Cultivation

Based on the preliminary data, no neuronal extensions were observed in the IOP alone group. However, with TF, neuronal extensions were observed on day 28 samples undergoing dynamic culture. Q-PCR data indicated (Figure 32) that combined IOP+TF cultivation increased the expression of CRCP and SCN compared to static cultivation. Through IHC, higher β III tubulin

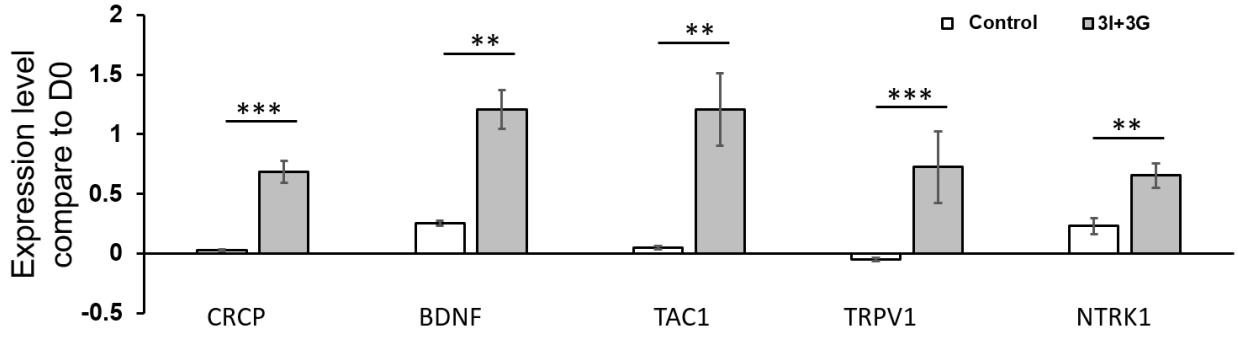

Figure 30. *Q-PCR result of day 14 differentiated neuronal stem cell reprogramed from human fibroblasts. Compared to control groups cultivated without inhibitors and growth factors, the 3I+3G differentiated group had higher expression of pain mediators (CRCP, BDNF, TAC1), temperature and capsaicin sensor (TRPV1), and neurotrophic factor receptor (NTRK1). The data were collected from n>3 from three independent experiments. ***P<0.0001; **P<0.001.*

expression was observed in the static culture samples than the IOP+TF culture, while NaV 1.8 - expression was improved by IOP+TF cultivation (Figure 31).

3.3 hCECs Responded to Dynamic Cultivation

In the IOP group, the mature corneal epithelium markers (IVL and connexin43) were not expressed. However, in the IOP+TF group, IVL and connexin immunostain signals were observed and were statistically upregulated when compared to the IOP group and static cultivated samples (Figure 31). In q-PCR result (Figure 32), greater expression of IVL, and GJA4 was detected in IOP+TF group compared to static cultivation, suggesting tears improved the maturity of the epithelium.

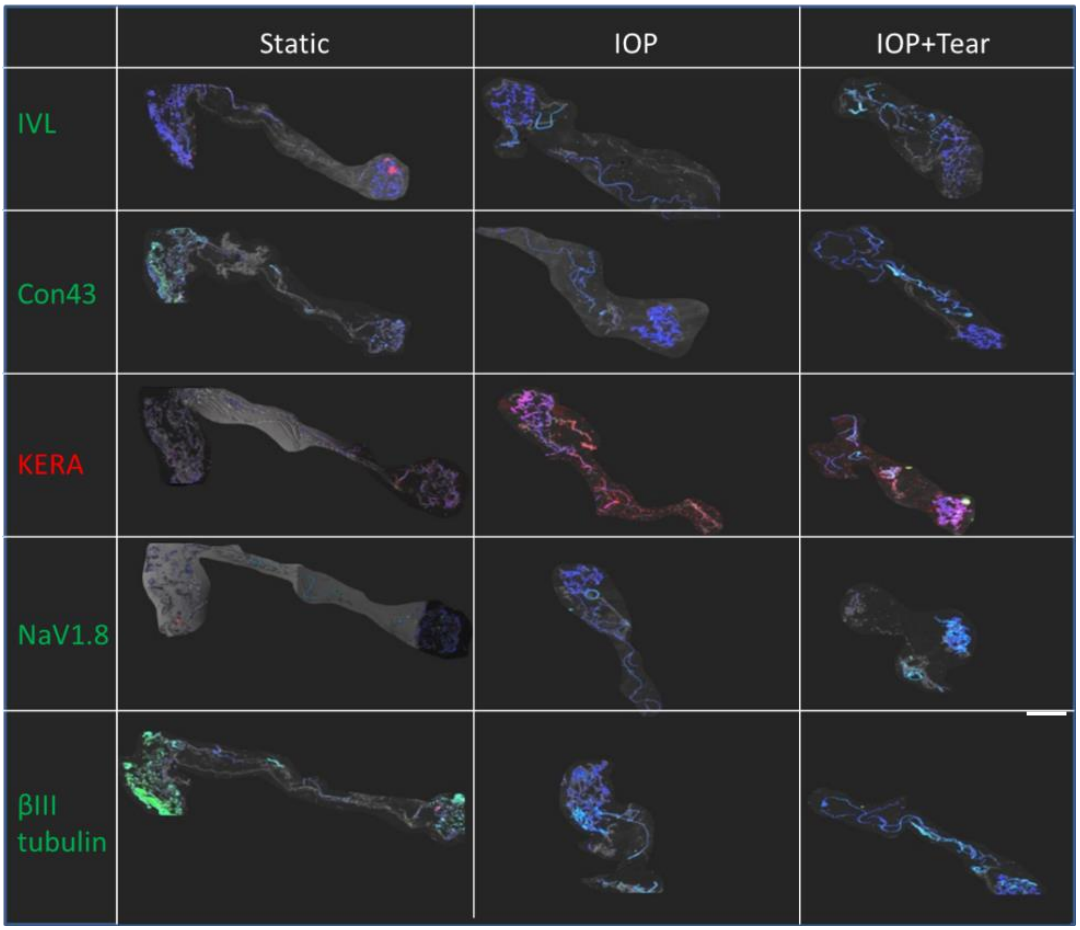

Figure 31. *Immunohistochemistry of corneal tissue models cultivated in static, IOP alone, and IOP+ tear wash bioreactors. Involucrin (IVL), connexin 43 (con 43), NaV1.8 and β III tubulin were stained green while keratocan was stained red. IOP+ tear wash group had most IVL, connexin 43, NaV 1.8. Whereas IOP and IOP+ tear wash groups both had higher keratocan expression than static cultivation. Scale bar=3mm*

3.4 hCSSCs Responded to Dynamic Cultivation

Higher KERA, LUM, and ALDH expression in the IOP+TF cultivation group was detected relative to the static cultured group in terms of both IHC (Figure 31) and q-PCR (Figure 32). These results indicated that IOP and TF improved the secretion of ECM components by hCSSCs.

IV. Discussion

To date, the impact of mechanical forces on corneal cells have been mainly studied in single cell type cultures [7, 219]. In order to further mimic the cellular component of human cornea we innervated the multicellular corneal tissue model with hNs differentiated from neuronal stem cells (hNSCs) derived from reprogrammed human dermal fibroblasts [216]. Previously, 3I+3G

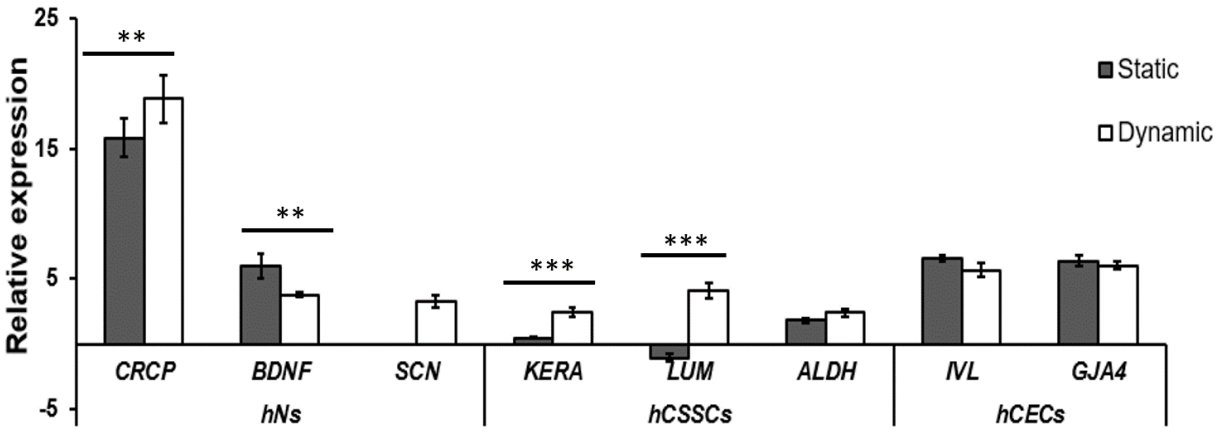

Figure 32. *HCSSCs, hCECs and neuron marker expression after IOP+TW dynamic cultivation. Q-PCR result for expression of CRCP, BDNF, SCN from neuron; KERA,LUM, ALDH from hCSSCs and IVL,GJA from hCECs in day 28 static and IOP + Tear wash samples. The dynamic cultivation appeared to improve the expression of CRCP, SCN, KERA, LUM, and ALDH. No significant difference was observed between static and dynamic cultivation in IVL and GJA4 expression level. The data were collected from n>3 from three independent experiments. ***P<0.0001; **P<0.001.*

neurobasal medium was shown to be effective for iPS cells differentiating towards sensory neurons [217, 220, 221]. Here we adopteded this method to differentiate the hNSCs. To evaluate

the differentiation efficacy, the expression level of sensory neuron markers Tac1, BDNF, CRCP, TRPV1 and NTRK1 were evaluated. Tac1[222], BDNF and CRCP [223] genes encode important peripheral pain mediators [220]. TRPV1 is linked to nociceptive nerve firing following temperature and capsaicin stimulation [224]. NTRK encodes neurotrophic factor receptors necessary for nerve cornea cross talk [64]. Here, all human sensory neuronal markers were significantly upregulated in the differentiation experimental conditions using the 3I+3G neurobasal medium, indicating the effectiveness of the differentiation protocol.

To mimic the IOP, we applied the artificial anterior chamber used in corneal transplantation to inflate the scaffold with culture medium. The IOP was maintained in the range of 15-20 mmHg mimicking human cornea pressure [218]. Maintaining pressure also served as an indicator that the bioreactor system remained sealed during the cultivation. In the human eye, the tear fluid is spread on the ocular surface by eye blink movement, with average rate of 10 times/min [225, 226]. To mimic these features, we designed the lid with a medium outlet to drip artificial tears on the scaffold surface with rate of 10 drops (5µl/drop) /min. In our preliminary experiments, the tear fluid was dropped from a 2-3 cm height onto the tissue model. In these samples, no hCECs or hCSSCs were observed due to the forces imposed by the tear dropping. To solve this problem, we lowered the medium outlet to a 1 mm height from the scaffold surface and gained improved cell growth. On the native ocular surface, the tear fluid is drained through the tear duct and into the lacrimal sac by the nose [226]. In our bioreactor, the tear fluid flowed off the surface due to the curvature of the pressurized tissue model. Thus, we placed a sterilized gauze pad underneath the anterior chamber to collect the tears.

The tissue model gained curvature and significantly increased secretion of stromal ECM (KERA, LUM) under stimulation of IOP, demonstrating the contribution of mechanical tension to corneal integrity. This result aggreed with the contribution of IOP in corneal curvature and thickness during mice corneal development [227], demonstrating the promise of this bioreactor as an effective tissue model for future studies.

A custom designed lid was used to protect the artificial anterior chamber, however, contamination still occurred in some of the IOP alone samples. In the IOP + TF group, however, no contamination was observed during the culture period, suggesting medium flushing on the scaffold surface was effective washing out potential contaminents or pathogens in a similar manner to a human tear flow [228]. In addition to preventing contamination, TF also improved the functionality of the corneal epithelium and innervation in the tissue model. As shown in IHC and Q-PCR results, TF enhanced the expression of IVL and connexin which indicated improvement of epithelial maturity. The higher expression of nociceptor NaV 1.8 in the IOP+TF group compared to the IOP alone group revealed the importance of TF to functional corneal innervation.

In vivo, aqueous humour generated IOP and air-liquid interface environment contribute to a healthy cornea [58, 218]. The aforementioned air-driven flex cell cannot fully replicate these physiological features. Currently, there is no bioreactor that combines the air-liquid interface environment, IOP and TF. Making use of our design, fluid generated IOP and ALIC provided a representative, physiologically relevant model. Additional tear flow elements provide the chance of studying tear function within an *in vitro* environment. By tunning the IOP, tear and aqueous

humour components , diseases like glaucoma, dry eye syndrome, and ocular surface infection can be mimicked *in vitro* using this new system.

V. Conclusions

A bioreactor was developed to mimic the mechanical and biochemical properties of IOP and TF. IOP improved stromal ECM secretion while TF promoted the maturity of the epithelium and neuronal extensions, as well as reducing contamination. Such responses match the functioning of native cornea, demonstrating the utility of this corneal tissue model and bioreactor system in studying corneal reactions to mechnical stimulation. The bioreactor allows adjustment of IOP pressure, tear fomulation and aqueous humour components, and can serve as a platform of mimicking the dynamic environment of healthy and diseased cornea.

Chapter VI. Corneal Tissue Model Response to Nociceptive Stimulation

I. Introduction

To evaluate functionality, the corneal tissue model with functional neuronal innervation was evaluated for the ability to respond to pain stimuli. The ability to react to and recover from trauma is also crucial for future applications in drug screening and toxicity testing. In this chapter, culture medium containing capsaicin, which triggers pain and cause epithelial ulcers [229] in human cornea [230], was used to stimulate the corneal tissue model. Following pain stimulation, serum supplemented medium, a clinically used treatment for corneal trauma, was applied. Decreased confluency and morphological changes in hCECs, hCSSCs, and neurons were observed following nociceptive stimulation. Pain mediator release was also observed following capsaicin stimulation, as detected by SP and CGRP directed ELISA. Recovery of hCECs and hCSSCs confluency and nerve density were observed after exposure to medium containing serum. Such reactions indicated that the tissue damage and pain mediator release during corneal trauma can be replicated by this *in vitro* tissue model.

II. Material and Methods

2.1 Q-PCR of hCSSCs and hCECs cultured in medium containing EGF and FBS

In order to encourage epithelial and stromal recovery following capsaicin stimulation, 4 types of medium (5% or 10% FBS, 25 or 50ng/ml EGF supplemented hCSSCs differentiation medium) were added to hCSSCs and hCECs monocultures. RNA was processed (extraction, reverse transcribed) on D14 samples following the method described in Chapter IV. Expression of lumical (LUM), keratocan (KERA), aldehyde dehydrogenase 3 family member A1(ALDH3A1), actin alpha 2 (ACTA2), involucrin (IVL), gap junction protein alpha 4 (GJA4) and keratin 3

(KRT3) was evaluated through q-PCR to evaluate cellular response also using the same methods with Chapter IV.

2.2 Capsaicin stimulation and Serum Treatment on Corneal Model

Following 28 days of culture of the tissue model at the air-liquid interface, 10µl DMEM containing 0.5%, 0.05%. 0.005%, 0.0005% capsaicin was pipetted on top of the scaffolds. Capsaicin supplemented DMEM was rinsed off with PBS following a 10 min incubation period. The scaffolds were then placed back on the floating shelf to continue cultivation. For convenience, day 28 co-culture is defined as day 0 after capsaicin stimulation in this Chapter (D0 cap). Three days after initial capsaicin stimulation, hCSSCs differentiation medium containing 10% FBS was added for 24h to improve the healing of corneal cells and neurons. Following the serum treatment, the samples were cultured in hCSSCs differentiation medium with 50ng/ml NGF until day 9. The serum treated (STSR), non-serum treated (ST), and non-stimulated (no ST) samples were collected on day 9 after capsaicin stimulation, for q-PCR and IHC analysis.

2.3 DiI and DiO Labeling of Cells

To observe cellular response to different concentrations of capsaicin, neurons were labelled with DiO and corneal cells with DiI (ThermoFisher) by diluting the dye at a ratio of 1:500 (v/v) in a 1,000,000cells /ml solution prior to seeding on the scaffolds. Images were collected every two days from 1 day before capsaicin stimulation (day-1) to day 9.

2.4 ELISA of SP and CGRP

SP and CGRP are mediators used to assess the pain reactions. Supernatant culture media samples were collected every 2 days after capsaicin stimulation and stored at -80°C. The frozen medium samples were lyophilized overnight and dissolved in 1 ml of deionized water. ELISAs for SP and

CGRP were processed using an SP parameter assay kit (R&D system) and human CGRP EIA kit (Cayman Chemistry, Ann Arbor, Michigan).

2.5 Immunohistochemistry and q-PCR

The IHC and q-PCR were processed following the same procedures outlined in previous chapters. SP8 CARS confocal microscopy (Leica) was used for 3D image acquisition.

III. Results

3.1 hCECs and hCSSCs Reaction to FBS and EGF

To optimize the concentration of FBS and EGF in the regrowth improving medium, 10 and 5% FBS, 25 and 50 ng/ml EGF supplemented hCSSCs differentiation medium were tested with D14 hCSSCs and hCECs mono-cultures grown on TCP. The q-PCR results showed hCECs maturity marker (IVL, GJA4 and KRT-3) expression improved in the 10% FBS and 25ng/ml EGF groups. HCSSCs ECM marker expression (KERA, LUM, ALDH) was increased by all 4 types of media, with the lowest amount of non-stromal differentiation marker (ACT) expression observed in the 10% FBS group. Thus, 10% FBS supplemented medium was chosen as the healing medium for the tissue model after capsaicin stimulation (Figure 33).

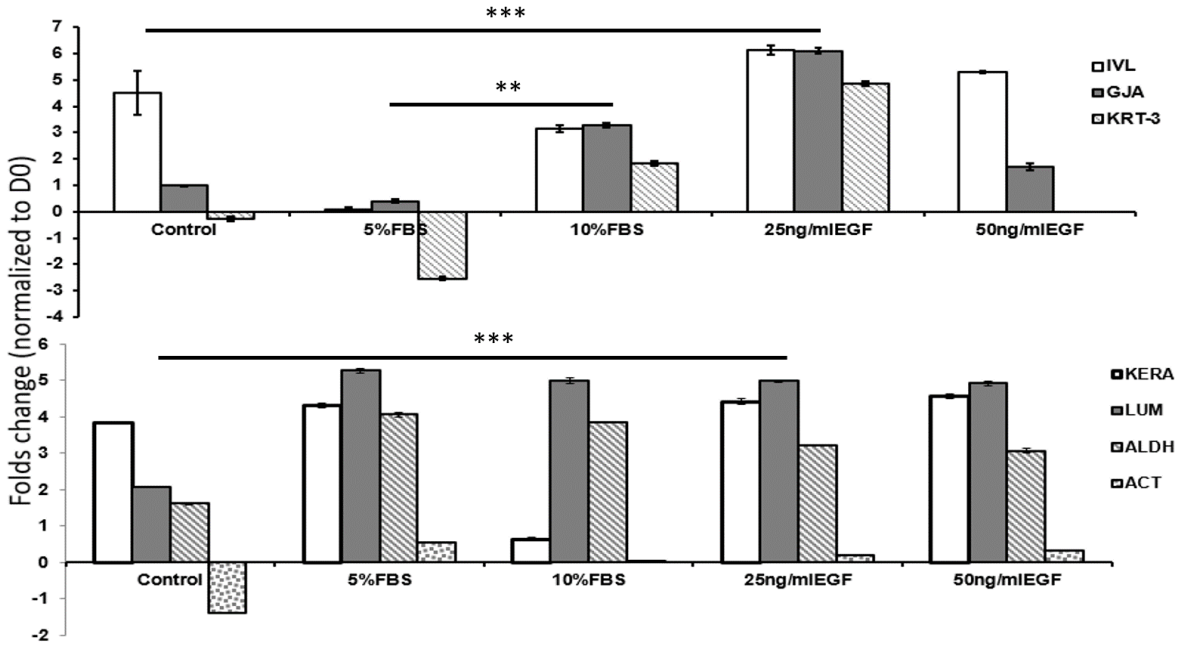

Figure 33. *Gene expression of hCSSCs and hCECs cultured in medium containing EGF and FBS. Q-PCR of IVL, GJA, KRT-3 expression from hCECs and KERA, LUM, ALDH and ACT expression from hCSSCs under stimulation of 5% 10% FBS, 25, and 50ng/ml EGF. The hCECs appeared to have higher IVL, GJA and KRT-3 marker expression in 25ng/ml and 10% FBS group than other groups. Whereas hCSSCs expressed most KERA, LUM, and ALDH in 5% FBS group. The data were collected from n>3 from three independent experiments. ***P<0.0001; **P<0.001.*

3.2 DiI labeled Corneal Cells Response to Capsaicin Stimulation

To seek the optimal stimulation concentration, tissue models containing DiI labeled corneal cells and DiO labeled hNs were stimulated by 0.5,0.05,0.005% capsaicin in DMEM. Figure 34 shows the stitched images of corneal tissue model on D2 before stimulation, D0 (immediately after stimulation), and D3 and D5 after stimulation. As shown in Figure 34, 0.5 and 0.05% capsaicin decreased the cell density upon stimulation. Reduction of cell coverage was observed 5 days after 0.005% capsaicin stimulation. Recovery of cell confluency was observed after serum treatment in all groups with the 0.005% group demonstrating the best regrowth (Figure 35). Thus we chose 0.005% capsaicin for all remaining experiments.

To study serum treatment, neurons were labeled green with DiO while corneal cells were labeled red with DiI. After the capsaicin exposure, a decrease of cellular confluency was found on day 3. The non-serum treated (ST) group showed continuous decrease of cellular confluency after the

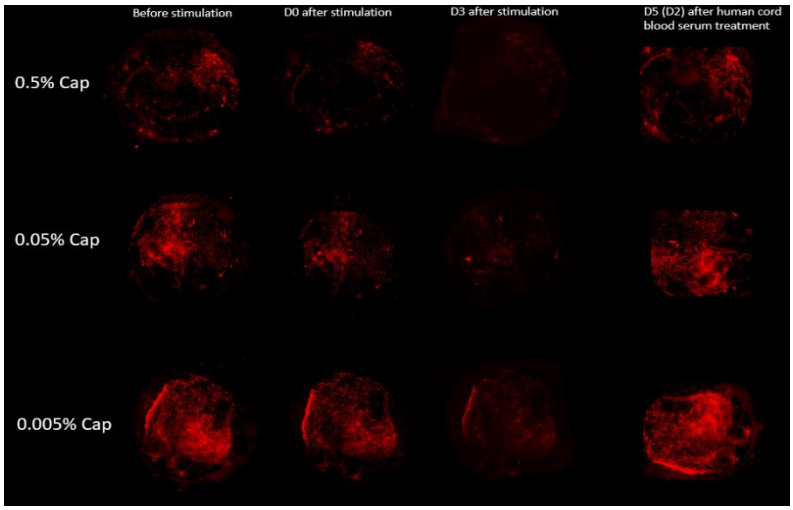

Figure 34. *Live cell image of corneal cell response to different concentration of capsaicin. DiI (red) labeled hCSSCs and hCECs reacted to 10 min exposure to 10μL capsaicin (0.5,0.05, 0.005%), day 3 after stimulation and after serum treatment. The 0.005% capsaicin appeared to provide decrease of cell coverage after exposure while recovered after the serum treatment.*

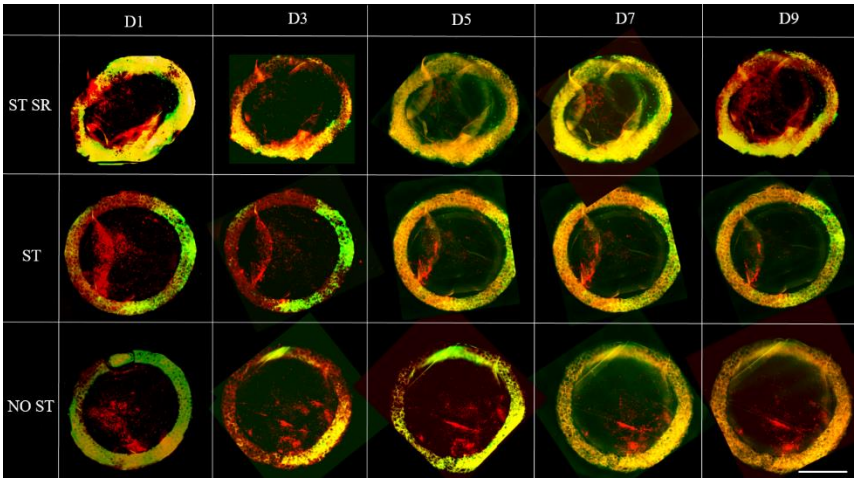

Figure 35. *Confluency change observed through live cell imaging. Stitched fluorescence images captured from stimulated (ST), stimulated and serum treated (STSR), and non-stimulated (NO ST) samples. The corneal cells were labeled red with DiI while neurons were labeled green with DiO. Scale bar =6mm*

capsaicin stimulation. For the serum treated group (STSR) we saw an increase of cell confluence on day 7 and 9 indicating the serum treatment improved regrowth of corneal cells.

3.3 Confocal Microscopy of Tissue Model After Capsaicin Stimulation and Serum Treatment

Confocal microscopy was utilized to assess cellular morphology in the scaffolds, with results shown in Figure 36. No neuronal extensions were observed in the ST group. HCECs and hCSSCs showed altered cell morphology and decreased cell number compared to the non-

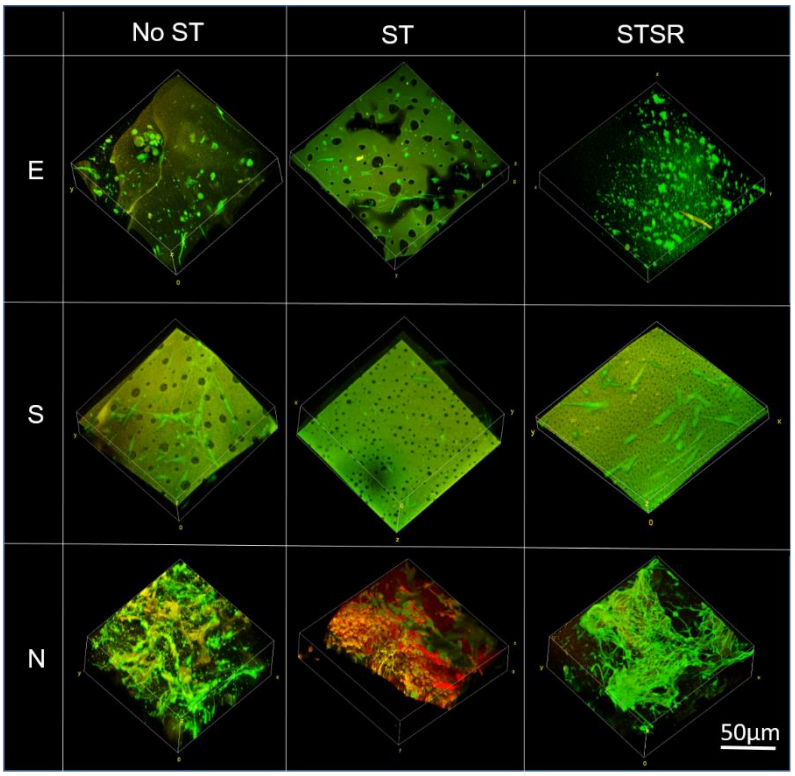

Figure 36. *Immunohistochemistry of corneal tissue model regions (E: epithelium, S: stroma, N: neuron) on day 14 after exposure to 0.005% capsaicin in ST(stimulated), NOST (non-stimulated) and STSR (serum treated) groups. β III tubulin was stained as green, red represent the auto fluorescence of silk scaffolds. Neuronal extension disappeared at samples at 3 days after capsaicin stimulation with change of cellular morphology in epithelium and stroma observed as well. The serum treatment improved the density axons and epithelial cells compared to the control group. While the D14 control has the elongated stromal cells. Scale bar=50µm.*

stimulated group (NO ST). After serum treatment (STSR), longer and denser axons were observed in the capsaicin stimulated group than the No ST and STSR samples. The STSR samples also had multilayer epithelium. However, the recovery of morphology and density of hCSSCs were not achieved in serum treated samples.

3.4 Substance P and CGRP Release

SP and CGRP in the medium was evaluated by ELISA. The SP and CGRP concentration increased following capsaicin treatment, and decreased on the day of serum treatment (Figure 37). Then SP was maintained at a lower level (~220pg/ml), whereas CGRP appeared to be increased 4 days after serum treatment. There was no significant secretion of SP and CGRP in

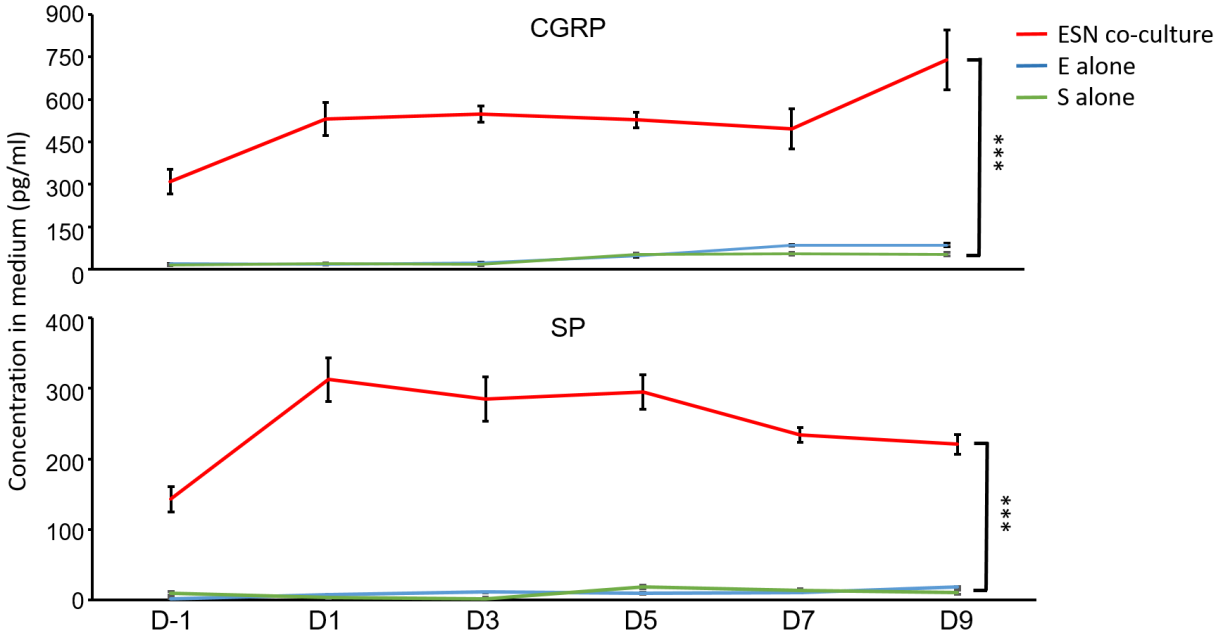

***Figure 37**. ELISA of substance P and CGRP secretion from capsaicin stimulated samples. The concentration of substance P and CGRP both increased after stimulation and was higher than in the control group. The data were collected from n>3 from three independent experiments. ***P<0.0001.*

the monoculture control group (Figure 37).

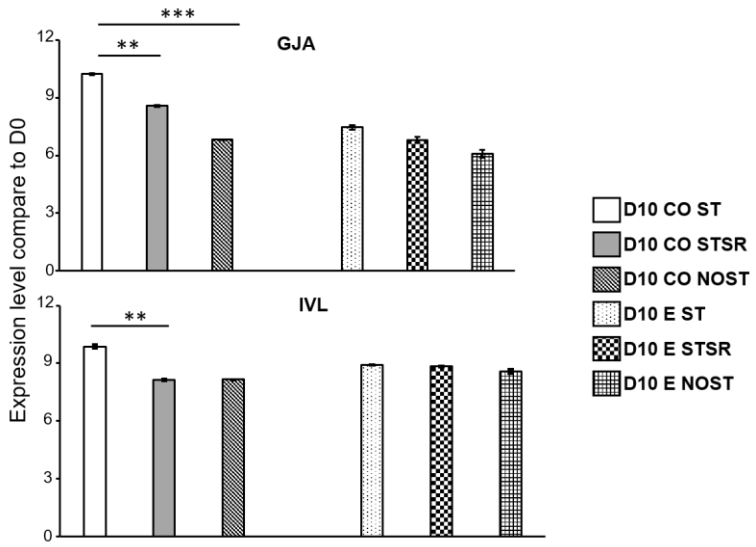

Figure 38. *Q-PCR result for GJA and IVL expression from hCECs after capsaicin stimulation. Samples are collected on day 10 after stimulation from co-cultures (D10 CO ST, D10 CO STSR, D10 CO NOST), and mono-cultures (D10 E ST, D10 E STSR, D10 E NOST). ST stand for stimulated but not treated with serum. The STSR group was treated with serum and NOST means non-stimulated group. GJA and IVL were upregulated in ST monoculture and co-culture groups. Serum treated samples had higher GJA expression than monoculture and non-stimulated groups. The data was collected from n>2 experiments. ***P<0.0001; **P<0.001.*

3.5 HCECs, hCSSCs and hNs Marker Expression After Capsaicin Stimulation

In Figure 38, both GJA and IVL had the highest expression in the capsaicin stimulated co-cultures (D10 CO ST). In Figure 39, LUM, ALDH3A1 and KERA expression were decreased for D10 CO ST samples. The serum treated group (D10 CO STSR) had comparable LUM, KERA and ALDH3A1 expression with non-stimulated co-cultures (D10 CO NOST). In hCSSCs mono-cultures, the LUM, KERA and ALDH3A1 expression were only detected in the non-stimulated group (D10 S NOST), while ACTA2 was down regulated in all the groups. The

expression of TAC1 and BDNF was highest D10 ST group, while CGRP expressed highest in serum treated group D10 STSR (Figure 40).

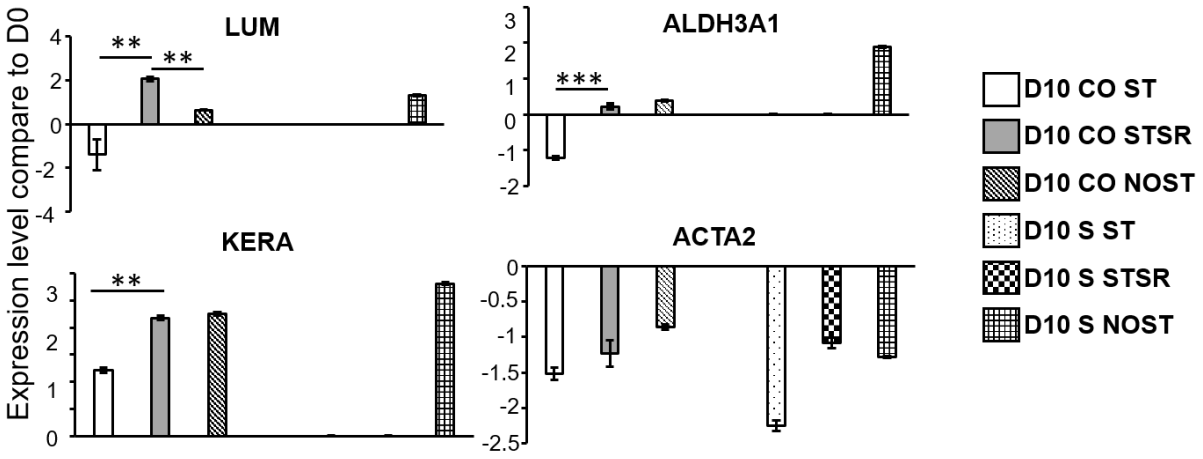

Figure 39. *Q-PCR results for LUM, ALDH3A1 KERA and ACTA2 expression from hCSSCs after capsaicin stimulation. Samples are collected on day 10 after stimulation from co-cultures (D10 CO ST, D10 CO STSR, D10 CO NOST), and mono-cultures (D10 S ST, D10 S STSR, D10 S NOST). ST stand for stimulated but not treated with serum. STSR group was treated with serum and NOST means non-stimulated group. LUM, ALDH3A1, KERA expression in ST groups were less than STSR group and NOST group. Expression of ACTA2 was down regulated in all the groups. No significant LUM, ALDH3A1 and KERA expression was detected in S, ST and S STSR groups. The data was collected from n>2 experiments. ***P<0.0001; **P<0.001.*

IV. Discussion

Being able to respond to damage and treatment in a physiological relevant manner indicates the functionality of *in vitro* model. Here we used capsaicin, which causes pain upon application [231] and epithelium ulcer and nerve degeneration in long term [229, 232]. In clinic, serum eye drops which contain a cocktail of growth factors including EGF, TGF-β, fibronectin, IGF-1 and

NGF is considered as one of the most effective treatments for corneal epithelium and nerve defect [233, 234]. Here we applied healing medium containing 10% FBS following capsaicin exposure, to mimic serum eye drop treatment and measure injury response using the innervated cornea model.

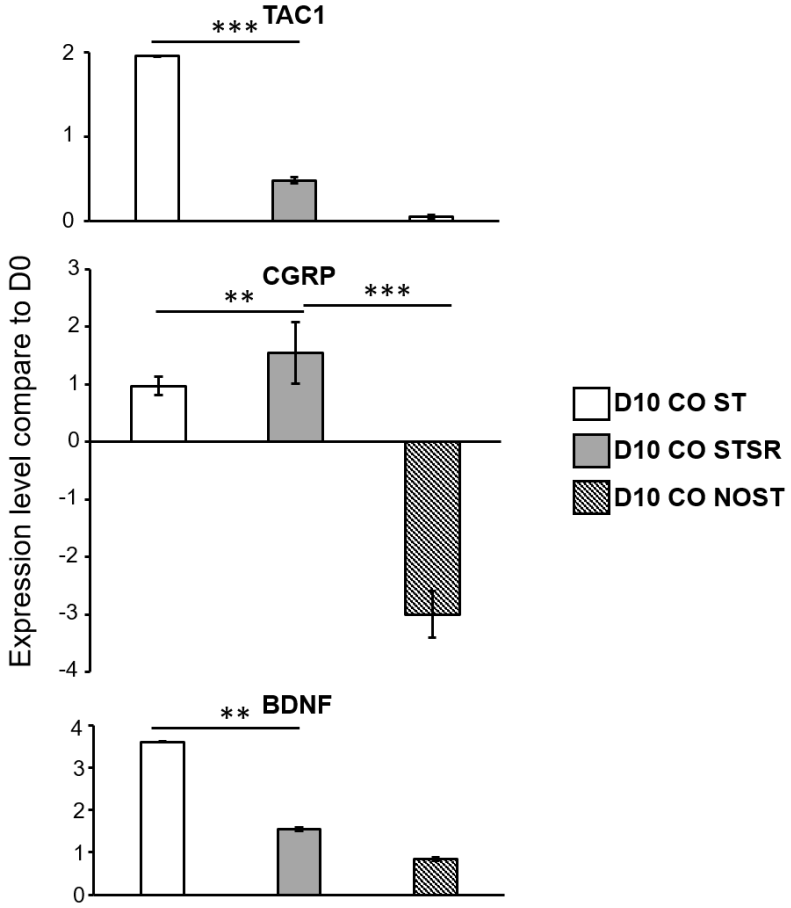

Figure 40. *Q-PCR result for TAC1, CGRP and BDNF from neuron after capsaicin stimulation. Samples are collected on day 10 after stimulation from co-cultures (D10 CO ST, D10 CO STSR, D10 CO NOST). ST stand for stimulated but not treated with serum. STSR group was treated with serum and NOST means non-stimulated group. TAC1, CGRP and BDNF expression was upregulate in ST groups. Serum treated group have lower BDNF, TAC1 and higher CGRP expression than ST group. The data was collected from n>2 experiments.*

Through confocal images, the decrease of axonal density, hCECs and hCSSCs confluency were observed in ST group indicating capsaicin caused *in vitro* tissue damage. Interestingly we observed increased GJA and IVL expression from hCECs in both co-cultured and monocultured ST groups, showing the capsaicin stimulation improved the maturity of the epithelium. In human cornea, epithelial cells respond to trauma by proliferating and migrating towards the injured site [235]. Thus, it is likely the hCECs increased the synthesis of its functional marker to perform its protective function. For hCSSCs, in confocal images, cell confluency was decreased in ST group compared to NOST group. This agreed with keratocytes apoptosis after epithelium injury observed in clinic[236]. In q-PCR results, the D10 S ST group showed no ECM marker expression. However, ECM markers were expressed in the D10 CO ST group. These results indicated the importance of neuronal innervation in maintaining the functionality of corneal stroma.

The healing medium containing 10% FBS improved the cell confluency of hCECs, hCSSCs, and the density of innervation after capsaicin exposure. The comparable ECM marker expression from hCSSCs in D10 CO STSR and D10 CO NOST groups showed the serum treatment is effective in restoring corneal stromal cell functionality. This matches the healing effect observed through the recovery of corneal epithelium[237-239] and innervation[240] in human patients that used serum eye drops.

SP and CGRP are found in tears during conreal pain cause by dry eye syndrome [241] and after capsaicin stimulation [223, 242]. These pain mediators are secreted by mature and functional

human sensory neurons[217, 243, 244]. Both SP and CGRP can regulate stratification of corneal epithelial cells, restoring epithelial barrier function, and improving wound healing in animal models [245, 246] [247]. Thus SP and CGRP are measured assessing the pain response on corneal tissue model. Here, we found the SP and CGRP concentration in culture medium increased after capsaicin stimulation and decreased after serum treatment. The SP and CGRP are secreted from hNs in the scaffold as no significant release was detected from the hCECs and hCSSCs monocultures. Q-PCR results demonstrated cellular expression of TAC1, CRCP which agreed with ELISA data. This study shows the first method able to to detect SP, CGRP release from capsaicin stimulated human sensory neurons in an *in vitro* environment. This demonstrated the maturity and functionality of innervaiton and further indicated the pain-like response in the innervated corneal tissue model may be achieved.

Futher, the data established the utility of the model for future drug toxicity testing, due to its ability to withstand trauma and to recover under certain treatments.

V. Conclusion

The innervated corneal tissue model responded to capsaicin stimulation, and generated pain-like reaction in a similar fashion to the human cornea. Furthermore, clinically suitable serum eye drops treatments that appear to be effective in human eye traumatic injury showed comparable healing effects within the tissue model. These results indicate the tissue model can potentially replace animal models for future toxicity testing and drug development.

Chapter VII Future Directions

I. Summary

The need for human corneal tissue models as research and drug screening tools continues to expand, with few available options currently on the market [248]. The tissue 3D *in vitro* corneal tissue model described in this thesis combined human corneal cells and sensory neurons. A custom bioreactor system was also designed to adjust aqueous humour and tear compositions. The reaction also allows user input for the TF rate and IOP. Taken together, the bioreactor system provides a platform for capturing corneal features in both native and pathological

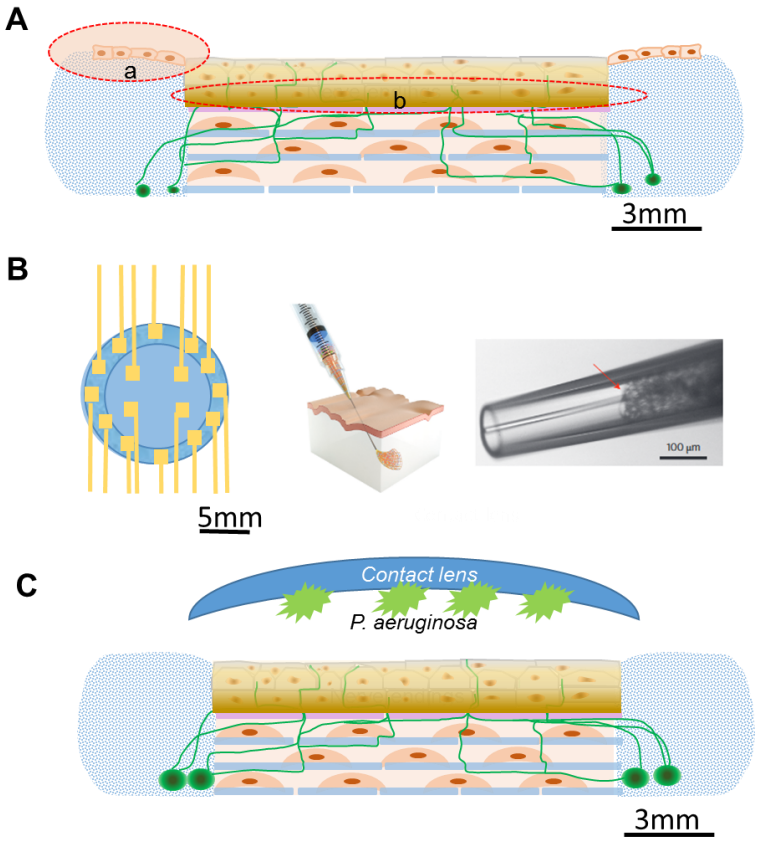

Figure 41. *Future directions. A: (a) Adding corneal limbus epithelial cells in the system, (b)optimizing stamped silk films to improve nerve and epithelium confluency. B: Electrode design on silk films and injectable electrodes for the detection of nerve firing [3]. C: Introducing bacteria to the surface as a corneal infectious disease model.*

environments. This tissue model and dynamic cultivation system is a state of the art technological advancement in the field for corneal *in vitro* models.

Our publications using this model have shown cornea-neuron crosstalk among multiple cell types that resulted from long-term culture [35, 36]. Further, we recorded pain-like reactions showing potential to replace animal models for studying corneal physiology, pathology, and drug development. A next step towards more fully replicating the anatomy and function of the cornea is the incorporation of limbus epithelial cells and endothelial cells into our multi-cellular and dynamic model system. The hypothesis for future directions is that by including corneal limbus epithelial cells, endothelial cells and native tear components, improved functional corneal tissue equivalents can be achieved. This tissue model can be used to mimic acute pain responses and corneal infectious diseases. The results from these studies will contribute towards our knowledge of treating corneal diseases, which remains the second major cause of blindness, affecting 7 million people around the world [4].

II. Specific Aims

Aim 1. Optimization of current tissue model

The objective is to further mimic corneal tissue structure including the confluence of epithelium, the density of innervation, the involvement of endothelial cells, and the components of tear fluid. We plan to: (a) introduce corneal limbus epithelial cells and endothelial cells to the current tissue model to represent the human corneal cellular components, (b) optimize the concentration of NGF and include GDNF and BDNF to gain physiologically relevant innervation density and length, (c) include the proteins in native tears and compare the function of the tissue models (e.g., nerve density, length, epithelial thickness, stromal ECM secretion) to reported human data (Figure 41A). The outcome of this effort will be more physiological relevant human tissue

corneal equivalents to assess the interaction between endothelial, epithelial, stromal cells and innervation.

Aim 2: Corneal pain model

The objective is to track tissue functions *in vitro* under nociceptive stimulation using trans-epithelial electrical resistance (TEER), and local field potential measurements (LFP). We will also track ECM remodeling under nociceptive stimulation using transmission electron microscopy (TEM). We plan to first design an electrode pattern on silk substrates for the corneal tissue model to detect nerve firing (Figure 41 B). E-Phys readouts and ECM organization will be compared between normal and stimulated samples to assess changes over time. The results will contribute to drug screening, accelerating wound healing and related needs.

Aim3: Corneal infectious disease model

The objective is to study corneal inflammatory responses and barrier functions *in vitro* by infecting the corneal equivalent with *Pseudomonas aeruginosa*. The approach will be to introduce *P. aeruginosa* through a contact lens and compare outcomes (e.g., LFP, TEER, innervation density, inflammation and pain mediator release) to current clinical results from human patients (Figure 41 C). These results will establish a foundation for the system regarding mimicking disease.

III. Aim 1. Optimization of Current System

1.1 Goal

We aim to optimize the current tissue model to achieve denser innervation and more confluence of the epithelium. We will incorporate additional endothelial cells to the current *in vitro* corneal tissue model to enhance functional relevance. Toward this goal we will optimize silk film surface topography and protein decoration to support innervation, epithelial and endothelial cell growth.

Table 4. *Summarize of current result and needed improvements*

Task	Current results	Improvement needed
Innervation	Density : 100termini/cm^2 Length: 3mm	Increased density and length
Epithelium	Regional multilayer growth	Increase confluence
Endothelial	No endothelial layer	Optimize scaffold to support endothelial layer
Tear component	Using hCSSCs differentiation medium with NGF	Involve different proteins in medium

1.2 Background

Human corneal limbus epithelial cells have been cultured on silk substrates.[249-252]. However the effect of these cells upon innervation and the corneal stroma remain unclear. Corneal limbus stem cells can differentiate into epithelial cells and migrate to cover the wound site during the corneal healing process[253] which will benefit future applications in corneal wound healing models.

Meanwhile, the corneal endothelium layer serves important pumping functions and is crucial for corneal transparency. Engineering of corneal endothelium has been explored mainly using type I

collagen, gelatin, chitosan, decellularized tissue matrices [254-256] and decellularized amniotic membrane [257]. However all of these materials have their limitations due to lack of transparency, degradability and mismatched mechanical properties with native tissue. Silk substrates as discussed in this thesis can be an ideal material for corneal endothelial cell cultivation. By including an additional silk film layer that contains endothelial cells, the corneal tissue model will more completely mimic the cellular composition and total function of the tissue. Aside from additional cellular components, the density of innervation may also be improved. The native cornea has an innervation density of ~300 termini/mm^2. The average density of axons in the chicken DRG innervated system reached 100 termini/mm^2, and for human sensory neurons (hNs), the innervation was less dense and did not reach the center of the scaffold. BDNF and GDNF were reported to improve nerve branching [258], and will be included in the silk film to improve hNs innervation.

To further improve cellular growth, tear components can also be optimized. Native tear films consist of 3 layers: lipid, aqueous and mucin [259].The combination of all three layers enhances functionality and biological relevance. The current medium-based tear flow can serve as the aqueous layer. The addition of a lipid layer can prevent evaporation of tears, enhancing the functionality of the epithelial layer [260]. A mucin layer may be used to entrap drug components [82] in the human eye and can provide a more relevant tissue model for drug development. With these optimization plans, the model will gain more complete corneal functions.

1.2 Experimental Design

1.2.1 Optimization of Epithelium

Improved corneal epithelial cell confluency can be achieved through optimization of cell source and scaffolds. The hCECs purchased from ThermoFisher can only be passaged 4 times, with the proliferation rate decreasing as passage number increases. To improve the viability of epithelial cells, human limbus epithelial cells will be isolated from donor cornea and cultured on the top layer of silk film stacks following the previously reported method [251, 261, 262]. Growth factors (KGF, NGF, HGF, EGF) embedded in silk films will be prepared and used as the top layer of the silk film stacks to support epithelial cell growth and guidance of innervation [263]. The concentration of growth factors will be adjusted for optimal confluency of the hCECs.

1.2.2 Optimization of Innervation

To improve the density and the length of innervation, the concentration of NGF will be increased to 100 ng/mL in the co-culture medium from the currently used 50 ng/mL. GDNF, BDNF, and NT-3, which are growth factors reported to improved neuronal extension and branching [264], will also be added to the stamped films or the medium (Figure 41 A). The concentration of growth factors (50,100,200,400 ng/ml) will be optimized to have improved density and length of innervation.

1.2.3 Optimization of tear film

Lipid and mucin layers will be mimicked in the tear films. Phosphatidylcholine and phosphatidylethanolamine account for 88±6% of all identified tear lipids [265]. These compounds will be added to hCSSCs differentiation medium and used as the tear fluid in the bioreactor. The concentration of phosphatidylcholine and phosphatidylethanolamine (1, 2, 4, 8, 16 %) will be adjusted to provide a multilayer homogenous epithelium. Goblet cells which secrete mucin on the ocular surface [266] in native cornea will be incorporated in the tissue model. Our collaborator (Darlene A. Dartt, Massachusetts Eye and Ear) has reported methods for cultivating goblet cells on RGD functionalized silk films [267]. The co-culture medium will be optimized to support goblet cell survival. Meanwhile, different proteins involved in the native aqueous layer (Table 4) can also be considered for inclusion in the tear medium to provide a more complete tear fluid.

Table 5. *Proteins in human tear*

Name	**Reference**	**Name**	**Reference**
Von Ebner's gland protein , serum albumin	[268]	Extracellular glycoprotein lacritin precursor	[269]
Transferrin: serotransferrin precursor	[79]	Oxygen-regulated protein 1	[270]
Lysozyme	[271]	Clusterin precursor	[79]
IgA, IgG, IgM	[272]	Mesothelin precursor	[273]
Lactoferrin	[274]	Lipophilin A precursor	[79]
Epidermal growth factor	[275]	Antileukoproteinase 1 precursor	[79]
Aquaporin 5	[276]	Aspartyl aminopeptide	[79]
a-Defensins	[277]	60S ribosomal protein L18a	[278]
G-rich sequence factor-1 (GRSF-1)	[278]	Phospholipid transfer protein precursor	[279]
Mammaglobin B	[280]	Chloride intracellular channel protein 2	[79]
Phospholipase A	[281]	KFLA590	[278]

Besides optimizing components of the tears, the methods to apply the tears on the scaffold surface can be improved. In the current model, a custom designed lid applied tear fluid dropwise onto the top surface of the scaffold. However, tear fluid in human cornea is pushed and spread

across the whole surface through eye blinking movement. An engineered device that lightly removes the liquid from the surface of the scaffold would better mimic the eyelid and tear film renewal, but this can also cause damage to the tissue model. An alternative strategy is moving the tear drop opening to the side of the scaffold, prompting fluid to flow across the scaffold surface, similar to blinking.

1.2.4 Inclusion of corneal endothelial cells

Cell culture and differentiation of human corneal endothelial cells (CEnCs) was described recently by Zhao & Afshari [282]. We will use the same protocols here, but with the goal to achieve co-culture and improve the efficiency and the integration of the endothelial layer into the corneal model for long-term cell culture (> 2 mo). An additional silk film layer embedded with ECM decoration including laminin, collagen type V and fibronectin will be applied on the bottom of the tissue model and contact the endothelium-seeded silk film. The concentration of ECM proteins and cultivation medium will be optimized to support endothelial cells co-culture with other cell types in the tissue model.

1.3 Evaluation

The optimization of the epithelium, innervation and tears are all aimed at improving the functionality of the tissue model. Trans-epithelial electrical resistance (TEER) measurements, and sodium fluorescein and rose bengal dye extrusion experiments will be used to reflect epithelium integrity[283]. Confocal imaging will be processed for the samples stained to reveal the tight junctions of the epithelium and β III tubulin of the neuronal innervation. The expression level of tight junction density and length of innervation will be quantified through Image J. Neuronal markers to be assessed by qPCR include calcitonin gene-related peptide (CRCP),

brain-derived neurotrophic factor (BDNF), tachykinin precursor 1(TAC1), transient receptor potential cation channel subfamily V member 1(TRPV1), Neurotrophic Receptor Tyrosine Kinase 1(NTRK1), melastatin-related receptor family 8 (TRPM8), Subtilisin-like serine protease 3 (SLP3) and transient receptor potential ion channels A (TRPA) as indicators of neural function. Confluency of endothelium along with the expression level of collagen III, IV, V , TJP1, CDH2, and ATP1A1 will be applied to evaluate endothelium function. The ideal concentration of lipid and proteins will be evaluated through the confluency of hCSSCs, hCECs , hCEnCs, and density of innervation.

Table 6. *Summary of variables, analysis and expected outcome for Aim 1*

Feature	***Variables***	***Analysis***	***Metric***
Cellular component			
Epithelium	Delivery method of growth factors (stamp and embedded) Concentration of HGF,KGF,EGF, NGF	TEER Confocal microscopy	Confluency of hCECs Numbers of cellular layers of epithelium
Innervation	NGF, BDNF, GDNF concentration (50, 100, 200ng/ml)	Confocal microscopy q-PCR	Nerve density and length Expression of sensory neuron markers (CRCP, BDNF, TAC1,TRPV1,NTRK1,TRPM8,TREK, SLP3,TRPA)
Endothelium	ECM decoration: laminin, collagen type V, fibronectin	TEM Fluorescence microscopy Immuno-histochemistry qPCR Proteomics	Surface morphology ECM production: increase of collagen III, IV, V, and interfibrillar distance Endothelial functionality: upregulated TJP1, CDH2, and ATP1A1 expression in endothelial cells cultured on optimized silk substrates; increased scaffold transparency and decreased tissue model thickness.
Physiological culture system			
Tear	Concentration of	Fluorescence microscopy Immuno-histochemistry qPCR Proteomics ELISA	Cell morphology: hCSSCs, hCECs, hCEnCs, neurons Proliferation (DNA content) Expression of corneal cell markers: GJA4, IVL, ALDH3A1, KERA, LUM, ACT2A, CK3, CK12

1.4 Expected Outcomes

We expect to observe improved TEER values and sodium fluorescein and rose bengal dye dot with defined edges when the optimum epithelium growth is achieved [284]. Human sensory nerve innervation with length ~4 mm and density ~100 termini /mm^2 will be considered as the optimal nerve outgrowth. Survival of endothelial cells and increased expression of TJP1, CDH2 and ATP1A1 as culture time is increased are expected when laminin, collagen type V and fibronectin are included in the scaffold. Epithelial confluency, corneal cell markers expression, innervation density and neuronal marker expression are foreseen to increase when lipid and tear proteins are involved in the tear fluid in dynamic cultivation.

IV. Aim 2. Corneal Wound Healing and Pain Model

2.1 Goal

We aim at utilizing electrical physiology measurement of the corneal tissue model to assess the tissue in both normal and wounded states to compare changes over time during recovery/repair. The goal is to utilize pain response as a suitable measure of the benefits of this multiple cell type tissue system towards proper healing for comparisons against suitable control systems.

2.2 Background

Corneal pain is a symptom associated with corneal diseases, such as inflammation, trauma and dry eye syndrome [59]. Often, the level of pain correlates to the effectiveness of a drug treatment [285]. However, this critical perspective is not included in current commercially available corneal tissue models [26] due to the lack of functional innervation. In Chapter VI we described the secretion of pain mediators SP and CGRP after capsaicin stimulation, indicating that the

tissue model can generate a pain-like response. However, nerve firing behavior detected through electrical physiology measurements (E-Phys) is considered the gold standard of measuring neuropathic pain [286] and needs to be evaluated to show the full functionality of the model. In 3D environment, local field potential (LFP) measurements, which capture the summed electric current flowing from nearby neurons, within a small volume of tissue [287] is an appropriate assessment of nerve firing upon stimulation. The occurrence of Allodynia (firing to non-painful stimuli) or hyperalgesia (heightened pain response to normal stimuli) is an indication of chronic pain which can also be characterized with LFP.

2.3 Experimental design

The tissue model will be cultured at the air-liquid interface for 28 days to achieve steady state, including cell confluency and innervation. The tissue model will then be injured in the epithelial layer or the epithelial and stromal layers. To generate acute pain response, both mechanical and chemical wound will be applied on the epithelial layer. To injure the epithelial layer, a rotating epithelial brush used in the clinic to remove epithelial cell and expose stroma will be applied. The brush will not penetrate the silk film while generating a controlled injury with the smooth edge of the brush head [288]. By gently placing the brush head (0.5, 1 and 3.5mm) on the top surface of the tissue model, a circular injury site will be generated. To injure the epithelial and stromal layers, a clinically used diamond blade will be applied to cut a 3mm long wound [289]. Different sizes of blades (0.1, 0.15, and 0.2 mm) will be tested to establish control of depth of injury and maintenance of tissue model integrity. The size of the brush, blade, and length of injury will be optimized to allow maintenance of tissue model integrity and complete cell regrowth within 2 weeks. The chemicals listed in Table 6 will be applied topically on the epithelium to generate chemical injury. The concentration of chemicals will be optimized to

avoid massive cell apoptosis. To accelerate wound healing, human serum which is used to improve corneal wound healing will be purchased from Thermofisher and added in the medium. The concentration of serum and duration of treatment will be optimized based on the rate of cell migration and growth, and marker expression from the hCECs and hCSSCs. The serum treatment effect will be compared with saline containing 5mg/ml albumin which mimic the protein concentration of tears [290]. Medium containing curcumin (EGF receptor inhibitor) and SU5402 (FGF receptor inhibitor) will be used to culture the negative control group. Different concentrations of curcumin (1, 2, 3X 10^{-4} M) and SU5402 (25, 50, 100 M) [291, 292] will be applied on the tissue model for optimal suppression of cell regrowth without causing apoptosis.

2.4 Evaluation

To detect nerve firing upon stimulation, calcium signaling during acute pain reactions should first be examined. Due to the change of firing threshold after each stimulation, a novel electrical signal recording device that captures the signal from the multiple locations on the scaffold simultaneously is needed to provide statistically significant results. A custom designed electrode (Figure 41 C) will be manufactured by sputter coating electrodes on silk films using photolithography [293]. The silk film works as a carrier for the electrodes which can be applied to the bottom of scaffold prior stimulation. The films will dissolve, leaving the electrodes in direct contact with neurons seeded on the bottom of the scaffold. Each electrode will have their own outlet. The electrodes located at the outer ring will collect neuronal response to stimuli, while the center electrodes will collect signals from the corneal cells. The electrode will be kept on the bottom surface of the scaffold for 28 days after the injury. The LFP measurements will be processed every 3 days to observe changes of firing threshold.

Table 7. *Summary of variables, analysis and expected outcomes of Aim 2*

Injury	***Variable***	***Analysis***	***Metric***
Epithelium Stroma	Brush head (0.5, 1, and 3.5mm) Diamond blade (0.1, 0.15, and 0.2 mm) Albumin, serum (5,10%) Macrophages/neutrophils (numbers and frequency) Cytokines (TNF-α, IL-1b, IL-12, IL-8, MIP-1 α/β) Treatment time (24 to 48h) Curcumin (1,2,3X10^{-4}M), SU5402 (25,50,100M) [291, 292]	TEER LFP TEM Histology Confocal microscopy Immuno-histochm qPCR ELISA	Epithelium barrier function – 400-500 Ω*cm^2 in non-injured samples, before injury [284], sodium fluorescein/rose Bengal dye (121) Nerve firing – peaks in LFP ECM organization – collagen misalignment injury site Cell morphology – regrowth of hCECs; elongated hCSSC, density and length of axons <u>Post injury marker expression</u>: hCECs: -TJA, +GJA4,+ IVL hNs: +CRCP, + BDNF, +TAC1, -TRPV1, -NTRK1, -TRPM8, -TREK, -SLP3, -TRPA, hCSSCs: -ALDH3A1, -KERA, -LUM, +ACT2A

2.5 Expected outcomes:

A wound healing model that provides pain response relevant outcomes to human systems, while also helping to assess the relative contributions of inflammatory components will be the main outcome. We expect the TEER value to decrease to less than 300 Ω*cm^2 [294] after injury followed by gradual increases as the epithelium heals and the cells form tight junctions. Further, we anticipate that this recovery phase will be accelerated in the cornea model with all cell types present; in contrast to the scaffolds where given cell types are missing. An LFP peak is expected upon scratching or exposure to chemicals on the tissue model, with a larger impact in the deeper wounds (epithelium and stroma vs. epithelium alone). Occurrence of allodynia (firing to non-painful stimuli) or hyperalgesia (heightened pain response to normal stimuli) is expected in long term LFP measurement as indications of chronic pain. The release of pain mediators in the culture medium including SP, CGRP, and BDNF is anticipated to increase after stimulation and decrease after treatment with antibiotics.

The injured sample is also expected to display an irregular ECM organization after healing in comparison to the uninjured control systems. The regrowth rate of hCECs and hCSSCs is anticipated to be faster in the serum treated group than in the non-treated group and inhibited

group. A change of hCSSCs cell shape could be observed at the healed injury site. A change of marker expression in hCECs, hCSSCs and sensory neurons (**Table 2**) is also anticipated.

2.6 Alternative plan:

We have observed DRG neuronal firing in response to menthol stimulation through calcium imaging. However, we have not captured hNs firing through calcium imaging. This is partially due to the hNs innervation occurred with much thinner axons than DRG neurons and are more difficult to locate in the scaffold. This can be solved by labeling neurons with DiI to visualize the nerves in the calcium imaging samples.

Contact between neuron cell soma and electrode is needed for the proposed electrode design. Additionally, the silk sponges and collagen hydrogel in the scaffold may interfere with signal detection. As an alternative method, an injectable electrode may be applied (Figure 41 C) with a mesh structure, to improve the contact with the neurons. These methods can provide a sensitive and high throughput assessment of the acute pain response [295].

After the methodology of electrophysiological recording is optimized, other nociceptive stimuli may be tested on the model to further support functional innervation. Menthol (above 2 mN) which activates TRPM8 [296] and mechanical stimulation (stress above 55 mmHg) that triggers TRPA1[297] may be tried. Temperature stimuli (above 50°C) should also be included due to nerve firing at low and high temperatures may occur as a function for eye blinking [298-300]. In animal corneal experiments, local pH was tuned by blowing CO_2 onto the corneal surface [301],

which created a pain response without damaging the tissue. A similar method can be used in our model to stimulate and observe acute pain reactions without causing injury.

III. Aim 3. Corneal Infectious Disease Model

3.1 Goal

To evaluate the function and utility of the cornea model for diseased tissue, the full thickness corneal tissue model will be assessed as an *in vitro* screening tool to sense and respond to inflammation stimuli. The ability to react to pathogens is crucial for application in drug screening.

3.2 Background

Worldwide, corneal infectious diseases have compromised the vision of more than 250 million people and have blinded over 6 million individuals [302]. Reduction of nerve fibers, bundles, and branching occurs when a cornea is infected [59]. *Pseudomonas aeruginosa* is one of the most feared contact related infectious pathogens that often leads to severe tissue damage due to its ability to secrete collagenase [303]. One of the common sources of corneal *P. aeruginosa* infection is through contact lenses [304]. Current treatment uses antibiotic-containing eye drops but are often unsuccessful in stopping the progression of the disease. A corneal tissue model exposed to *Pseudomonas aeruginosa* can provide opportunities to study the infections and to identify new models for drug development.

3.2 Experimental design

The corneal tissue model will be cultivated at an air-liquid interface for 28 days prior and transferred to bioreactor for cultivation with *P. aeruginosa*. TF and IOP will be applied to the

tissue model. Then, a contact lens carrying GFP-labeled *P. aeruginosa* will be applied on the top surface of the scaffold. The number (10,50,100 bacteria/cm^2) and viability of *P. aeruginosa* as well as contacting time (5,10,15 seconds) will be optimized to allow inflammation response without causing massive apoptosis of corneal cells. After the exposure to bacteria, the tissue models will be cultured in a bioreactor using antibiotics-free artificial tear fluid to allow bacterial spreading. Afterward, gentamicin and amikacin supplemented artificial tear fluid will be applied to improve tissue healing. Antibiotics type and concentration (0.7,1.4,2.8 %) will be optimized to provide effective treatment. The treatment will last for 7 days with culture medium collected every 2 days.

3.3 Characterization

Real-time Z-axis confocal images will be taken every 30 min on the first day and every 4 hours from day 2 to 7. The maximum projected image on XZ-axis will be generated through image J. The distance from GFP-labeled bacteria to the surface of tissue model will be quantified in each image to evaluate the speed of bacteria penetration. Beside the real-time confocal imaging, samples will also be fixed on day 1,3,5,7 and stained with anti-β III tubulin antibody to observe the change of cell morphology. Western-blot against inflammation mediators (TNF-α, IL-1b, IL-12, IL-8, MIP-1 α/β) and pain mediators (SP, CGRP, BDNF) will be tested on the medium collected from the samples. TEER and LFP measurement will be applied to evaluate the change of epithelial barrier function and neuronal sensitivity during infection. The outcomes will be compared between infected, non-infected and antibiotic treated groups.

***Table 8**: Summary of variables, analysis and expected outcomes of Aim 3*

Task	***Variable***	***Analysis***	***Metric***
Infection	Amount of bacteria (10,50,100/cm^2) Viability of bacteria (culturable and non-culturable) Contacting time (5,10,15 seconds) Timing of infection (1, 2, 3 months in dynamic cultivation)	TEER LFP Real- time Confocal microscopy Westernblot	Epithelium barrier function – 400-500 Ω*cm^2 in non-infected samples, before infection [284] and after antibiotics treatment. Nerve firing – decrease of firing threshold in LFP Bacterial penetration-GFP labeled bacteria move deeper into the tissue model as time. Cell morphology – regrowth of hCECs; elongated hCSSC, decreased density and length of axons <u>Post infection marker expression</u>: hCECs: -TJA, +GJA4,+ IVL hNs: +CRCP, + BDNF, +TAC1, -TRPV1, -NTRK1, -TRPM8, -TREK, -SLP3, -TRPA, hCSSCs: -ALDH3A1, -KERA, -LUM, +ACT2A
Treatment	Choice of antibiotics (gentamicin or amikacin) Concentration of antibiotics (0.7,1.4 2.8%) Timing of treatment (day 1,3)		

3.4 Expected outcome:

A corneal infection model can be utilized as a platform for drug development. We anticipate to observe less than 10% of GFP-labeled *P. aeruginosa* penetrate the tissue model with the majority of the bacteria blocked by the epithelium. In the epithelium infected by more viable bacteria, the TEER value is expected to decrease after the infection. Inflammation reaction will be observed through elevated secretion of inflammation mediators (TNF-α, IL-1b, IL-12, IL-8, MIP-1 α/β) and pain mediators (SP, CGRP, BDNF). These mediators are anticipated to be secreted less from tissue model after antibiotics treatment. Inflammation status caused chronic pain will be observed by an increased firing threshold in LFP measurement. Cell confluency and innervation density are expected to decrease after infection and increase after antibiotics treatment in epithelium and stroma.

3.5 Alternative plan:

Co-cultivation of mammalian cells and bacteria could be challenging. Alternatively, inflammation mediators can be used to mimick a diseased environment. Cytokine interleukin-6 (Il-6) is associated with keratitis and corneal ulcers caused by *Pseudomonas aeruginosa* infection [305]. Il-6 can be directly added in the tear solution or the scaffold to mimic the inflammation environment. The concentration and loading time of IL-6 can be optimized to have an effect on the corneal and neuronal cells without triggering abundant cell apoptosis.

IV. Conclusions

The disease models for acute pain, chronic pain and corneal infectious diseases can be built using the current corneal tissue models described here. By evaluating the response to pathological cues, the functionality of the tissue model can be further investigated. The establishment of corneal *in vitro* disease models should open a new page in ocular disease research and drug development.

Chapter VIII. References

1. Rocha, G., *Use of a disposable artificial anterior chamber for trans-epithelial trephination and endothelial keratoplasty.* 2007.
2. Abraham, T., et al., *Quantitative assessment of forward and backward second harmonic three dimensional images of collagen Type I matrix remodeling in a stimulated cellular environment.* Journal of structural biology, 2012. **180**(1): p. 17-25.
3. Liu, J., et al., *Syringe-injectable electronics.* Nature nanotechnology, 2015. **10**(7): p. 629-636.
4. Whitcher, J.P., M. Srinivasan, and M.P. Upadhyay, *Corneal blindness: a global perspective.* Bulletin of the world health organization, 2001. **79**(3): p. 214-221.
5. Wipperman, J.L. and J.N. Dorsch, *Evaluation and management of corneal abrasions.* American family physician, 2013. **87**(2).
6. Rozsa, A.J. and R.W. Beuerman, *Density and organization of free nerve endings in the corneal epithelium of the rabbit.* Pain, 1982. **14**(2): p. 105-120.
7. Orwin, E., et al., *Bioreactor design for cornea tissue engineering: Material–cell interactions.* Acta biomaterialia, 2007. **3**(6): p. 1041-1049.
8. Nishida, K., et al., *Corneal reconstruction with tissue-engineered cell sheets composed of autologous oral mucosal epithelium.* New England Journal of Medicine, 2004. **351**(12): p. 1187-1196.
9. Belmonte, C., et al., *What causes eye pain?* Current ophthalmology reports, 2015. **3**(2): p. 111-121.
10. Wu, J., et al., *Bioengineering organized, multilamellar human corneal stromal tissue by growth factor supplementation on highly aligned synthetic substrates.* Tissue Engineering Part A, 2013. **19**(17-18): p. 2063-2075.
11. Liu, W., et al., *Recombinant human collagen for tissue engineered corneal substitutes.* Biomaterials, 2008. **29**(9): p. 1147-1158.
12. Short, B.G., *Safety evaluation of ocular drug delivery formulations: techniques and practical considerations.* Toxicologic pathology, 2008. **36**(1): p. 49-62.
13. Trials.gov, C., *List of Clinical Trial Sponsors.* 2008.
14. Gower, N.J., et al., *Drug discovery in ophthalmology: past success, present challenges, and future opportunities.* BMC ophthalmology, 2016. **16**(1): p. 1.
15. Watch, C. *FDA Approved Drugs for Ophthalmology*. 2016; Available from: https://www.centerwatch.com/drug-information/fda-approved-drugs/therapeutic-area/13/ophthalmology.
16. Huml, R.A. and C.R. RAC, *Key challenges to US topical ocular drug development.* Regulatory Focus, 2009. **14**: p. 47-52.
17. Mitra, A.K., *Ophthalmic drug delivery systems*. Vol. 130. 2003: Informa Health Care.
18. York, M. and W. Steiling, *A critical review of the assessment of eye irritation potential using the Draize rabbit eye test.* Journal of Applied Toxicology, 1998. **18**(4): p. 233-240.
19. Kupferberg, H., *Animal models used in the screening of antiepileptic drugs.* Epilepsia, 2001. **42**(s4): p. 7-12.
20. Smee, D.F. and R.W. Sidwell, *A review of compounds exhibiting anti-orthopoxvirus activity in animal models.* Antiviral research, 2003. **57**(1): p. 41-52.
21. Davila, J.C., et al., *Predictive value of in vitro model systems in toxicology.* Annual review of pharmacology and toxicology, 1998. **38**(1): p. 63-96.
22. Curren, R.D. and J.W. Harbell, *Ocular safety: a silent (in vitro) success story.* ATLA-NOTTINGHAM-, 2002. **30**: p. 69-74.

23. Jester, J., et al., *Extent of initial corneal injury as a basis for alternative eye irritation tests.* Toxicology in vitro, 2001. **15**(2): p. 115-130.
24. Muir, C., *A simple method to assess surfactant-induced bovine corneal opacity in vitro: preliminary findings.* Toxicology letters, 1984. **22**(2): p. 199-203.
25. Xiang, G., et al., *Prediction of ocular irritancy of 26 chemicals and 26 cosmetic products with isolated rabbit eye (IRE) test.* Biomedical and Environmental Sciences, 2012. **25**(3): p. 359-366.
26. Shafaie, S., et al., *In Vitro Cell Models for Ophthalmic Drug Development Applications.* BioResearch open access, 2016. **5**(1): p. 94-108.
27. Mishima, S. and T. Kudo, *In vitro incubation of rabbit cornea.* Investigative Ophthalmology & Visual Science, 1967. **6**(4): p. 329-339.
28. Ware, L.B., *Modeling human lung disease in animals.* American Journal of Physiology-Lung Cellular and Molecular Physiology, 2008. **294**(2): p. L149-L150.
29. Madhan, K. and S. Raju, *Comparative histology of human and cow, goat and sheep liver.* Journal of Surgical Academia, 2014. **4**(1): p. 10-13.
30. Dunn, S.P., et al., *Corneal Graft Rejection Ten Years after Penetrating Keratoplasty in the Cornea Donor Study.* Cornea, 2014. **33**(10): p. 1003.
31. Griffith, M., et al., *Functional human corneal equivalents constructed from cell lines.* Science, 1999. **286**(5447): p. 2169-2172.
32. Doillon, C., et al., *A collagen-based scaffold for a tissue engineered human cornea: physical and physiological properties.* The International journal of artificial organs, 2003. **26**(8): p. 764-773.
33. Han, B., et al., *A fibrin-based bioengineered ocular surface with human corneal epithelial stem cells.* Cornea, 2002. **21**(5): p. 505-510.
34. Ramaesh, K. and B. Dhillon, *Ex vivo expansion of corneal limbal epithelial/stem cells for corneal surface reconstruction.* European journal of ophthalmology, 2003. **13**(6): p. 515-524.
35. Wang, S., et al., *Coculture of dorsal root ganglion neurons and differentiated human corneal stromal stem cells on silk‐based scaffolds.* Journal of Biomedical Materials Research Part A, 2015. **103**(10): p. 3339-3348.
36. Wang, S., et al., *In vitro 3D corneal tissue model with epithelium, stroma, and innervation.* Biomaterials, 2017. **112**: p. 1-9.
37. Cassin, B., S. Solomon, and M.L. Rubin, *Dictionary of eye terminology*. 1984: Triad Pub. Co.
38. Klintworth, G.K., *The cornea--structure and macromolecules in health and disease. A review.* The American journal of pathology, 1977. **89**(3): p. 718.
39. Yanez, B., et al., *Interfacial properties of corneal epithelial cells at different degrees of differentiation.* Investigative Ophthalmology & Visual Science, 2014. **55**(13): p. 1482-1482.
40. Leonard, B.C., et al., *Species variation and spatial differences in mucin expression from corneal epithelial cells.* Experimental Eye Research, 2016. **152**: p. 43-48.
41. Eghrari, A.O., S.A. Riazuddin, and J.D. Gottsch, *Chapter Two-Overview of the Cornea: Structure, Function, and Development.* Progress in molecular biology and translational science, 2015. **134**: p. 7-23.
42. Maurice, D.M., *The structure and transparency of the cornea.* The Journal of physiology, 1957. **136**(2): p. 263-286.
43. Beales, M.P., et al., *Proteoglycan synthesis by bovine keratocytes and corneal fibroblasts: maintenance of the keratocyte phenotype in culture.* Investigative ophthalmology & visual science, 1999. **40**(8): p. 1658-1663.
44. Robert, L., et al., *Corneal collagens.* Pathologie Biologie, 2001. **49**(4): p. 353-363.
45. Michelacci, Y.M., *Collagens and proteoglycans of the corneal extracellular matrix.* Brazilian Journal of Medical and Biological Research, 2003. **36**(8): p. 1037-1046.

46. Gipson, I.K. and T. Inatomi, *Extracellular matrix and growth factors in corneal wound healing.* Current opinion in ophthalmology, 1995. **6**(4): p. 3-10.
47. Schultz, G.S. and A. Wysocki, *Interactions between extracellular matrix and growth factors in wound healing.* Wound repair and regeneration, 2009. **17**(2): p. 153-162.
48. Radner, W., et al., *Interlacing and cross-angle distribution of collagen lamellae in the human cornea.* Cornea, 1998. **17**(5): p. 537-543.
49. Bron, A. and R. Tripathi, *The anterior corneal mosaic.* The British journal of physiological optics, 1969. **25**(1): p. 8-13.
50. Freund, D., et al., *Ultrastructure in anterior and posterior stroma of perfused human and rabbit corneas. Relation to transparency.* Investigative ophthalmology & visual science, 1995. **36**(8): p. 1508-1523.
51. Turss, R., et al., *Glucose concentration and hydration of the corneal stroma.* Ophthalmic Research, 1971. **2**(5): p. 253-260.
52. Komai, Y. and T. Ushiki, *The three-dimensional organization of collagen fibrils in the human cornea and sclera.* Investigative ophthalmology & visual science, 1991. **32**(8): p. 2244-2258.
53. Poole, C.A., N.H. Brookes, and G.M. Clover, *Keratocyte networks visualised in the living cornea using vital dyes.* Journal of cell science, 1993. **106**(2): p. 685-691.
54. Scott, J. *Keratan sulphate--a'reserve'polysaccharide?* in *European journal of clinical chemistry and clinical biochemistry: journal of the Forum of European Clinical Chemistry Societies*. 1994.
55. Meek, K.M., et al., *The organisation of collagen fibrils in the human corneal stroma: a synchrotron X-ray diffraction study.* Current eye research, 1987. **6**(7): p. 841-846.
56. Nucci, P., et al., *Normal endothelial cell density range in childhood.* Archives of Ophthalmology, 1990. **108**(2): p. 247-248.
57. Senoo, T. and N.C. Joyce, *Cell cycle kinetics in corneal endothelium from old and young donors.* Investigative ophthalmology & visual science, 2000. **41**(3): p. 660-667.
58. Maurice, D.M., *The cornea and sclera.* The eye, 1984. **1**: p. 1-158.
59. Shaheen, B.S., M. Bakir, and S. Jain, *Corneal nerves in health and disease.* survey of ophthalmology, 2014. **59**(3): p. 263-285.
60. Goldstein, E.B. and J. Brockmole, *Sensation and perception*. 2016: Cengage Learning.
61. Marfurt, C.F., et al., *Anatomy of the human corneal innervation.* Experimental eye research, 2010. **90**(4): p. 478-492.
62. Al-Aqaba, M.A., et al., *Architecture and distribution of human corneal nerves.* British Journal of Ophthalmology, 2010. **94**(6): p. 784-789.
63. He, J., N.G. Bazan, and H.E. Bazan, *Mapping the entire human corneal nerve architecture.* Experimental eye research, 2010. **91**(4): p. 513-523.
64. Müller, L.J., et al., *Corneal nerves: structure, contents and function.* Experimental eye research, 2003. **76**(5): p. 521-542.
65. Madduri, S., M. Papaloïzos, and B. Gander, *Synergistic effect of GDNF and NGF on axonal branching and elongation in vitro.* Neuroscience research, 2009. **65**(1): p. 88-97.
66. You, L., S. Ebner, and F.E. Kruse, *Glial Cell–Derived Neurotrophic Factor (GDNF)–Induced Migration and Signal Transduction in Corneal Epithelial Cells.* Investigative ophthalmology & visual science, 2001. **42**(11): p. 2496-2504.
67. You, L., F.E. Kruse, and H. Volcker, *Neurotrophic factors in the human cornea.* Investigative Ophthalmology and Visual Science, 2000. **41**(3): p. 692-702.
68. Hollows, F. and P. Graham, *Intra-ocular pressure, glaucoma, and glaucoma suspects in a defined population.* The British journal of ophthalmology, 1966. **50**(10): p. 570.
69. Karabatakis, V., et al., *Correlating intraocular pressure, blood pressure, and heart rate changes after jogging.* European journal of ophthalmology, 2004. **14**(2): p. 117-122.

70. Dielemans, I., et al., *Primary open-angle glaucoma, intraocular pressure, and systemic blood pressure in the general elderly population: the Rotterdam Study.* Ophthalmology, 1995. **102**(1): p. 54-60.
71. Cooper, R., et al., *Continual monitoring of intraocular pressure: effect of central venous pressure, respiration, and eye movements on continual recordings of intraocular pressure in the rabbit, dog, and man.* British Journal of Ophthalmology, 1979. **63**(12): p. 799-804.
72. Shimmyo, M., et al., *Intraocular pressure, Goldmann applanation tension, corneal thickness, and corneal curvature in Caucasians, Asians, Hispanics, and African Americans.* American journal of ophthalmology, 2003. **136**(4): p. 603-613.
73. Douthwaite, W.A. and A.K. Lam, *The effect of an artificially elevated intraocular pressure on the central corneal curvature.* Ophthalmic and Physiological Optics, 1997. **17**(1): p. 18-24.
74. Argus, W.A., *Ocular hypertension and central corneal thickness.* Ophthalmology, 1995. **102**(12): p. 1810-1812.
75. Schmid, K.L., et al., *Relationship between intraocular pressure and eye growth in chick.* Ophthalmic and Physiological Optics, 2003. **23**(1): p. 25-33.
76. Toris, C.B., C.B. Camras, and M.E. Yablonski, *Acute versus chronic effects of brimonidine on aqueous humor dynamics in ocular hypertensive patients.* American journal of ophthalmology, 1999. **128**(1): p. 8-14.
77. Gagnon, M.-M., et al., *Corneal endothelial cell density in glaucoma.* Cornea, 1997. **16**(3): p. 314-318.
78. Petroll, W.M., M. Vishwanath, and L. Ma, *Corneal fibroblasts respond rapidly to changes in local mechanical stress.* Investigative ophthalmology & visual science, 2004. **45**(10): p. 3466-3474.
79. Ohashi, Y., M. Dogru, and K. Tsubota, *Laboratory findings in tear fluid analysis.* Clinica chimica acta, 2006. **369**(1): p. 17-28.
80. Holly, F.J., *Formation and rupture of the tear film.* Experimental eye research, 1973. **15**(5): p. 515-525.
81. Jumblatt, M.M., R.W. McKenzie, and J.E. Jumblatt, *MUC5AC mucin is a component of the human precorneal tear film.* Investigative ophthalmology & visual science, 1999. **40**(1): p. 43-49.
82. Davidson, H.J. and V.J. Kuonen, *The tear film and ocular mucins.* Veterinary Ophthalmology, 2004. **7**(2): p. 71-77.
83. Doughty, M.J., *Assessment of short‐term variability in human spontaneous blink rate during video observation with or without head/chin support.* Clinical and Experimental Optometry, 2016. **99**(2): p. 135-141.
84. Pascolini, D. and S.P. Mariotti, *Global estimates of visual impairment: 2010.* British Journal of Ophthalmology, 2011: p. bjophthalmol-2011-300539.
85. Guthoff, R.F., et al., *Epithelial innervation of human cornea: a three-dimensional study using confocal laser scanning fluorescence microscopy.* Cornea, 2005. **24**(5): p. 608-613.
86. Von Korff, M. and K.M. Dunn, *Chronic pain reconsidered.* Pain, 2008. **138**(2): p. 267-276.
87. Apkarian, A.V., et al., *Human brain mechanisms of pain perception and regulation in health and disease.* European journal of pain, 2005. **9**(4): p. 463-463.
88. Aragona, P. and R. Di Pietro, *Is it safe to use topical NSAIDs for corneal sensitivity in Sjögren's syndrome patients?* Expert opinion on drug safety, 2007. **6**(1): p. 33-43.
89. Paton, L., *The trigeminal and its ocular lesions.* The British journal of ophthalmology, 1926. **10**(6): p. 305.
90. Kingsley, R.E. and C.F. Marfurt, *Topical substance P and corneal epithelial wound closure in the rabbit.* Investigative ophthalmology & visual science, 1997. **38**(2): p. 388-395.
91. Robin, J.B., et al., *Lack of effect of pilocarpine on corneal epithelial wound healing.* Current eye research, 1984. **3**(3): p. 403-406.

92. MANNIS, M.J. and C.J. MURPHY, *Synergistic effects of substance P with insulin-like growth factor-1 on epithelial migration of the cornea.* Journal of cellular physiology, 1996. **169159**: p. 166.
93. Nakamura, M., T.-i. Chikama, and T. Nishida, *Up-regulation of integrin α5 expression by combination of substance P and insulin-like growth factor-1 in rabbit corneal epithelial cells.* Biochemical and biophysical research communications, 1998. **246**(3): p. 777-782.
94. MIKULEC, A.A. and D.L. TANELIAN, *CGRP increases the rate of corneal re-epithelialization in an in vitro whole mount preparation.* Journal of ocular pharmacology and therapeutics, 1996. **12**(4): p. 417-423.
95. Tran, M.T., et al., *Calcitonin gene-related peptide induces IL-8 synthesis in human corneal epithelial cells.* The Journal of Immunology, 2000. **164**(8): p. 4307-4312.
96. Candia, O.A. and A.H. Neufeld, *Topical epinephrine causes a decrease in density of β-adrenergic receptors and catecholamine-stimulated chloride transport in the rabbit cornea.* Biochimica et Biophysica Acta (BBA)-General Subjects, 1978. **543**(3): p. 403-408.
97. McDermott, A.M., et al., *Effect of substance P, insulin-like growth factor-1 and vasoactive intestinal polypeptide on corneal re-epithelialization in galactosemic rats.* Current eye research, 1998. **17**(12): p. 1143-1149.
98. Bourcier, T., et al., *Expression of neurotensin receptors in human corneal keratocytes.* Investigative ophthalmology & visual science, 2002. **43**(6): p. 1765-1771.
99. Hamrah, P., et al., *Corneal sensation and subbasal nerve alterations in patients with herpes simplex keratitis: an in vivo confocal microscopy study.* Ophthalmology, 2010. **117**(10): p. 1930-1936.
100. Ahuja, Y., et al., *Decreased corneal sensitivity and abnormal corneal nerves in Fuchs endothelial dystrophy.* Cornea, 2012. **31**(11): p. 1257.
101. Al-Aqaba, M., et al., *Corneal nerve aberrations in bullous keratopathy.* American journal of ophthalmology, 2011. **151**(5): p. 840-849. e1.
102. Hu, Y., et al., *Corneal in vivo confocal scanning laser microscopy in patients with atopic keratoconjunctivitis.* Ophthalmology, 2008. **115**(11): p. 2004-2012.
103. Molnár, I. and Á. Bokk, *Decreased nerve growth factor levels in hyperthyroid Graves' ophthalmopathy highlighting the role of neuroprotective factor in autoimmune thyroid diseases.* Cytokine, 2006. **35**(3): p. 109-114.
104. He, J. and H.E. Bazan, *Mapping the nerve architecture of diabetic human corneas.* Ophthalmology, 2012. **119**(5): p. 956-964.
105. Hossain, P., A. Sachdev, and R.A. Malik, *Early detection of diabetic peripheral neuropathy with corneal confocal microscopy.* The Lancet, 2005. **366**(9494): p. 1340-1343.
106. Hargus, N.J. and M.K. Patel, *Voltage-gated Na+ channels in neuropathic pain.* Expert opinion on investigational drugs, 2007. **16**(5): p. 635-646.
107. Malik, R.A., et al., *Corneal confocal microscopy: a non-invasive surrogate of nerve fibre damage and repair in diabetic patients.* Diabetologia, 2003. **46**(5): p. 683-688.
108. Engel, G.L., *The need for a new medical model: a challenge for biomedicine.* Holistic Medicine, 1989. **4**(1): p. 37-53.
109. Rosenthal, P. and D. Borsook, *Ocular neuropathic pain.* British Journal of Ophthalmology, 2015: p. bjophthalmol-2014-306280.
110. Carr, D.B. and L.C. Goudas, *Acute pain.* The Lancet, 1999. **353**(9169): p. 2051-2058.
111. Breivik, H., et al., *Survey of chronic pain in Europe: prevalence, impact on daily life, and treatment.* European journal of pain, 2006. **10**(4): p. 287-287.
112. Brewitt, H. and F. Sistani, *Dry eye disease: the scale of the problem.* Survey of ophthalmology, 2001. **45**: p. S199-S202.

113. Rosenthal, P. and D. Borsook, *The corneal pain system. Part I: the missing piece of the dry eye puzzle.* The ocular surface, 2012. **10**(1): p. 2-14.
114. Tuominen, I.S., et al., *Corneal innervation and morphology in primary Sjogren's syndrome.* Investigative ophthalmology & visual science, 2003. **44**(6): p. 2545-2549.
115. Marfurt, C.F. and D.R. Del Toro, *Corneal sensory pathway in the rat: a horseradish peroxidase tracing study.* Journal of Comparative Neurology, 1987. **261**(3): p. 450-459.
116. Todorovic, S.M. and V. Jevtovic-Todorovic, *The role of T-type calcium channels in peripheral and central pain processing.* CNS & Neurological Disorders-Drug Targets (Formerly Current Drug Targets-CNS & Neurological Disorders), 2006. **5**(6): p. 639-653.
117. Woolf, C.J., et al., *Nerve growth factor contributes to the generation of inflammatory sensory hypersensitivity.* Neuroscience, 1994. **62**(2): p. 327-331.
118. Woolf, C.J. and M.W. Salter, *Neuronal plasticity: increasing the gain in pain.* Science, 2000. **288**(5472): p. 1765-1768.
119. Pergolizzi, J., et al., *The development of chronic pain: physiological CHANGE necessitates a multidisciplinary approach to treatment.* Current medical research and opinion, 2013. **29**(9): p. 1127-1135.
120. You, L., S. Ebner, and F.E. Kruse, *Glial Cell–Derived Neurotrophic Factor (GDNF)–Induced Migration and Signal Transduction in.*
121. You, L., F.E. Kruse, and H.E. Völcker, *Neurotrophic factors in the human cornea.* Investigative ophthalmology & visual science, 2000. **41**(3): p. 692-702.
122. Tripathi, B. and R. Tripathi, *Cytotoxic effects of benzalkonium chloride and chlorobutanol on human corneal epithelial cells in vitro.* Lens and eye toxicity research, 1988. **6**(3): p. 395-403.
123. Wilson, S.L., M. Ahearne, and A. Hopkinson, *An overview of current techniques for ocular toxicity testing.* Toxicology, 2015. **327**: p. 32-46.
124. Van Goethem, F., et al., *Prevalidation of a new in vitro reconstituted human cornea model to assess the eye irritating potential of chemicals.* Toxicology in vitro, 2006. **20**(1): p. 1-17.
125. Mohan, R.R., et al., *Development of genetically engineered tet HPV16-E6/E7 transduced human corneal epithelial clones having tight regulation of proliferation and normal differentiation.* Experimental eye research, 2003. **77**(4): p. 395-407.
126. Minami, Y., H. Sugihara, and S. Oono, *Reconstruction of cornea in three-dimensional collagen gel matrix culture.* Investigative ophthalmology & visual science, 1993. **34**(7): p. 2316-2324.
127. Zieske, J.D., et al., *Basement membrane assembly and differentiation of cultured corneal cells: importance of culture environment and endothelial cell interaction.* Experimental cell research, 1994. **214**(2): p. 621-633.
128. Suuronen, E.J., et al., *Innervated human corneal equivalents as in vitro models for nerve-target cell interactions.* The FASEB journal, 2004. **18**(1): p. 170-172.
129. Roeder, B.A., et al., *Tensile mechanical properties of three-dimensional type I collagen extracellular matrices with varied microstructure.* Journal of biomechanical engineering, 2002. **124**(2): p. 214-222.
130. Elsheikh, A., et al., *Assessment of corneal biomechanical properties and their variation with age.* Current eye research, 2007. **32**(1): p. 11-19.
131. Becker, R.A., et al., *Report of an ISRTP Workshop: Progress and barriers to incorporating alternative toxicological methods in the US.* Regulatory Toxicology and Pharmacology, 2006. **46**(1): p. 18-22.
132. Jin, H.J., et al., *Water‐Stable Silk Films with Reduced β‐Sheet Content.* Advanced Functional Materials, 2005. **15**(8): p. 1241-1247.
133. Hu, X., et al., *Regulation of silk material structure by temperature-controlled water vapor annealing.* Biomacromolecules, 2011. **12**(5): p. 1686-1696.

134. Zeng, Y., et al., *A comparison of biomechanical properties between human and porcine cornea.* Journal of biomechanics, 2001. **34**(4): p. 533-537.
135. Last, J.A., et al., *Determining the mechanical properties of human corneal basement membranes with atomic force microscopy.* Journal of structural biology, 2009. **167**(1): p. 19-24.
136. Wu, J., et al., *Corneal stromal bioequivalents secreted on patterned silk substrates.* Biomaterials, 2014. **35**(12): p. 3744-3755.
137. Tang-Schomer, M.D., et al., *Bioengineered functional brain-like cortical tissue.* Proceedings of the National Academy of Sciences, 2014. **111**(38): p. 13811-13816.
138. COULOMBRE, A.J. and J.L. COULOMBRE, *The role of intraocular pressure in the development of the chick eye: IV. Corneal curvature.* AMA archives of ophthalmology, 1958. **59**(4): p. 502-506.
139. Orssengo, G.J. and D.C. Pye, *Determination of the true intraocular pressure and modulus of elasticity of the human cornea in vivo.* Bulletin of mathematical biology, 1999. **61**(3): p. 551-572.
140. Hopkins, A.M., et al., *Silk hydrogels as soft substrates for neural tissue engineering.* Advanced Functional Materials, 2013. **23**(41): p. 5140-5149.
141. Man, A.J., et al., *Neurite outgrowth in fibrin gels is regulated by substrate stiffness.* Tissue Engineering Part A, 2011. **17**(23-24): p. 2931-2942.
142. Hoffman-Kim, D., J.A. Mitchel, and R.V. Bellamkonda, *Topography, cell response, and nerve regeneration.* Annual review of biomedical engineering, 2010. **12**: p. 203.
143. Clements, I.P., et al., *Thin-film enhanced nerve guidance channels for peripheral nerve repair.* Biomaterials, 2009. **30**(23): p. 3834-3846.
144. Jenkins, P.M., et al., *A nerve guidance conduit with topographical and biochemical cues: potential application using human neural stem cells.* Nanoscale research letters, 2015. **10**(1): p. 1-7.
145. Cao, X. and M. Shoichet, *Defining the concentration gradient of nerve growth factor for guided neurite outgrowth.* Neuroscience, 2001. **103**(3): p. 831-840.
146. Kemp, S.W., et al., *A novel method for establishing daily in vivo concentration gradients of soluble nerve growth factor (NGF).* Journal of neuroscience methods, 2007. **165**(1): p. 83-88.
147. Tang, S., et al., *The effects of gradients of nerve growth factor immobilized PCLA scaffolds on neurite outgrowth in vitro and peripheral nerve regeneration in rats.* Biomaterials, 2013. **34**(29): p. 7086-7096.
148. Griscom, L., et al., *Techniques for patterning and guidance of primary culture neurons on micro-electrode arrays.* Sensors and Actuators B: Chemical, 2002. **83**(1): p. 15-21.
149. Lykissas, M.G., et al., *The role of neurotrophins in axonal growth, guidance, and regeneration.* Current neurovascular research, 2007. **4**(2): p. 143-151.
150. Uebersax, L., et al., *Silk fibroin matrices for the controlled release of nerve growth factor (NGF).* Biomaterials, 2007. **28**(30): p. 4449-4460.
151. Bhang, S.H., et al., *The effect of the controlled release of nerve growth factor from collagen gel on the efficiency of neural cell culture.* Biomaterials, 2009. **30**(1): p. 126-132.
152. Pruniéras, M., M. Régnier, and D. Woodley, *Methods for cultivation of keratinocytes with an air-liquid interface.* Journal of Investigative Dermatology, 1983. **81**.
153. Chang, J.-E., S.K. Basu, and V.H. Lee, *Air-interface condition promotes the formation of tight corneal epithelial cell layers for drug transport studies.* Pharmaceutical research, 2000. **17**(6): p. 670-676.
154. Liu, X.-Y., et al., *In vitro tissue engineering of lamellar cornea using human amniotic epithelial cells and rabbit cornea stroma.* International journal of ophthalmology, 2013. **6**(4): p. 425.
155. Bodle, J.C., et al., *Primary cilia: the chemical antenna regulating human adipose-derived stem cell osteogenesis.* PloS one, 2013. **8**(5): p. e62554.

156. Mauretti, A., et al., *Cardiomyocyte progenitor cell mechanoresponse unrevealed: strain avoidance and mechanosome development.* Integrative Biology, 2016. **8**(9): p. 991-1001.
157. French, K.M., et al., *Fibronectin and Cyclic Strain Improve Cardiac Progenitor Cell Regenerative Potential In Vitro.* Stem Cells International, 2016. **2016**.
158. Leonard, E.K., et al., *Design and validation of a corneal bioreactor.* Biotechnology and bioengineering, 2012. **109**(12): p. 3189-3198.
159. Springs, C.L., et al., *Predictability of donor lamellar graft diameter and thickness in an artificial anterior chamber system.* Cornea, 2002. **21**(7): p. 696-699.
160. Hubert, T., et al., *Collagens in the developing and diseased nervous system.* Cellular and molecular life sciences, 2009. **66**(7): p. 1223-1238.
161. Wang, X., et al., *Sonication-induced gelation of silk fibroin for cell encapsulation.* Biomaterials, 2008. **29**(8): p. 1054-1064.
162. Du, Y., et al., *Multipotent stem cells in human corneal stroma.* Stem Cells, 2005. **23**(9): p. 1266-1275.
163. Gil, E.S., et al., *Response of human corneal fibroblasts on silk film surface patterns.* Macromolecular bioscience, 2010. **10**(6): p. 664-673.
164. Gil, E.S., et al., *Helicoidal multi-lamellar features of RGD-functionalized silk biomaterials for corneal tissue engineering.* Biomaterials, 2010. **31**(34): p. 8953-8963.
165. Meijering, E., et al., *Design and validation of a tool for neurite tracing and analysis in fluorescence microscopy images.* Cytometry Part A, 2004. **58**(2): p. 167-176.
166. Leclere, P.G., et al., *Impaired axonal regeneration by isolectin B4-binding dorsal root ganglion neurons in vitro.* The Journal of neuroscience, 2007. **27**(5): p. 1190-1199.
167. Willits, R.K. and S.L. Skornia, *Effect of collagen gel stiffness on neurite extension.* Journal of Biomaterials Science, Polymer Edition, 2004. **15**(12): p. 1521-1531.
168. Chernousov, M.A., R.C. Stahl, and D.J. Carey, *Schwann cell type V collagen inhibits axonal outgrowth and promotes Schwann cell migration via distinct adhesive activities of the collagen and noncollagen domains.* The Journal of Neuroscience, 2001. **21**(16): p. 6125-6135.
169. Sajanti, J., et al., *Increase of collagen synthesis and deposition in the arachnoid and the dura following subarachnoid hemorrhage in the rat.* Biochimica et Biophysica Acta (BBA)-Molecular Basis of Disease, 1999. **1454**(3): p. 209-216.
170. Vitale, P., et al., *Mechanisms of transcriptional activation of the col6a1 gene during Schwann cell differentiation.* Mechanisms of development, 2001. **102**(1): p. 145-156.
171. Tucker, K.L., M. Meyer, and Y.-A. Barde, *Neurotrophins are required for nerve growth during development.* Nature neuroscience, 2001. **4**(1): p. 29-37.
172. Moore, K., M. Macsween, and M. Shoichet, *Immobilized concentration gradients of neurotrophic factors guide neurite outgrowth of primary neurons in macroporous scaffolds.* Tissue engineering, 2006. **12**(2): p. 267-278.
173. Bae, J.S., et al., *Bone marrow‐derived mesenchymal stem cells promote neuronal networks with functional synaptic transmission after transplantation into mice with neurodegeneration.* Stem cells, 2007. **25**(5): p. 1307-1316.
174. Kaselis, A., et al., *DRG axon elongation and growth cone collapse rate induced by Sema3A are differently dependent on NGF concentration.* Cellular and molecular neurobiology, 2014. **34**(2): p. 289-296.
175. Fan, C., et al., *Effect of type-2 astrocytes on the viability of dorsal root ganglion neurons and length of neuronal processes.* Neural regeneration research, 2014. **9**(2): p. 119.
176. Daud, M.F., et al., *An aligned 3D neuronal-glial co-culture model for peripheral nerve studies.* Biomaterials, 2012. **33**(25): p. 5901-5913.

177. Wilkins, A., et al., *Oligodendrocytes promote neuronal survival and axonal length by distinct intracellular mechanisms: a novel role for oligodendrocyte-derived glial cell line-derived neurotrophic factor.* The Journal of neuroscience, 2003. **23**(12): p. 4967-4974.
178. Kowtharapu, B.S., et al., *Corneal epithelial and neuronal interactions: role in wound healing.* Experimental eye research, 2014. **125**: p. 53-61.
179. Lindsay, R.M., *Nerve growth factors (NGF, BDNF) enhance axonal regeneration but are not required for survival of adult sensory neurons.* The Journal of neuroscience, 1988. **8**(7): p. 2394-2405.
180. Wang, C.-Y., et al., *The effect of aligned core–shell nanofibres delivering NGF on the promotion of sciatic nerve regeneration.* Journal of Biomaterials Science, Polymer Edition, 2012. **23**(1-4): p. 167-184.
181. White, J.D., et al., *Silk–tropoelastin protein films for nerve guidance.* Acta biomaterialia, 2015. **14**: p. 1-10.
182. Hardy, J.G., et al., *Into the groove: instructive silk-polypyrrole films with topographical guidance cues direct DRG neurite outgrowth.* Journal of Biomaterials Science, Polymer Edition, 2015. **26**(17): p. 1327-1342.
183. Altman, G.H., et al., *Silk-based biomaterials.* Biomaterials, 2003. **24**(3): p. 401-416.
184. Altman, G.H., et al., *Silk matrix for tissue engineered anterior cruciate ligaments.* Biomaterials, 2002. **23**(20): p. 4131-4141.
185. Hofmann, S., et al., *Cartilage-like tissue engineering using silk scaffolds and mesenchymal stem cells.* Tissue engineering, 2006. **12**(10): p. 2729-2738.
186. Lawrence, B.D., et al., *Silk film biomaterials for cornea tissue engineering.* Biomaterials, 2009. **30**(7): p. 1299-1308.
187. Chen, Y., et al., *Robust bioengineered 3D functional human intestinal epithelium.* Scientific reports, 2015. **5**.
188. Xu, T., et al., *Inkjet printing of viable mammalian cells.* Biomaterials, 2005. **26**(1): p. 93-99.
189. Jakab, K., et al., *Tissue engineering by self-assembly and bio-printing of living cells.* Biofabrication, 2010. **2**(2): p. 022001.
190. Delaney, J.T., P.J. Smith, and U.S. Schubert, *Inkjet printing of proteins.* Soft Matter, 2009. **5**(24): p. 4866-4877.
191. Derby, B., *Inkjet printing of functional and structural materials: fluid property requirements, feature stability, and resolution.* Annual Review of Materials Research, 2010. **40**: p. 395-414.
192. Wang, Q., et al., *High Throughput Screening of Dynamic Silk-Elastin-Like Protein Biomaterials.* Advanced Functional Materials, 2014. **24**(27): p. 4303-4310.
193. Hu, X., et al., *Biomaterials derived from silk-tropoelastin protein systems.* Biomaterials, 2010. **31**(32): p. 8121-8131.
194. Yamada, K., Y. Tsuboi, and A. Itaya, *AFM observation of silk fibroin on mica substrates: morphologies reflecting the secondary structures.* Thin Solid Films, 2003. **440**(1-2): p. 208-216.
195. Barroso, M.M.S.A., et al., *Artificial laminin polymers assembled in acidic pH mimic basement membrane organization.* Journal of Biological Chemistry, 2008. **283**(17): p. 11714-11720.
196. Zhou, J., et al., *Influence of assembling pH on the stability of poly (l-glutamic acid) and poly (l-lysine) multilayers against urea treatment.* Colloids and Surfaces B: Biointerfaces, 2008. **62**(2): p. 250-257.
197. Dinis, T.M., et al., *Method to form a fiber/growth factor dual-gradient along electrospun silk for nerve regeneration.* ACS applied materials & interfaces, 2014. **6**(19): p. 16817-16826.
198. Pritchard, E.M., et al., *Physical and chemical aspects of stabilization of compounds in silk.* Biopolymers, 2012. **97**(6): p. 479-498.

199. Yao, D., et al., *Salt-leached silk scaffolds with tunable mechanical properties.* Biomacromolecules, 2012. **13**(11): p. 3723-3729.
200. Wu, J., et al., *Corneal stromal stem cells versus corneal fibroblasts in generating structurally appropriate corneal stromal tissue.* Experimental eye research, 2014. **120**: p. 71-81.
201. Chomczynski, P. and N. Sacchi, *Single-step method of RNA isolation by acid guanidinium thiocyanate-phenol-chloroform extraction.* Analytical biochemistry, 1987. **162**(1): p. 156-159.
202. Chen, J., et al., *Human bone marrow stromal cell and ligament fibroblast responses on RGD‐modified silk fibers.* Journal of Biomedical Materials Research Part A, 2003. **67**(2): p. 559-570.
203. Jester, J.V., *Corneal crystallins and the development of cellular transparency.* Seminars in cell & developmental biology, 2008. **19**(2): p. 82-93.
204. Du, Y., et al., *Adipose-derived stem cells differentiate to keratocytes in vitro.* Molecular Vision, 2010. **16**: p. 2680-2689.
205. Suuronen, E.J., et al., *Functional innervation in tissue engineered models for in vitro study and testing purposes.* Toxicological Sciences, 2004. **82**(2): p. 525-533.
206. Rockwood, D.N., et al., *Materials fabrication from Bombyx mori silk fibroin.* Nature protocols, 2011. **6**(10): p. 1612-1631.
207. Salehi, H., et al., *Neuronal induction and regional identity by co-culture of adherent human embryonic stem cells with chicken notochords and somites.* International Journal of Developmental Biology, 2011. **55**(3): p. 321-326.
208. Chen, C.-C., et al., *A sensory neuron-specific, proton-gated ion channel.* Proceedings of the National Academy of Sciences, 1998. **95**(17): p. 10240-10245.
209. Reichl, S., J. Bednarz, and C. Müller-Goymann, *Human corneal equivalent as cell culture model for in vitro drug permeation studies.* British Journal of Ophthalmology, 2004. **88**(4): p. 560-565.
210. Tegtmeyer, S., I. Papantoniou, and C.C. Müller-Goymann, *Reconstruction of an in vitro cornea and its use for drug permeation studies from different formulations containing pilocarpine hydrochloride.* European journal of pharmaceutics and biopharmaceutics, 2001. **51**(2): p. 119-125.
211. Lambiase, A., et al., *Corneal changes in neurosurgically induced neurotrophic keratitis.* JAMA ophthalmology, 2013. **131**(12): p. 1547-1553.
212. Semeraro, F., et al., *Neurotrophic keratitis.* Ophthalmologica, 2014. **231**(4): p. 191-197.
213. Blanco-Mezquita, T., et al., *Nerve Growth Factor Promotes Corneal Epithelial Migration by Enhancing Expression of Matrix Metalloprotease-9NGF Promotes Epithelial Migration.* Investigative ophthalmology & visual science, 2013. **54**(6): p. 3880-3890.
214. Gingras, M., et al., *In vitro development of a tissue-engineered model of peripheral nerve regeneration to study neurite growth.* The FASEB journal, 2003. **17**(14): p. 2124-2126.
215. Bryce, G. and R. Ribchester, *Culture of isolated embryonic chick dorsal root ganglia at an air-liquid interface: a simple method for studying the mechanism and control of neurite outgrowth.* Journal of neuroscience methods, 1993. **48**(1): p. 89-97.
216. Cairns, D.M., et al., *Expandable and Rapidly Differentiating Human Induced Neural Stem Cell Lines for Multiple Tissue Engineering Applications.* Stem Cell Reports, 2016. **7**(3): p. 557-570.
217. Chambers, S.M., et al., *Combined small-molecule inhibition accelerates developmental timing and converts human pluripotent stem cells into nociceptors.* Nature biotechnology, 2012. **30**(7): p. 715-720.
218. Kontiola, A.I., et al., *The induction/impact tonometer: a new instrument to measure intraocular pressure in the rat.* Experimental eye research, 2001. **73**(6): p. 781-785.
219. Teixeira, A.I., et al., *The effect of environmental factors on the response of human corneal epithelial cells to nanoscale substrate topography.* Biomaterials, 2006. **27**(21): p. 3945-3954.

220. Lee, J.-H., et al., *Single transcription factor conversion of human blood fate to NPCs with CNS and PNS developmental capacity.* Cell reports, 2015. **11**(9): p. 1367-1376.
221. Wainger, B.J., et al., *Modeling pain in vitro using nociceptor neurons reprogrammed from fibroblasts.* Nature neuroscience, 2015. **18**(1): p. 17-24.
222. Henry, J.L., *Substance P and pain: an updating.* Trends in Neurosciences, 1980. **3**(4): p. 95-97.
223. Yang, Y., et al., *Wakayama Symposium: Dependence of Corneal Epithelial Homeostasis on Transient Receptor Potential Function.* The ocular surface, 2013. **11**(1): p. 8-11.
224. Lewinter, R.D., et al., *Immunoreactive TRPV‐2 (VRL‐1), a capsaicin receptor homolog, in the spinal cord of the rat.* Journal of Comparative Neurology, 2004. **470**(4): p. 400-408.
225. Schlote, T., G. Kadner, and N. Freudenthaler, *Marked reduction and distinct patterns of eye blinking in patients with moderately dry eyes during video display terminal use.* Graefe's archive for clinical and experimental ophthalmology, 2004. **242**(4): p. 306-312.
226. Doane, M.G., *Blinking and the mechanics of the lacrimal drainage system.* Ophthalmology, 1981. **88**(8): p. 844-851.
227. Copt, R.-P., R. Thomas, and A. Mermoud, *Corneal thickness in ocular hypertension, primary open-angle glaucoma, and normal tension glaucoma.* Archives of ophthalmology, 1999. **117**(1): p. 14-16.
228. Selinger, D.S., R.C. Selinger, and W.P. Reed, *Resistance to infection of the external eye: the role of tears.* Survey of ophthalmology, 1979. **24**(1): p. 33-38.
229. Vesaluoma, M., et al., *Effects of oleoresin capsicum pepper spray on human corneal morphology and sensitivity.* Investigative ophthalmology & visual science, 2000. **41**(8): p. 2138-2147.
230. Gazerani, P., O.K. Andersen, and L. Arendt-Nielsen, *A human experimental capsaicin model for trigeminal sensitization. Gender-specific differences.* Pain, 2005. **118**(1): p. 155-163.
231. Caterina, M.J., et al., *Impaired nociception and pain sensation in mice lacking the capsaicin receptor.* science, 2000. **288**(5464): p. 306-313.
232. Lockwood, A., M. Hope-Ross, and P. Chell, *Neurotrophic keratopathy and diabetes mellitus.* Eye, 2006. **20**(7): p. 837-839.
233. Poon, A.C., et al., *Autologous serum eyedrops for dry eyes and epithelial defects: clinical and in vitro toxicity studies.* British Journal of Ophthalmology, 2001. **85**(10): p. 1188-1197.
234. Pan, Q., et al., *Autologous serum eye drops for dry eye.* The Cochrane Library, 2013.
235. Gallar, J., et al., *Effects of capsaicin on corneal wound healing.* Investigative ophthalmology & visual science, 1990. **31**(10): p. 1968-1974.
236. Wilson, S.E., et al., *The Corneal Wound Healing Response:: Cytokine-mediated Interaction of the Epithelium, Stroma, and Inflammatory Cells.* Progress in retinal and eye research, 2001. **20**(5): p. 625-637.
237. Lekhanont, K., et al., *Undiluted Serum Eye Drops for the Treatment of Persistent Corneal Epitheilal Defects.* Scientific Reports, 2016. **6**: p. 38143.
238. Geerling, G., S. Maclennan, and D. Hartwig, *Autologous serum eye drops for ocular surface disorders.* British Journal of Ophthalmology, 2004. **88**(11): p. 1467-1474.
239. Noble, B.A., et al., *Comparison of autologous serum eye drops with conventional therapy in a randomised controlled crossover trial for ocular surface disease.* British Journal of Ophthalmology, 2004. **88**(5): p. 647-652.
240. Noda-Tsuruya, T., et al., *Autologous serum eye drops for dry eye after LASIK.* Journal of Refractive Surgery, 2006. **22**(1): p. 61-66.
241. Lambiase, A., et al., *Alterations of tear neuromediators in dry eye disease.* Archives of Ophthalmology, 2011. **129**(8): p. 981-986.
242. Bring, D.K.I., et al., *Residual substance P levels after capsaicin treatment correlate with tendon repair.* Wound Repair and Regeneration, 2012. **20**(1): p. 50-60.

243. Tervo, K., et al., *Substance P-immunoreactive nerves in the human cornea and iris.* Investigative ophthalmology & visual science, 1982. **23**(5): p. 671-674.
244. He, J., et al., *Changes in Corneal Innervation after HSV-1 Latency Established with Different Reactivation Phenotypes.* Current Eye Research, 2016: p. 1-6.
245. Ko, J.-A., et al., *Neuropeptides Released From Trigeminal Neurons Promote the Stratification of Human Corneal Epithelial CellsEffects of Neural Cells on HCE Cells.* Investigative ophthalmology & visual science, 2014. **55**(1): p. 125-133.
246. Garcia-Hirschfeld, J., L.G. Lopez-Briones, and C. Belmonte, *Neurotrophic influences on corneal epithelial cells.* Experimental eye research, 1994. **59**(5): p. 597-605.
247. Nagano, T., et al., *Effects of substance P and IGF-1 in corneal epithelial barrier function and wound healing in a rat model of neurotrophic keratopathy.* Investigative ophthalmology & visual science, 2003. **44**(9): p. 3810-3815.
248. Elliott, N.T. and F. Yuan, *A review of three‐dimensional in vitro tissue models for drug discovery and transport studies.* Journal of pharmaceutical sciences, 2011. **100**(1): p. 59-74.
249. Rama, P., et al., *Limbal stem-cell therapy and long-term corneal regeneration.* New England Journal of Medicine, 2010. **363**(2): p. 147-155.
250. Pellegrini, G., et al., *Long-term restoration of damaged corneal surfaces with autologous cultivated corneal epithelium.* The Lancet, 1997. **349**(9057): p. 990-993.
251. Chen, S.-Y., et al., *A new isolation method of human limbal progenitor cells by maintaining close association with their niche cells.* Tissue Engineering Part C: Methods, 2011. **17**(5): p. 537-548.
252. Huang, A. and S. Tseng, *Corneal epithelial wound healing in the absence of limbal epithelium.* Investigative ophthalmology & visual science, 1991. **32**(1): p. 96-105.
253. Dua, H.S. and A. Azuara-Blanco, *Limbal stem cells of the corneal epithelium.* Survey of ophthalmology, 2000. **44**(5): p. 415-425.
254. Mimura, T., et al., *Cultured human corneal endothelial cell transplantation with a collagen sheet in a rabbit model.* Investigative ophthalmology & visual science, 2004. **45**(9): p. 2992-2997.
255. Chen, J., et al., *Study on biocompatibility of complexes of collagen–chitosan–sodium hyaluronate and cornea.* Artificial organs, 2005. **29**(2): p. 104-113.
256. Lai, J.-Y., et al., *Effect of charge and molecular weight on the functionality of gelatin carriers for corneal endothelial cell therapy.* Biomacromolecules, 2006. **7**(6): p. 1836-1844.
257. Ishino, Y., et al., *Amniotic membrane as a carrier for cultivated human corneal endothelial cell transplantation.* Investigative ophthalmology & visual science, 2004. **45**(3): p. 800-806.
258. Numakawa, T., et al., *BDNF function and intracellular signaling in neurons.* Histology and histopathology, 2010. **25**(2): p. 237-258.
259. Sweeney, D.F., T.J. Millar, and S.R. Raju, *Tear film stability: a review.* Experimental eye research, 2013. **117**: p. 28-38.
260. Bron, A., et al., *Functional aspects of the tear film lipid layer.* Experimental eye research, 2004. **78**(3): p. 347-360.
261. Espana, E.M., et al., *Novel enzymatic isolation of an entire viable human limbal epithelial sheet.* Investigative ophthalmology & visual science, 2003. **44**(10): p. 4275-4281.
262. Du, Y., et al., *Functional reconstruction of rabbit corneal epithelium by human limbal cells cultured on amniotic membrane.* Molecular vision, 2003. **9**: p. 635.
263. Thassu, D. and G.J. Chader, *Ocular drug delivery systems: barriers and application of nanoparticulate systems*. 2012: CRC Press.
264. Snider, W.D., *Functions of the neurotrophins during nervous system development: what the knockouts are teaching us.* Cell, 1994. **77**(5): p. 627-638.
265. Rantamäki, A.H., et al., *Human tear fluid lipidome: from composition to function.* PloS one, 2011. **6**(5): p. e19553.

266. Gipson, I.K. and T. Inatomi, *Cellular origin of mucins of the ocular surface tear film*, in *Lacrimal Gland, Tear Film, and Dry Eye Syndromes 2*. 1998, Springer. p. 221-227.
267. He, M., et al., *Artificial Polymeric Scaffolds as Extracellular Matrix Substitutes for Autologous Conjunctival Goblet Cell ExpansionArtificial Scaffolds for Conjunctival Goblet Cell Growth.* Investigative Ophthalmology & Visual Science, 2016. **57**(14): p. 6134-6146.
268. Reitz, C., et al., *Analysis of tear proteins by one-and two-dimensional thin-layer iosoelectric focusing, sodium dodecyl sulfate electrophoresis and lectin blotting. Detection of a new component: cystatin C.* Graefe's archive for clinical and experimental ophthalmology, 1998. **236**(12): p. 894-899.
269. Zhou, L., et al., *Quantitative Analysis of N-Linked Glycoproteins in Tear Fluid of Climatic Droplet Keratopathy by Glycopeptide Capture and iTRAQ†.* Journal of proteome research, 2009. **8**(4): p. 1992-2003.
270. Jay, N.L. and M. Gillies, *Proteomic analysis of ophthalmic disease.* Clinical & experimental ophthalmology, 2012. **40**(7): p. 755-763.
271. Covey, W., P. Perillie, and S.C. Finch, *The origin of tear lysozyme.* Experimental Biology and Medicine, 1971. **137**(4): p. 1362-1363.
272. German, A., E. Hall, and M. Day, *Measurement of IgG, IgM and IgA concentrations in canine serum, saliva, tears and bile.* Veterinary immunology and immunopathology, 1998. **64**(2): p. 107-121.
273. Perumal, N., et al., *Characterization of human reflex tear proteome reveals high expression of lacrimal proline‐rich protein 4 (PRR4).* Proteomics, 2015. **15**(19): p. 3370-3381.
274. Broekhuyse, R., *Tear lactoferrin: a bacteriostatic and complexing protein.* Investigative Ophthalmology & Visual Science, 1974. **13**(7): p. 550-554.
275. van Setten, G.-B., *Epidermal growth factor in human tear fluid: increased release but decreased concentrations during reflex tearing.* Current eye research, 1990. **9**(1): p. 79-83.
276. Ohashi, Y., et al., *Abnormal protein profiles in tears with dry eye syndrome.* American journal of ophthalmology, 2003. **136**(2): p. 291-299.
277. Zhou, L., et al., *Proteomic analysis of human tears: defensin expression after ocular surface surgery.* Journal of proteome research, 2004. **3**(3): p. 410-416.
278. Li, N., et al., *Characterization of human tear proteome using multiple proteomic analysis techniques.* Journal of proteome research, 2005. **4**(6): p. 2052-2061.
279. Dean, A.W. and B.J. Glasgow, *Mass Spectrometric Identification of Phospholipids in Human Tears and Tear LipocalinPhospholipids in Tears and Tear Lipocalin.* Investigative ophthalmology & visual science, 2012. **53**(4): p. 1773-1782.
280. Evans, V., et al., *Lacryglobin in human tears, a potential marker for cancer.* Clinical & experimental ophthalmology, 2001. **29**(3): p. 161-163.
281. Qu, X.-D. and R.I. Lehrer, *Secretory phospholipase A2 is the principal bactericide for staphylococci and other gram-positive bacteria in human tears.* Infection and immunity, 1998. **66**(6): p. 2791-2797.
282. Zhao, J.J. and N.A. Afshari, *Generation of Human Corneal Endothelial Cells via In Vitro Ocular Lineage Restriction of Pluripotent Stem Cells.* Invest Ophthalmol Vis Sci, 2016. **57**(15): p. 6878-6884.
283. Argüeso, P., et al., *Mucin characteristics of human corneal-limbal epithelial cells that exclude the rose bengal anionic dye.* Investigative ophthalmology & visual science, 2006. **47**(1): p. 113-119.
284. Barar, J., et al., *Ocular drug delivery; impact of in vitro cell culture models.* Journal of ophthalmic & vision research, 2009. **4**(4): p. 238-252.
285. Cohen, S. and J. Mao, *Neuropathic Pain: Mechanisms & Clinical Implications+ MP3.* British Medical Journal, 2014. **348**: p. f7656.

286. Kandel, E.R., et al., *Principles of neural science*. Vol. 4. 2000: McGraw-hill New York.
287. Logothetis, N.K. and S. Panzeri, *Local field potential, relationship to BOLD signal*, in *Encyclopedia of Computational Neuroscience*. 2015, Springer. p. 1560-1568.
288. Pallikaris, I.G., et al., *Rotating brush for fast removal of corneal epithelium.* Journal of Refractive Surgery, 1994. **10**(4): p. 439-442.
289. Melles, G.R., et al., *A surgical technique for posterior lamellar keratoplasty.* Cornea, 1998. **17**(6): p. 618-626.
290. Fullard, R.J. and D.L. Tucker, *Changes in human tear protein levels with progressively increasing stimulus.* Invest Ophthalmol Vis Sci, 1991. **32**(8): p. 2290-301.
291. Das, R.K., N. Kasoju, and U. Bora, *Encapsulation of curcumin in alginate-chitosan-pluronic composite nanoparticles for delivery to cancer cells.* Nanomedicine: Nanotechnology, Biology and Medicine, 2010. **6**(1): p. 153-160.
292. Grand, E., et al., *Targeting FGFR3 in multiple myeloma: inhibition of t (4; 14)-positive cells by SU5402 and PD173074.* Leukemia, 2004. **18**(5): p. 962-966.
293. Tang‐Schomer, M.D., et al., *Film‐Based Implants for Supporting Neuron–Electrode Integrated Interfaces for The Brain.* Advanced functional materials, 2014. **24**(13): p. 1938-1948.
294. Rönkkö, S., et al., *Human corneal cell culture models for drug toxicity studies.* Drug Delivery and Translational Research, 2016. **6**(6): p. 660-675.
295. Jin, C., et al., *Injectable 3-D fabrication of medical electronics at the target biological tissues.* Scientific reports, 2013. **3**.
296. Bautista, D.M., et al., *The menthol receptor TRPM8 is the principal detector of environmental cold.* Nature, 2007. **448**(7150): p. 204-208.
297. Kwan, K.Y., et al., *TRPA1 contributes to cold, mechanical, and chemical nociception but is not essential for hair-cell transduction.* Neuron, 2006. **50**(2): p. 277-289.
298. Vachon, P., et al., *Alleviation of chronic neuropathic pain by environmental enrichment in mice well after the establishment of chronic pain.* Behavioral and brain functions, 2013. **9**(1): p. 1.
299. Tramullas, M., T.G. Dinan, and J.F. Cryan, *Chronic psychosocial stress induces visceral hyperalgesia in mice.* Stress, 2012. **15**(3): p. 281-292.
300. Serra, J., et al., *Hyperexcitable C nociceptors in fibromyalgia.* Annals of neurology, 2014. **75**(2): p. 196-208.
301. Chen, X., et al., *CO2 stimulation of the cornea: a comparison between human sensation and nerve activity in polymodal nociceptive afferents of the cat.* European Journal of Neuroscience, 1995. **7**(6): p. 1154-1163.
302. Campoccia, D., L. Montanaro, and C.R. Arciola, *A review of the clinical implications of anti-infective biomaterials and infection-resistant surfaces.* Biomaterials, 2013. **34**(33): p. 8018-8029.
303. Heck, L., et al., *Specific cleavage of human type III and IV collagens by Pseudomonas aeruginosa elastase.* Infection and immunity, 1986. **51**(1): p. 115-118.
304. Todokoro, D., et al., *Contact lens-related infectious keratitis with white plaque formation caused by Corynebacterium propinquum.* Journal of clinical microbiology, 2015. **53**(9): p. 3092-3095.
305. Osthoff, M., et al., *Activation of the lectin pathway of complement in experimental human keratitis with Pseudomonas aeruginosa.* 2014.